ERRATA

AFOSR-106
TECHNICAL REPORT

Contract No. AF 29(600)-1711
Project No. 7856
Task No. 78548

DYNAMICS OF SEPARATING BODIES
VOLUME II
MEASUREMENTS AT MACH 2, 4, AND 5

H. L. Wackelin
R. O Fredette

March, 1961

Section III, page 36

On graph showing C_m as a function of Y/D for X/D = .625, two lower curves should read $\alpha = 0^o$ and $+15^o$ reading down.

Section IV, page 60

On graph showing C_A and A_B and on graph of C_N and A_{CON} as functions of percent exposure, vertical axis ordinates should read 0, .5, 1.0.

Appendix I, Section III

Page 16

Following the equation of motion for the carrier vehicle in center of page, add notation:

ϑ_o is positive when measured downward from the horizontal

On equation of motion for ejected pilot device at bottom of page, the last term on the right hand side of the equation should read:

$$+ K_p (x - x_p - \lambda_p)\left(1 + \frac{\dot{x} - \dot{x}_p}{k_p}\right)$$

Page 17

Starting on the 4th line of the page, the paragraph should read:

When lines are employed, the mass term $\rho_p (x - x_p)$ is maximum at λ_p, or is equal to $\rho_p \lambda_p$ at the time when full extension of the unstretched length occurs. However, during the period of line stretch, $(x - x_p) > \lambda_p$, the effective mass.....

Page 18

On first line of page, the second algebraic term should read:

$K_c (x_v - x_c - \lambda_c)$

Page 19

Add statement to end of paragraph in middle of page:

....angle of attack at the centroid. This analysis was conducted for bodies whose planes of symmetry are characterized by right angles between all faces, i.e., cylinders and rectangular shapes.

Two equations at bottom of page should read:

$$x_j = \dot{x}_c - K_j \dot{\theta} \sin(\theta + \tau_j)$$

$$\dot{y}_j = \dot{y}_c + K_j \dot{\theta} \cos(\theta + \tau_j)$$

Page 20

First line on page should read:

where K_j is the distance....

Page 21

Equation for F_{x_j} should read:

$$F_{x_j} = - \left[\begin{Bmatrix} P_{B_{jE}} \\ P_{F_{jE}} \end{Bmatrix} A_{jE} + \begin{Bmatrix} P_{B_{jw}} \\ P_{F_{jw}} \end{Bmatrix} (A_j - A_{jE}) \right] \cos (\theta + j \tfrac{\pi}{2})$$

$$= - \left[B_{jE} + B_{jw} \right] \cos (\theta + j \tfrac{\pi}{2})$$

Page 22

Fourth equation on page should read:

$$M_{j-} = - B_{jE-} \quad a_{jE-} - B_{jw-} \cdot a_{jw-}$$

List of Symbols for Appendix I, Page 29

On second line, delete definition given for B and substitute:

B Force on capsule face, lbs

Add definition of K_j:

K_j Distance from centroid of half-face to capsule c.g., ft

On eighth line, delete definition given for P and substitute:

P Pressure on capsule face, lbs/ft^2

AIR FORCE OFFICE OF SCIENTIFIC RESEARCH

TECHNICAL REPORT

Contract No. AF 29(600)-1711
Project No. 7856
Task No. 78548

DYNAMICS OF SEPARATING BODIES

VOLUME II

MEASUREMENTS AT MACH 2, 4, AND 5

H. L. Wackelin
R. O. Freaette

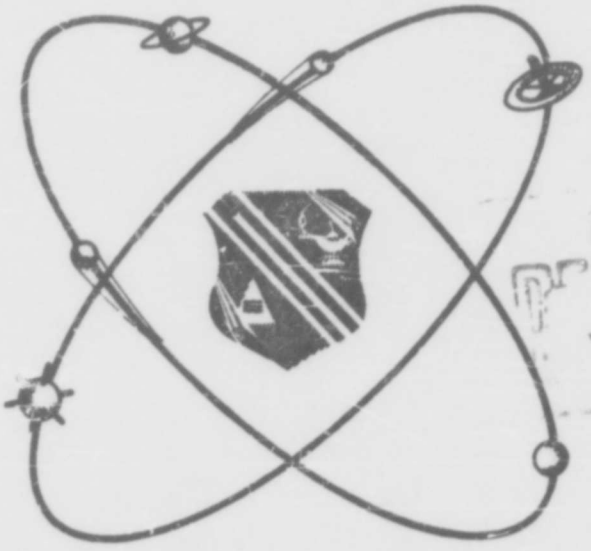

DIRECTORATE OF RESEARCH ANALYSIS

HOLLOMAN AIR FORCE BASE

NEW MEXICO

March 1961

AFOSR-106

Contract No. AF 29(600)-1711
Project No. 7856
Task No. 78548

DYNAMICS OF SEPARATING BODIES

VOLUME II*

MEASUREMENTS AT MACH 2, 4, AND 5

by

H. L. Wackelin
R. O. Fredette

Cook Research Laboratories
A Division of
Cook Electric Company
Chicago, Illinois

Science and Engineering Division

Directorate of Research Analysis

AIR FORCE OFFICE OF SCIENTIFIC RESEARCH
AIR FORCE RESEARCH DIVISION
AIR RESEARCH AND DEVELOPMENT COMMAND
UNITED STATES AIR FORCE
Holloman Air Force Base, New Mexico

March 1961

*See Foreword

FOREWORD

This report was prepared under Air Force Contract No. AF 29(600)-1711, Project No. 7856, Task No. 78548, by the Cook Research Laboratories, a division of the Cook Electric Company, Chicago, Illinois. This contract is monitored by the Directorate of Research Analysis, Science and Engineering Division. The contract monitor is Mr. F. Utech.

The work was conducted in the Aerodynamics Section of the Cook Research Laboratories under the direction of Mr. R. O. Fredette, Associate Director, with Mr. H. L. Wackelin as Project Engineer. The section of the report which presents the wake characteristics and the equations of motion presented in Appendix I were prepared by Mr. R. D. Turner and Dr. J. S. Thale, respectively.

The wind tunnel tests were conducted in wind tunnel A of the von Karman Gas Dynamics Facility, Arnold Engineering Development Center. The cooperation and effort afforded this test program by the Air Force and ARC personnel concerned, and in particular by the ARO Project Engineer, Mr. J. Don Gray, was especially valuable.

Volume I, THEORETICAL ANALYSIS and Volume III, MEASUREMENTS AT MACH 8 AND RESULTS of the series DYNAMICS OF SEPARATING BODIES, will be published at a later date.

ABSTRACT

Wind tunnel tests were conducted on a data capsule shape in the interference field of a carrier vehicle model at Mach numbers of 4.0 and 5.0 with limited data at M = 2.0. The data obtained were analyzed and a preliminary evaluation made as to the agreement with methods of prediction. It is shown that in areas where the flow field is known, estimated values of the derivatives obtained with relatively simple calculation techniques agree reasonably well with the data. A discussion of the direct application of these data to capsule separation analyses is presented.

TABLE OF CONTENTS

LIST OF ILLUSTRATIONS

LIST OF ILLUSTRATIONS (cont'd)

LIST OF SYMBOLS

A	Axial force
A_B	Capsule base area
C_A	Axial force coefficient, $A/q_\infty A_B$
C_{A_T}	Total axial force coefficient
C_{A_B}	Base pressure coefficient, $(P_\infty - P_B)/q_\infty$
C_M	Pitching moment coefficient, $M/q_\infty A_B L$
C_{M_α}	Pitching moment curve slope, per degree, $\partial C_M/\partial \alpha$
C_N	Normal force coefficient, $N/q_\infty A_B$
C_{N_α}	Normal force curve slope, per degree, $\partial C_N/\partial \alpha$
D	Carrier vehicle body diameter
L	Capsule length
M	Free stream Mach number, pitching moment about capsule center of gravity
N	Normal force
P	Pressure
P_B	Base Pressure
P_o	Wind tunnel stilling chamber pressure
q	Dynamic pressure
R_e	Free stream Reynolds number based on capsule centerbody diameter
r/r_o	Ratio of radial displacement from wake centerline and wake radius
U	Velocity depression in wake as a function of radial displacement

V_w	Local velocity in wake in streamwise direction
X	Streamwise direction, measurement or position coordinate
X/D	Axial displacement, in calibers, from reference station of carrier model. For wake studies X/D is referenced to the carrier model base
$X_{C.P.}$	Center of pressure location on capsule model, measured from the nose
Y	Direction, measurement, or position coordinate in pitch plane, transverse to the stream direction
Y/D	Lateral displacement, in calibers, from reference station of carrier model, i.e., carrier model centerline

---

α	Angle of attack of capsule model centerline to the free stream direction
δ	Local stream deflection angle
$\Delta\alpha$	Local stream deflection angle, to be added to α for capsule local angle of attack in influence of carrier model flow field (equal to δ)
ρ	Air density
∞	Subscript refers to free stream conditions

SECTION I

INTRODUCTION

This report presents a summary of the wind tunnel tests conducted and the evaluation of data obtained therefrom under the second phase of work performed in the pursuit of this contract. The first phase of the contract on Dynamics of Separation consisted of a study program conducted to obtain basic data on the influence of mutual interference and other factors on the dynamic properties of capsule bodies separating from high performance vehicles, and to predict capsule ejection forces and velocities required to effect separation and the trajectories resulting therefrom. The results of this work were presented in an Interim Summary Report. That report, however, exists in only a limited number of copies and is not generally available. Therefore, an unclassified condensation of that report has been included as Appendix I to this present report in order to provide background information on the study program conducted, and the theoretical analyses developed therein, prior to the conduct of the wind tunnel tests.

The wind tunnel tests reported on herein were conducted to provide static data on a capsule shape at various positions in the interference field of a carrier vehicle. These tests represent what would be a first step in a comprehensive test program that would provide a validation of initial conclusions reached in the study program and would provide data for analytic treatment of separation problems. These tests were conducted in the AEDC wind tunnel A at Mach numbers of 4.0 and 5.0 with limited data at Mach 2.0. The models used for these tests consisted of a flared body capsule model chosen in the study program for its over-all desirable qualities and a carrier vehicle model representative of a high performance rocket vehicle. These models are discussed in Section II along with the test procedures followed. The most important capsule data obtained are presented in Section III and Schlieren photographs of various run sequences are shown. A correlation of the test data to the Schlieren pictures points up the effect of interference at close proximity between models and the occurrence of maximum forces and moments on the capsule at proximity to the carrier bow wave. A preliminary evaluation of the static data and the correlation with predicted values are presented in Section IV and the application of the data to the development of empirical-theoretical procedures is considered. Section V discusses the direct application of the data to separation analyses.

Manuscript released by the author August 1960 for publication.

SECTION II

WIND TUNNEL TESTS

Two separate wind tunnel tests were conducted for the acquisition of static data for the Cook Research Laboratories' capsule model. The first test was essentially a scale-effect test of a large model of the capsule shape. This model had a cylinder diameter of six inches and an over-all length of 15 inches. The tests were conducted in the AEDC wind tunnel A between 21 July and 27 July 1959 to provide basic data on the sensitivity of the Cook Research Laboratories' capsule shape to Reynolds number variation, these data being necessary to the evaluation of the small scale tests of the capsule and carrier vehicle in combination.

The proximity tests were conducted in tunnel A between 5 October and 17 October 1959. These tests consisted of static measurements of capsule data while in the interference field surrounding the side and base regions of the carrier model. For these tests a small capsule model with cylinder diameter of 0.8 inch and an over-all length of two inches was used in conjunction with a carrier model with a 4-inch diameter and 24-inch length. Data were obtained during the partial exposure phase of the capsule emerging from a port in the side of the carrier body; close-in data were obtained by positioning the capsule model laterally and axially in the side flow field of the carrier model; wake-penetration data were obtained by traversing the capsule model across the wake boundary behind the carrier base; and wake-capsule interaction data were obtained by traversing the capsule axially down the wake centerline. These four phases of testing represent the most important aspects of separation from the side or base of a carrier vehicle.

A. AEDC Wind Tunnel A

The AEDC tunnel A is a 40 by 40 inch continuous, closed circuit, variable density, supersonic wind tunnel with a Mach number range of 1.5 to 6.0. The Reynolds number in the test section is varied by varying the stilling chamber pressure. The test section is equipped with a horizontal sector which provides an angle of attach variation of -5 to +15 degrees with a straight sting. A double-pass Schlieren system is provided for observation of flow fields. The outputs of balance strain gage bridges are digitized and punched into a raw data tape which is later fed into an ERA 1102 digital computer together with the desired program to yield force and moment coefficient data. Pressure taps on the models are connected to transducers and the output is digitized and punched into the raw data tape along with the force data and tunnel conditions.

B. Models and Equipments

The capsule model balance, capsule and carrier vehicle models, stings, and the auxiliary positioning equipments used in these tests, with the exception of the ARO axial actuator, were designed and manufactured by the Cook Research Laboratories for these tests, as part of the contract requirements. Figure 1 shows the general dimensions of the capsule and carrier vehicle models used in the proximity tests.

For the partial exposure phase, a positioning mechanism was installed in the carrier model to move the capsule model in and out of the ejection port to obtain data at various partially exposed positions. The carrier model was sting mounted to the ARO axial actuator which in turn was mounted in the sector hub. The ARO axial actuator is a device providing axial traverse in the tunnel.

For the close-in phase of testing, an auxiliary sting positioner, (ASP), was mounted on the ARO axial actuator and carried the capsule model. The positioner provides an angle of attack range of ±20 degrees and lateral traverse for the capsule model. Figure 2 shows the installation of equipments for these tests. In the figure, letter A is the small capsule model and balance assembly; B is the CRL auxiliary sting positioner (called ASP); C is the carrier vehicle model; D is the carrier vehicle sting; and E is the ARO axial actuator.

The wake penetration tests were conducted by wall mounting a second carrier model and probing in the wake edge region with the Cook Research Laboratories' capsule model mounted on the ASP.

The wake core survey was conducted by mounting the capsule model on a sting carried by the ARO axial actuator. This installation is shown in Figure 3. In this figure, letter A is the wake survey carrier model; B is the wall strut; C is the capsule model and balance assembly; D is the capsule model sting; and E is the sting adaptor on the ARO axial actuator. The wall strut and carrier model shown were the same for both the wake penetration and wake core tests. In all of these test, the sector was used only to provide a basic mounting for the equipment. Yaw angle was not varied.

Figure 4 shows the large capsule model used in the scale-effect tests. The model was sting mounted to the sector and the sector was used to provide angle of attack variation.

In order to measure the forces and moments on the small capsule model employed in the proximity tests, a miniature internal electric strain gage balance was developed. The Cook Research Laboratories' capsule model balance

is a compound, split-sting, three-component type designed to measure normal force, axial force, and pitching moment in a single plane.

The balance and capsule model assembly was calibrated at AEDC prior to the tests. The design calibration loads were six pounds of normal force and six pounds of axial force. As stated in Reference 1, statistical analysis of the calibration results indicated that uncertainties in the moment and forces were less than one percent of the design loads. However, because of zero shifts due to temperature, which occurred during tests, the uncertainties were frequently as high as five percent of the design loads.

C. Test Procedure

The test positions surveyed in the proximity tests are shown in Figure 5. For the close-in tests and wake penetration tests, angle of attack was varied at each data point. Angle of attack is referenced to the wind tunnel centerline. For the partial exposure and wake core tests, the angle of attack was zero.

Data were obtained for the following conditions

	Mach No.	P_o(psia)	R_e
Partial Exposure	5.0	150	0.42×10^6
	5.0	75	0.21×10^6
	4.0	72	0.38×10^6
	4.0	35	0.18×10^6
	2.0	20	0.34×10^6
	2.0	10	0.17×10^6
Close-in Effects	5.0	150	0.42×10^6
	5.0	75	0.21×10^6
	4.0	72	0.38×10^6
	4.0	35	0.18×10^6
Wake Penetration	5.0	150	0.42×10^6
	5.0	75	0.21×10^6
	4.0	72	0.38×10^6
Wake-Capsule Interaction	4.0	72	0.38×10^6

P_o = Tunnel stilling chamber pressure
R_e = Reynolds number based on capsule cylinder diameter

In addition to these data, free stream polars were taken at Mach 4.0 and 5.0 at various Reynolds numbers. The free stream data were taken to provide reference for the data analysis and comparison with the data obtained from the scale-effect tests.

The capsule data obtained were load, moment, and base pressure coefficients. Schlieren photographs were taken at most of the data points.

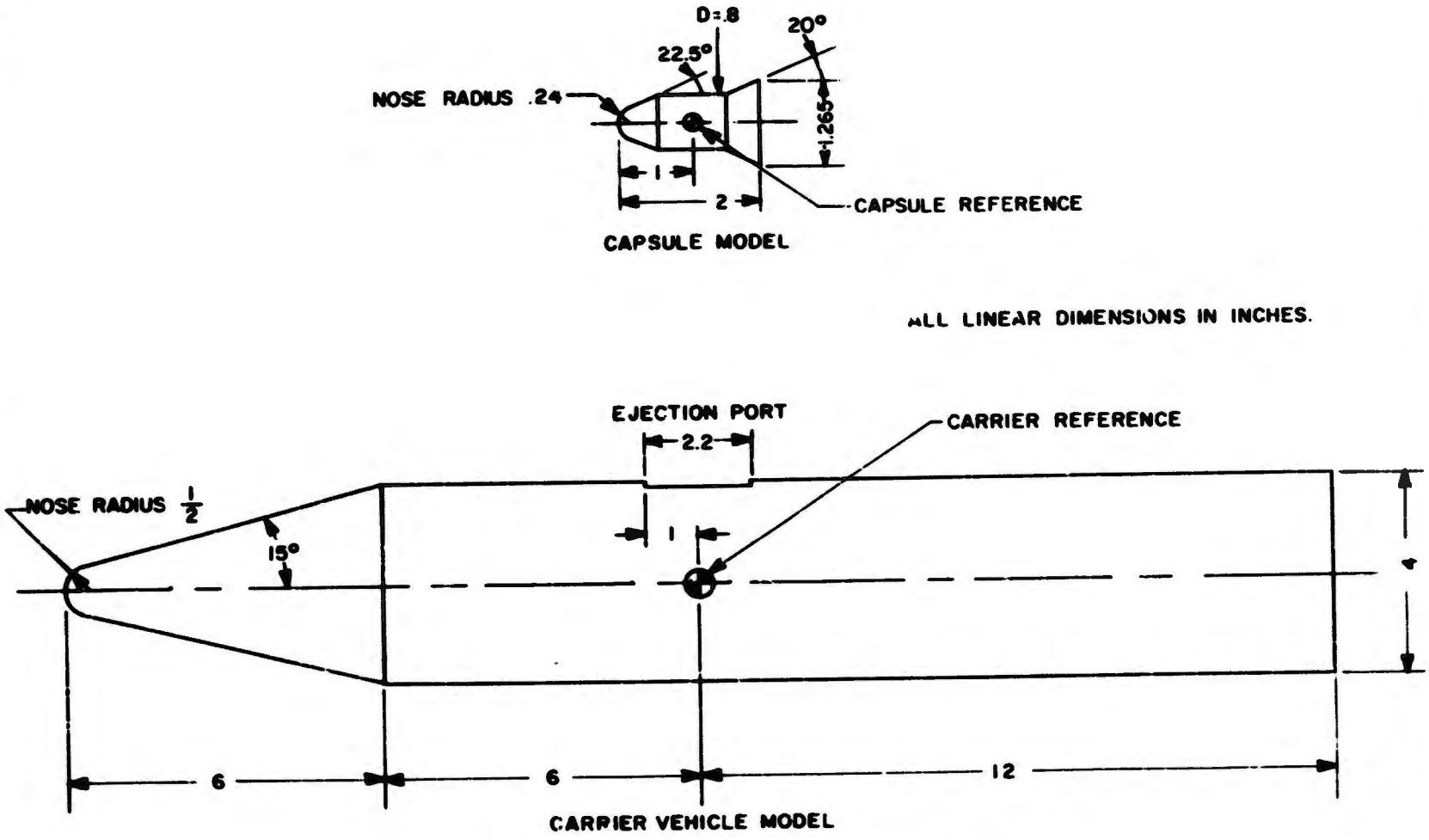

Figure 1. Dimensions of Models Employed in Proximity Tests

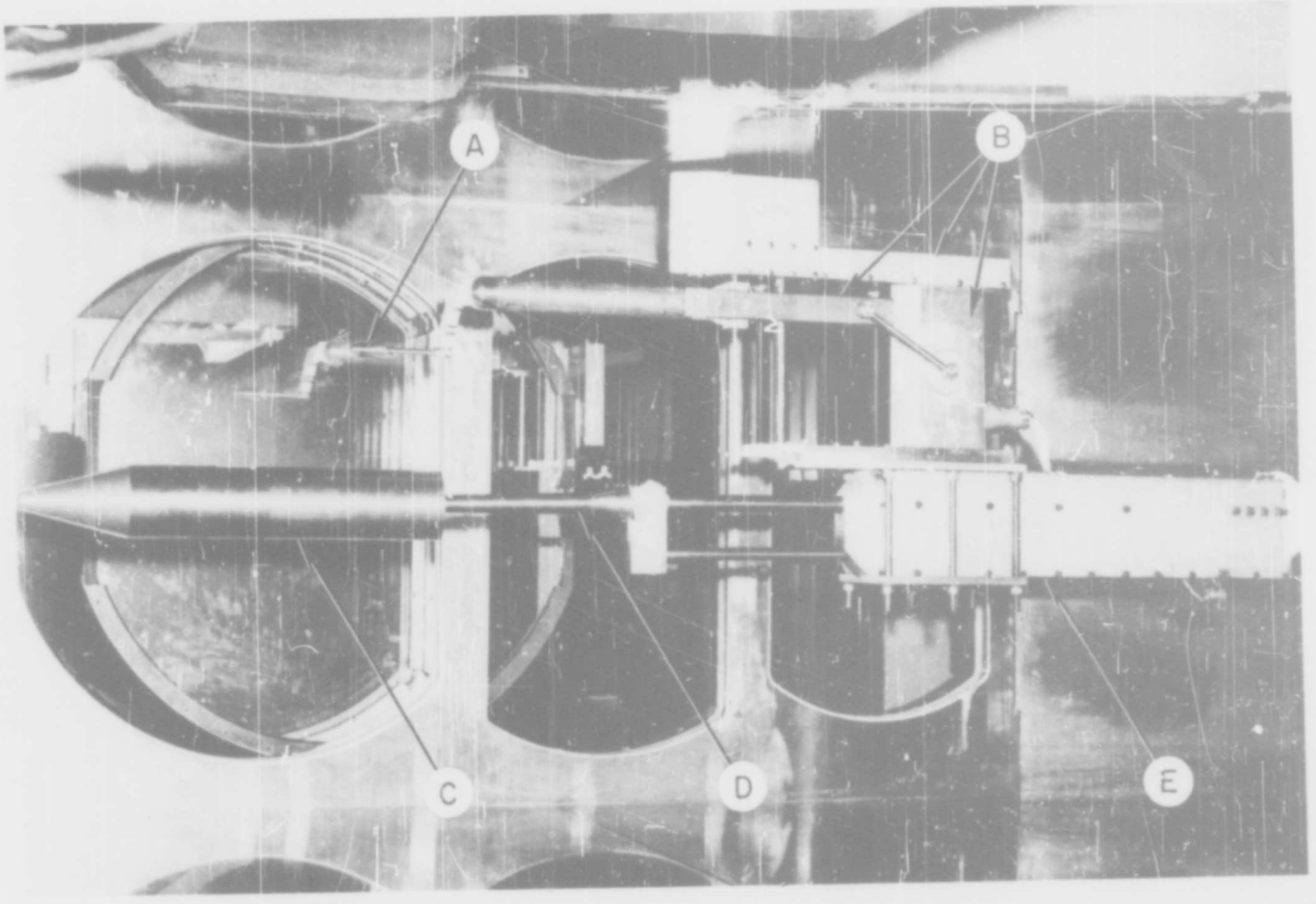

Figure 2. Tunnel A Installation - Side Separation Test, Close-in Phase

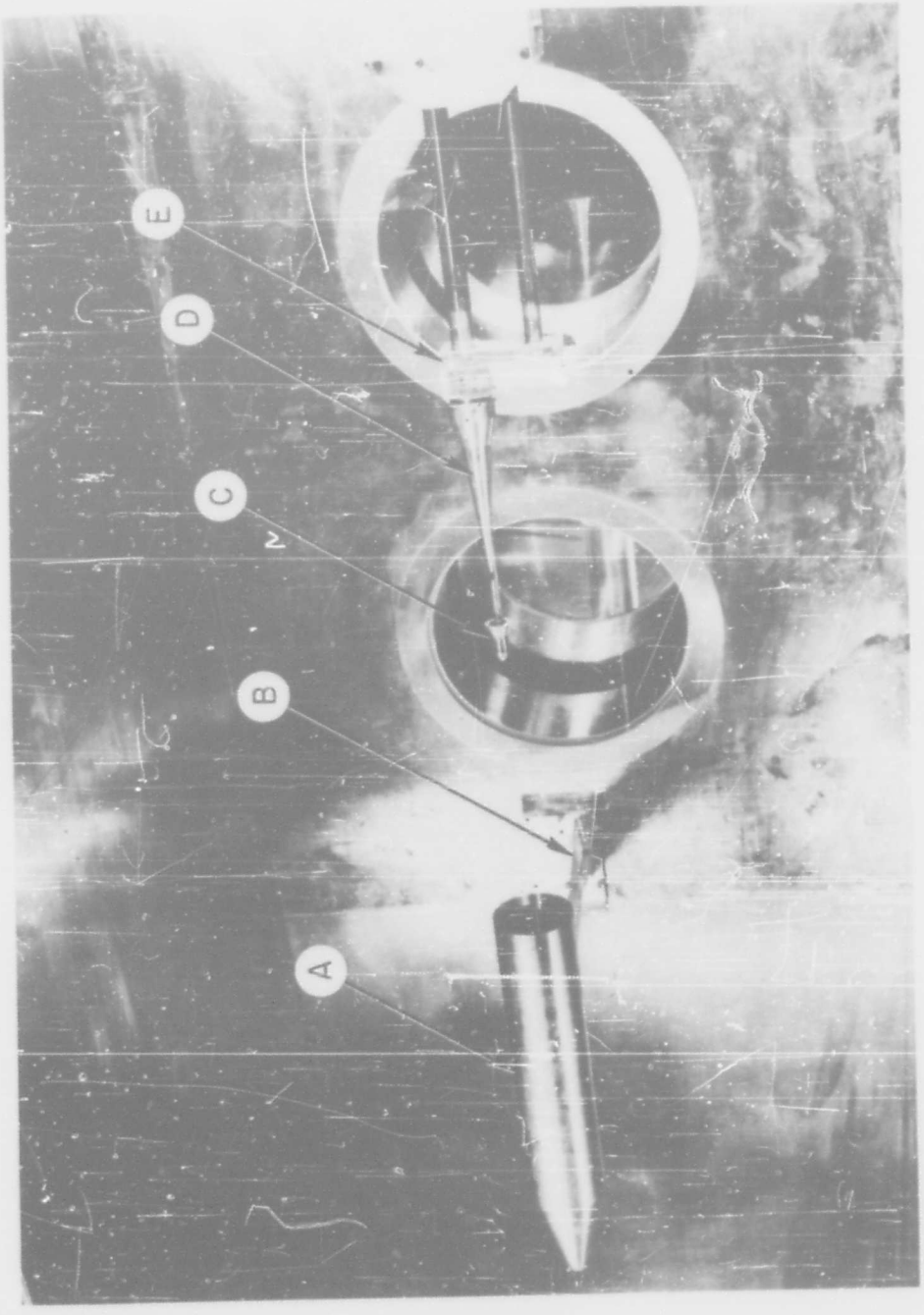

Figure 3. Tunnel A Installation - Wake Core Survey

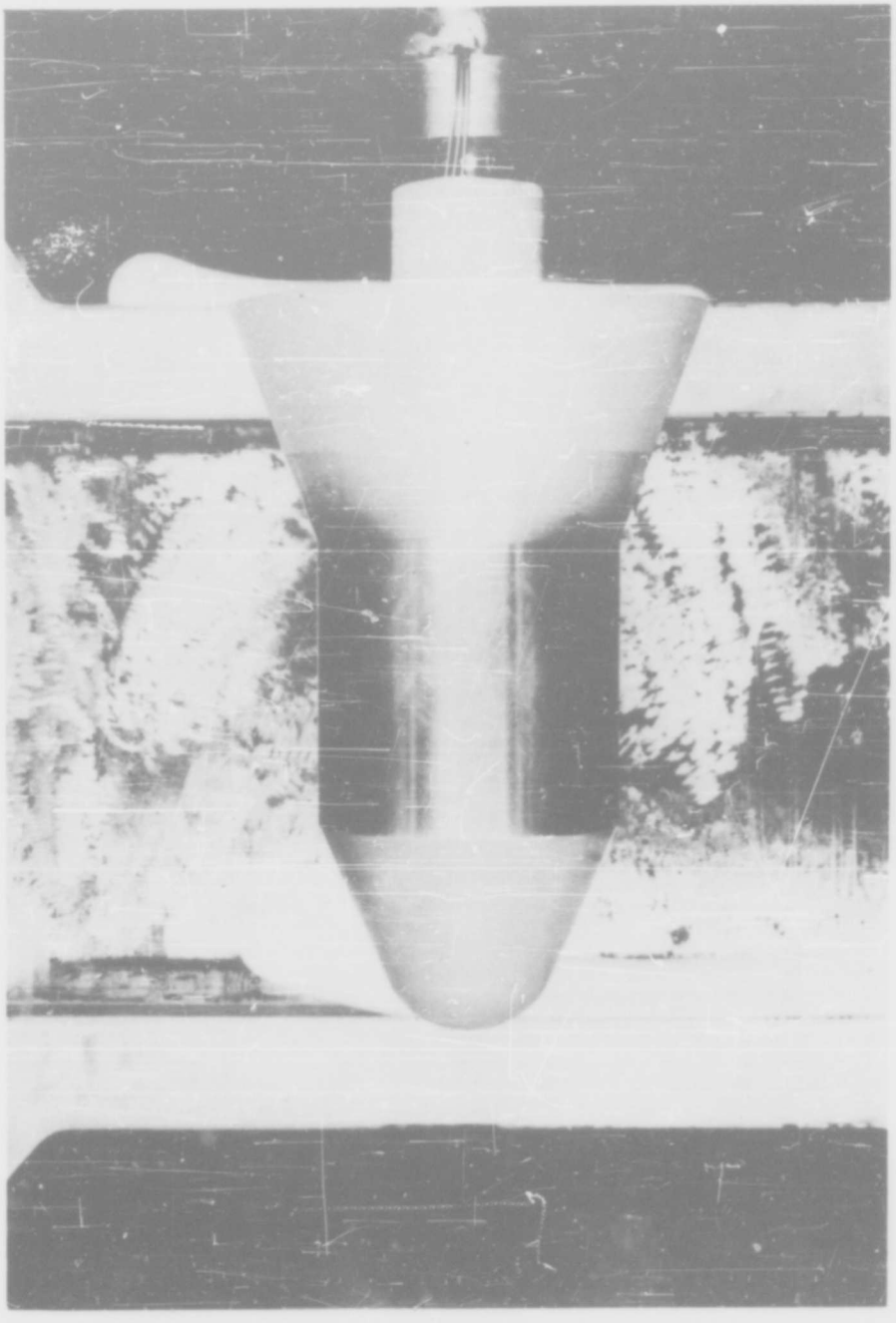

Figure 4. Tunnel A Installation - Scale-Effect Tests, 15 Inch Long Capsule Model

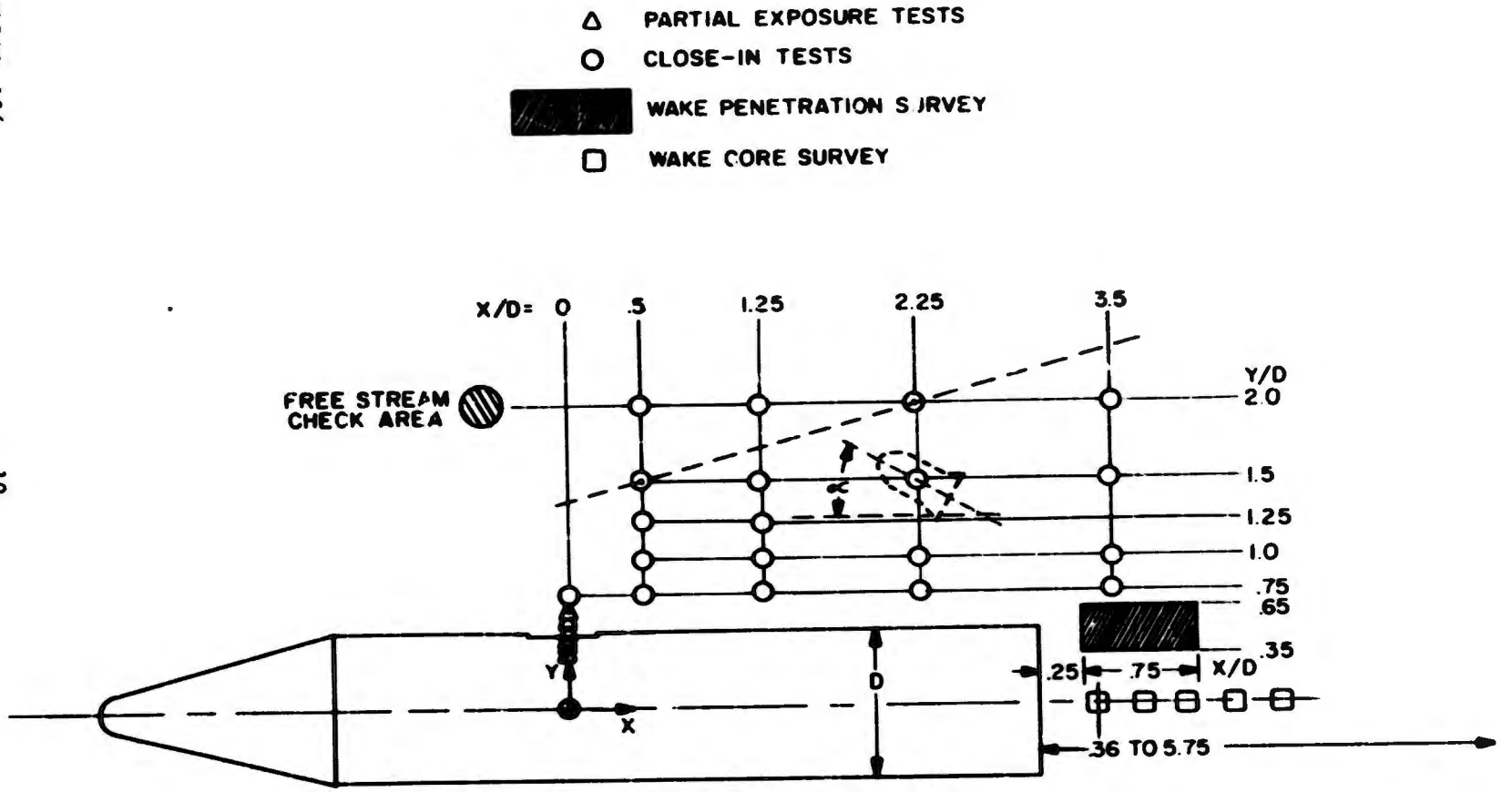

Figure 5. Coordinate System and Test Positions Surveyed

SECTION III

SUMMARY OF DATA

A summary of the most important data obtained is presented in graphic form in Figures 6a through 10. The data, for the most part, are plotted as printed out from the computer program. Some adjustment for zero shifts was made where the shifts were obvious.

Figures 6a through 6f present free stream polars taken at M = 4.0 and 5.0 and various Reynolds numbers for the capsule model. These data show the variation of the coefficients of axial force, normal force and pitching moment with angle of attack. These data were obtained by positioning the capsule as far ahead of the carrier bow wave as possible. The approximate area of free stream data acquisition is shown in Figure 5. The individual polars are presented to show the data scatter. Figures 6g and 6h show the effect of Reynolds number on the measured data. In Figure 6h, the data from the scale-effect tests of the large capsule model are included for comparison. The data show relatively small variations with Reynolds number at the higher values tested approaching independence of Reynolds number as it increases, and good correlation of normal force curve slope between the two models tested.

Figures 7a through 7d present data for all of the partial exposure conditions tested. The partial exposure data were taken with the capsule model at a fixed axial station of X/D = zero, which is the reference station on the carrier model. The lateral position of the capsule model was varied from a flush or zero exposure position to the full out or 100 percent position. Zero exposure is defined as the position of internal tangency of the capsule model base circle to the carrier model cylinder and full exposure the position of external tangency. The percent of exposure is the percent of capsule model base diameter lying external to the carrier model cylinder. The lateral position of the capsule model with respect to the carrier model is given by

$$\frac{Y}{D} = 0.341875 + 0.0031625E$$

where

E is the exposure in percent.

As shown in the curves, the Reynolds number effect is not great but a strong Mach number effect exists between the Mach 2.0 and the Mach 4.0 and 5.0 data. Figures 11 and 12 show a Schlieren record of typical exposure sequences at Mach 5.0 and 2.0.

Close-in data are shown in Figures 8a through 8i. Data variation with both lateral and axial travel in the flow field are shown. Figures 13, 14, and 15 show Schlieren sequences that can be correlated with the test data and show the shock wave interaction at the carrier surface and at bow wave intersection.

Wake penetration data are presented in Figures 9a through 9e. Two axial positions of the wall mounted carrier model were used to obtain these data. At each axial position, capsule lateral position and angle of attack were varied. However, because of the increment in axial position resulting from the angle of attack variation, data at different angles of attack could not be obtained at the same axial positions. Therefore, the data were first plotted against axial travel for fixed angles. Slight extrapolation of these data segments allowed the reading of data at fixed X/D values and these points are plotted. Figure 9a represents the middle range of the extrapolation and should be reliable as extrapolation errors in this range should be negligible. Figure 9b represents the fore and aft extremes of the extrapolations and may not be as accurate. Figure 16 shows a Schlieren sequence of a typical wake boundary traverse.

Limited data on wake capsule interaction were obtained. The variation of C_N and C_M in the wake was extremely slight and should be zero. Therefore, only the variation of C_A along the centerline is significant and is presented in Figure 10.

For both the wake penetration data and the wake capsule interaction data, the axial position of the capsule model (X/D) is referenced to the carrier model base.

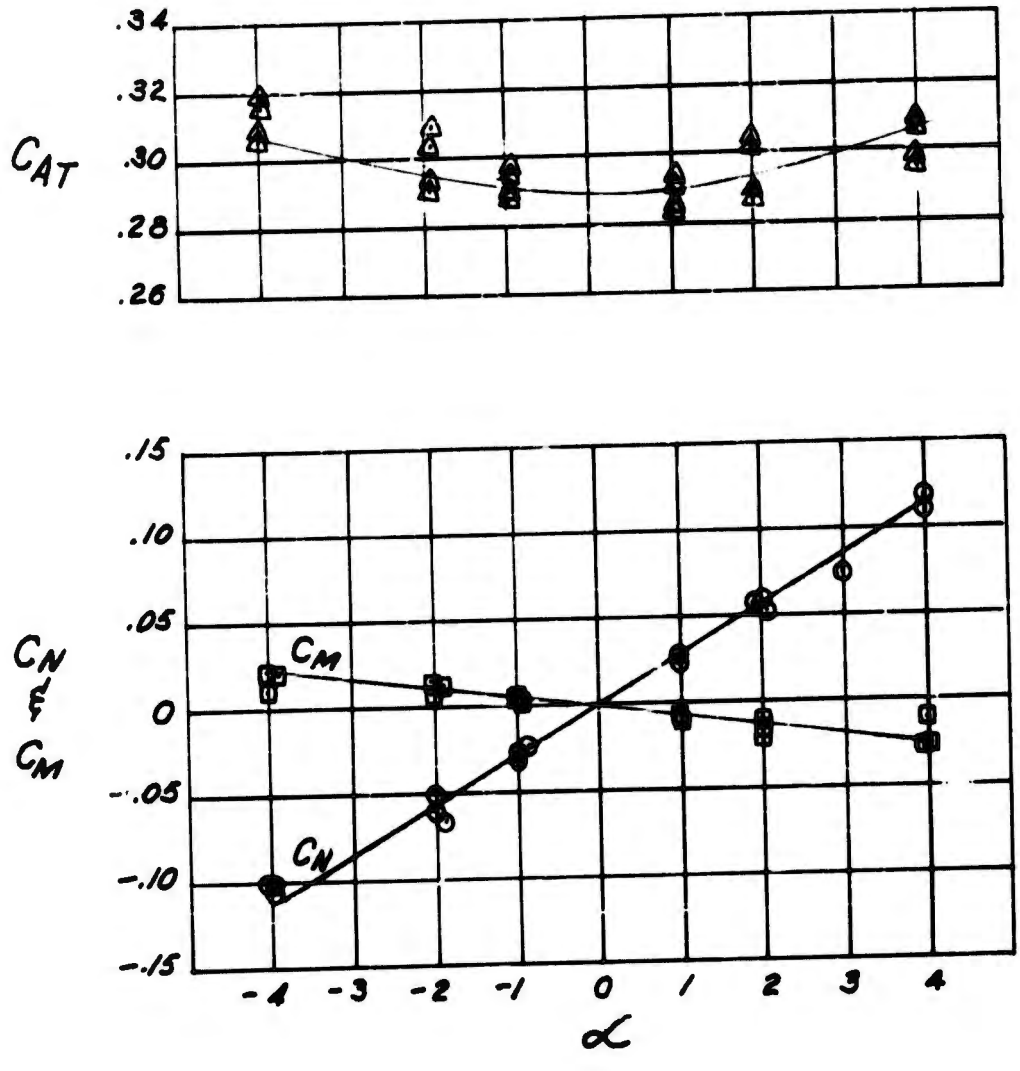

Figure 6a. Free Stream Capsule Characteristics - Variation of Axial Force, Normal Force and Pitching Moment Coefficients with Angle of Attack - M = 5.0, P_o = 150, R_e = 420,000

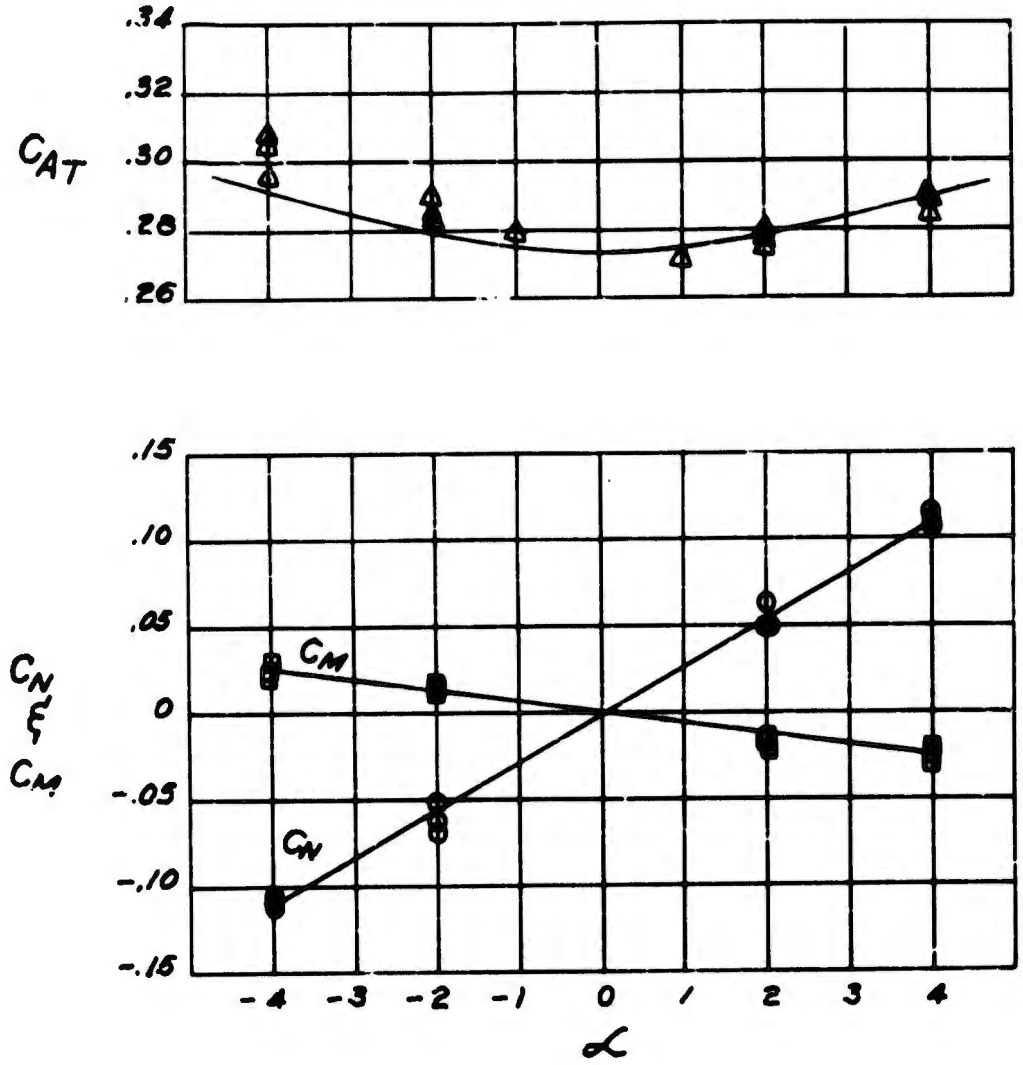

Figure 6b. Free Stream Capsule Characteristics - M = 5.0, P_o = 75, R_e = 211,000

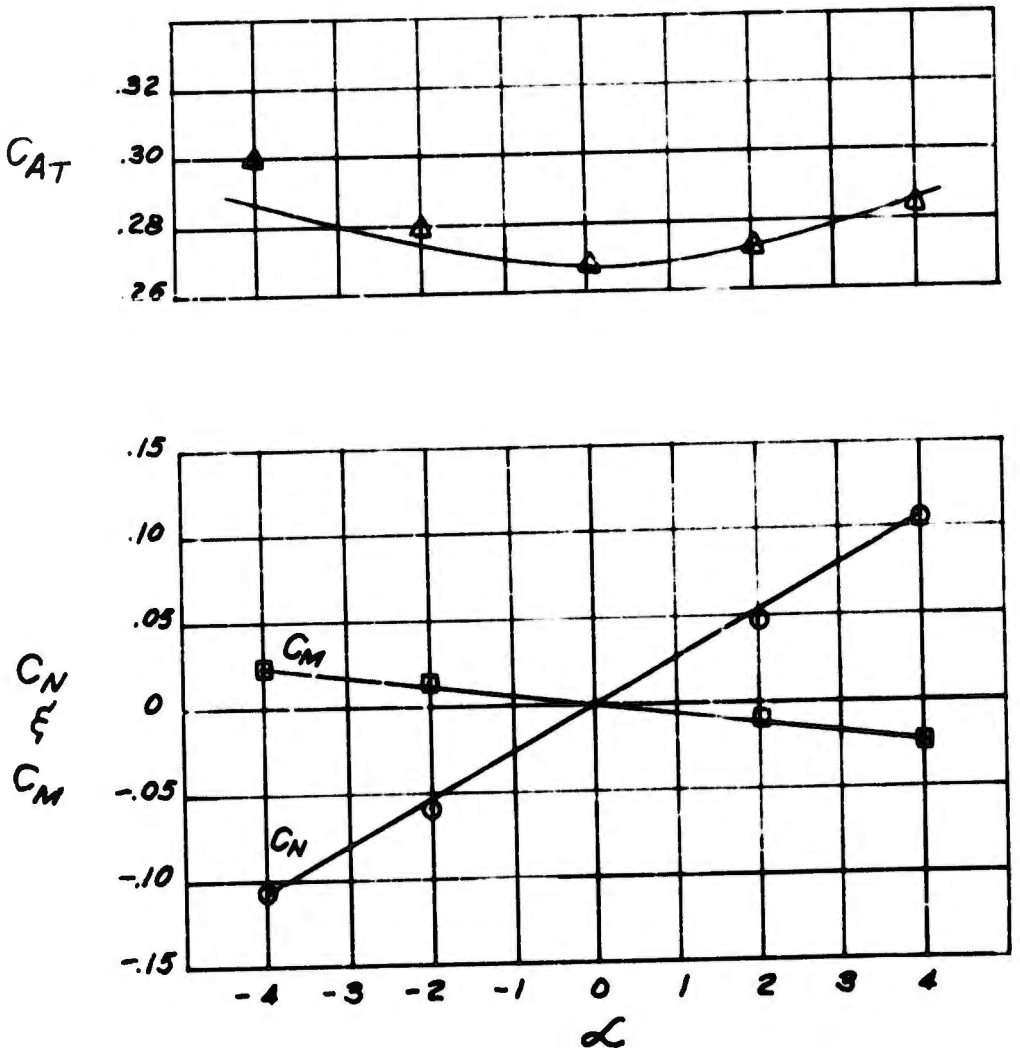

Figure 6c. Free Stream Capsule Characteristics - M = 5.0, P_o = 38, R_e = 108,000

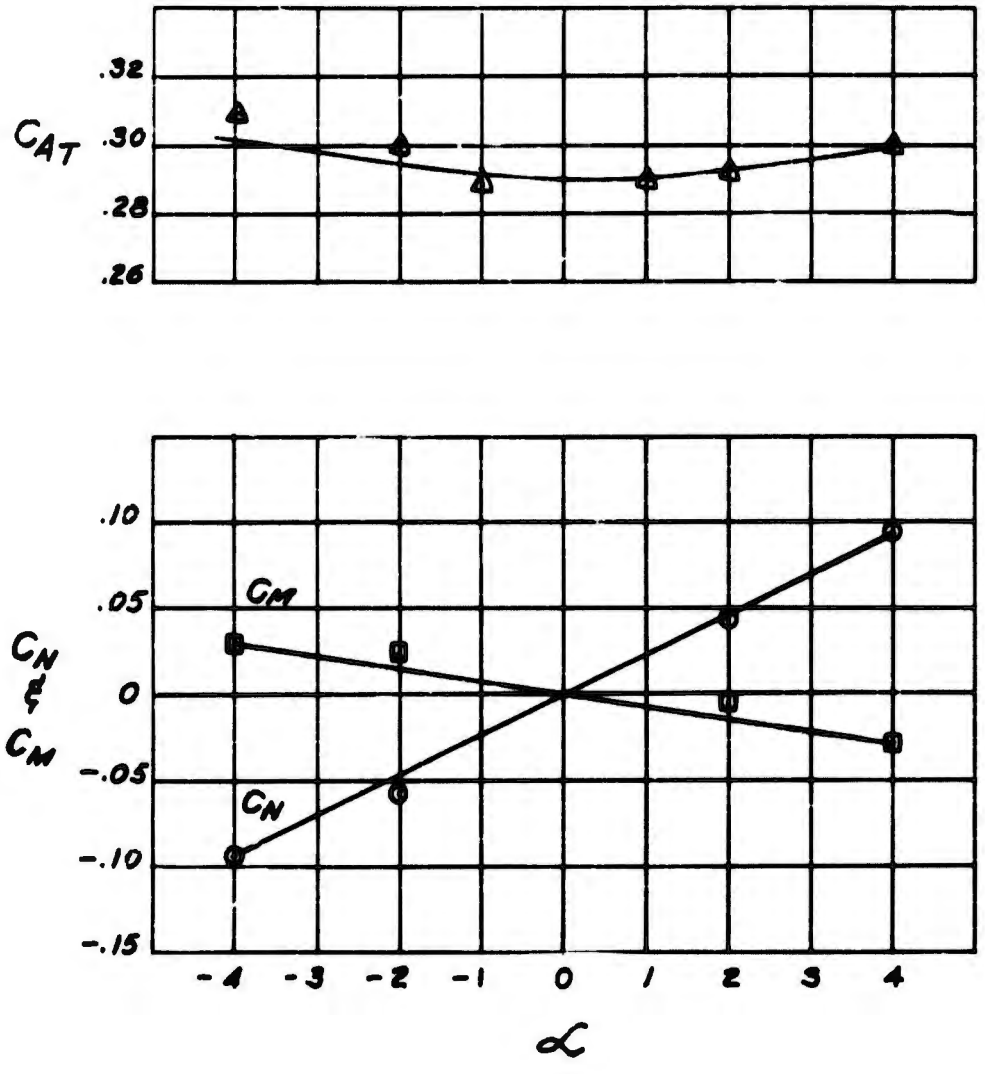

Figure 6d. Free Stream Capsule Characteristics - M = 5.0, P_o = 20, R_e = 57,000

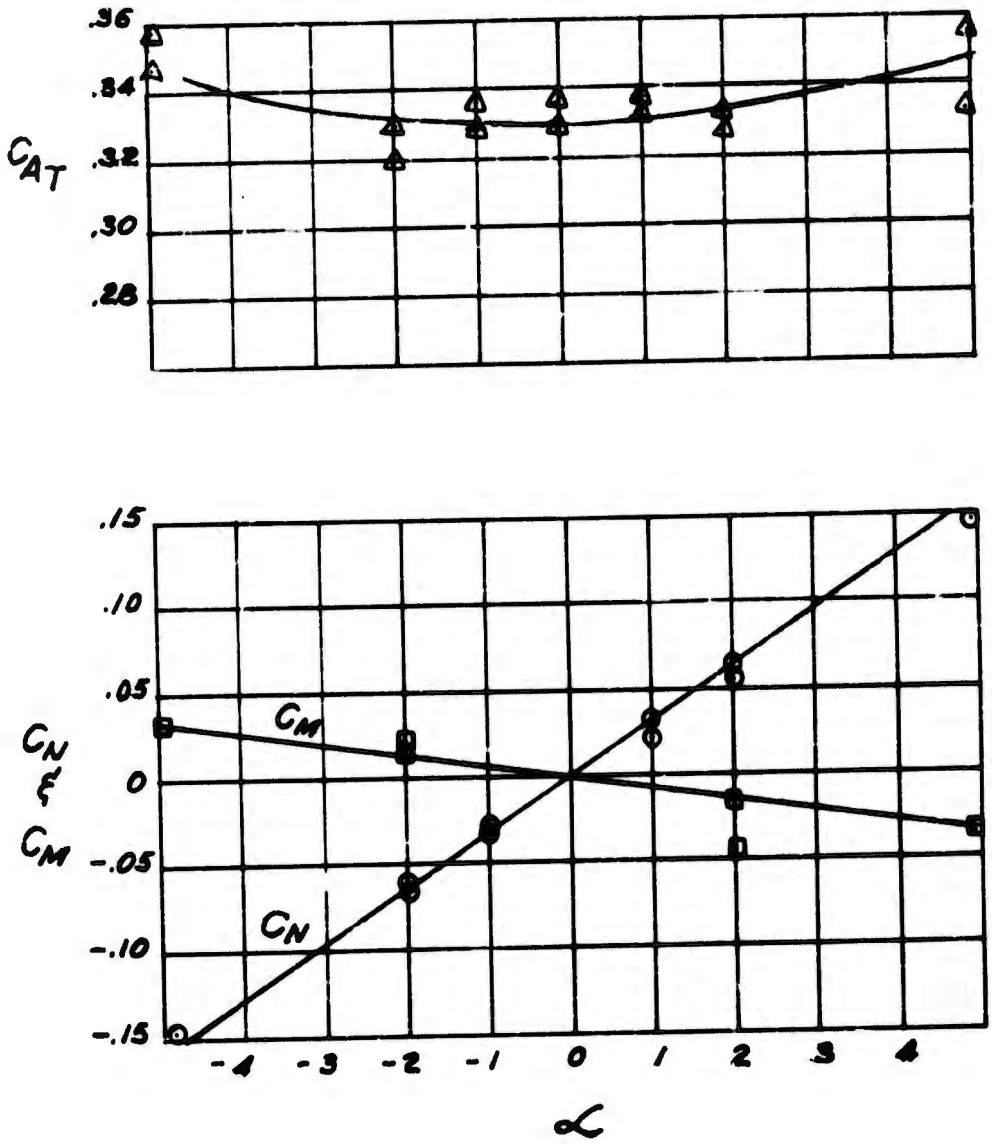

Figure 6e. Free Stream Capsule Characteristics - M = 4.0, P_o = 72, R_e = 380,000

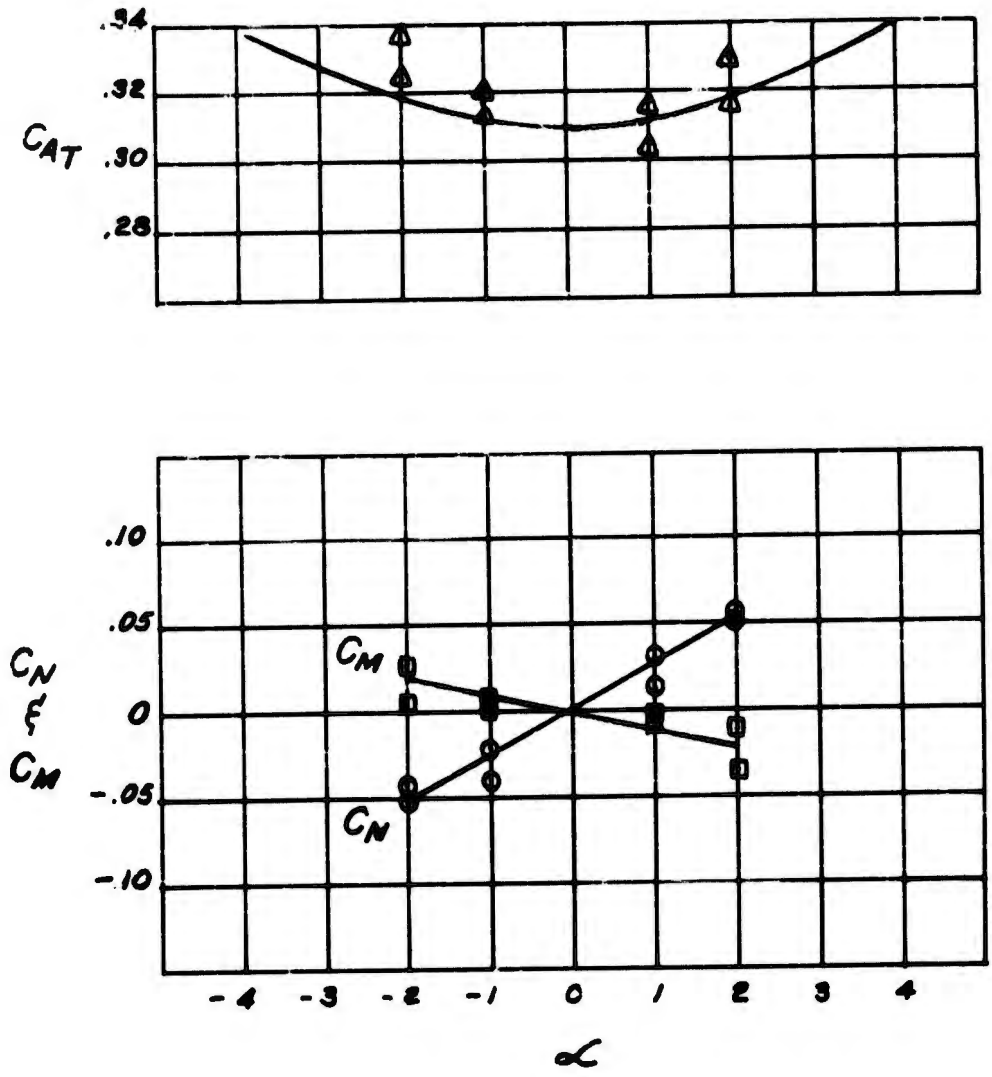

Figure 6f. Free Stream Capsule Characteristics - M = 4.0, P_o = 35, R_e = 182,000

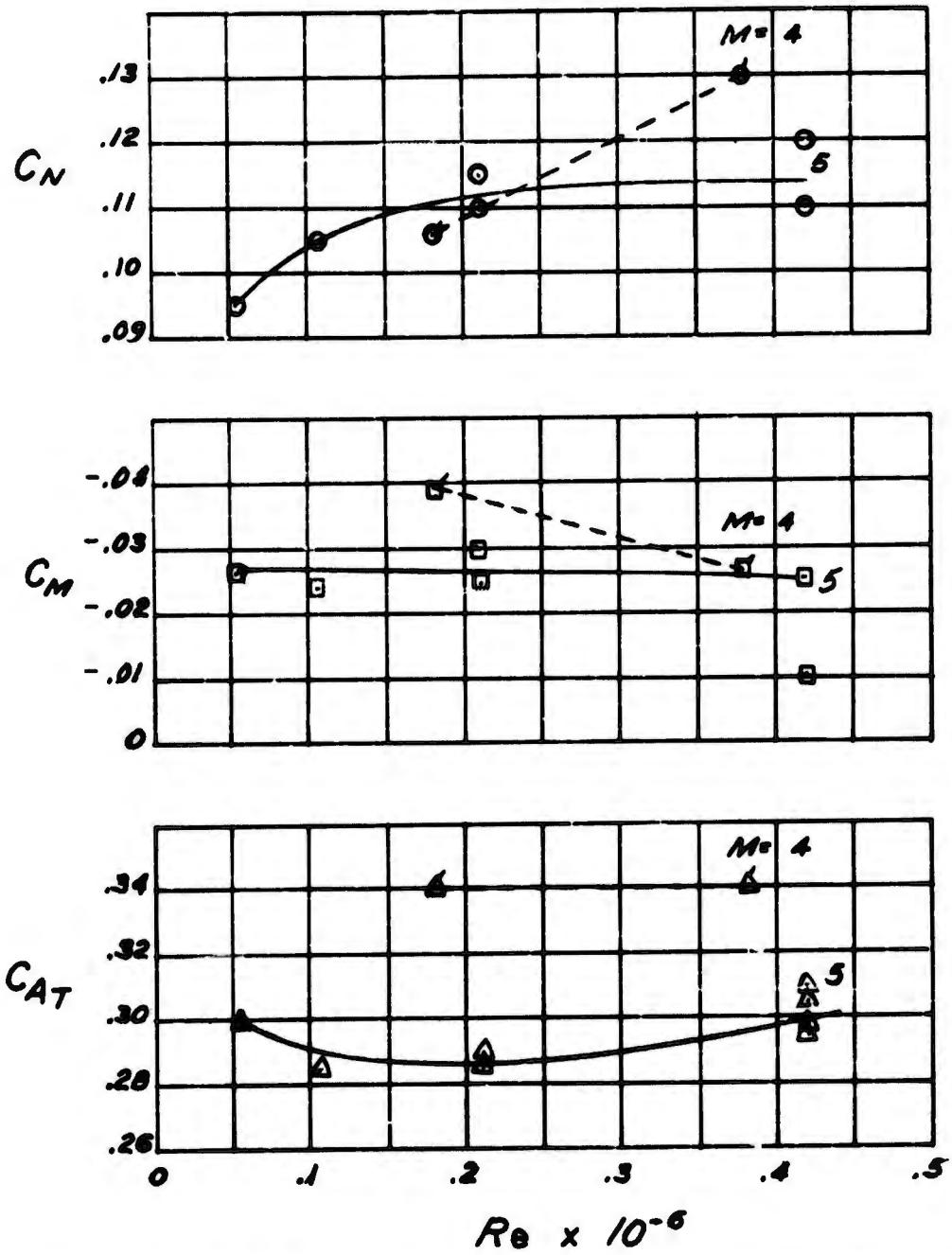

Figure 6g. Free Stream Capsule Characteristics Variation with Reynolds Number at $\alpha = 4^{\circ}$, M = 4.0 and 5.0

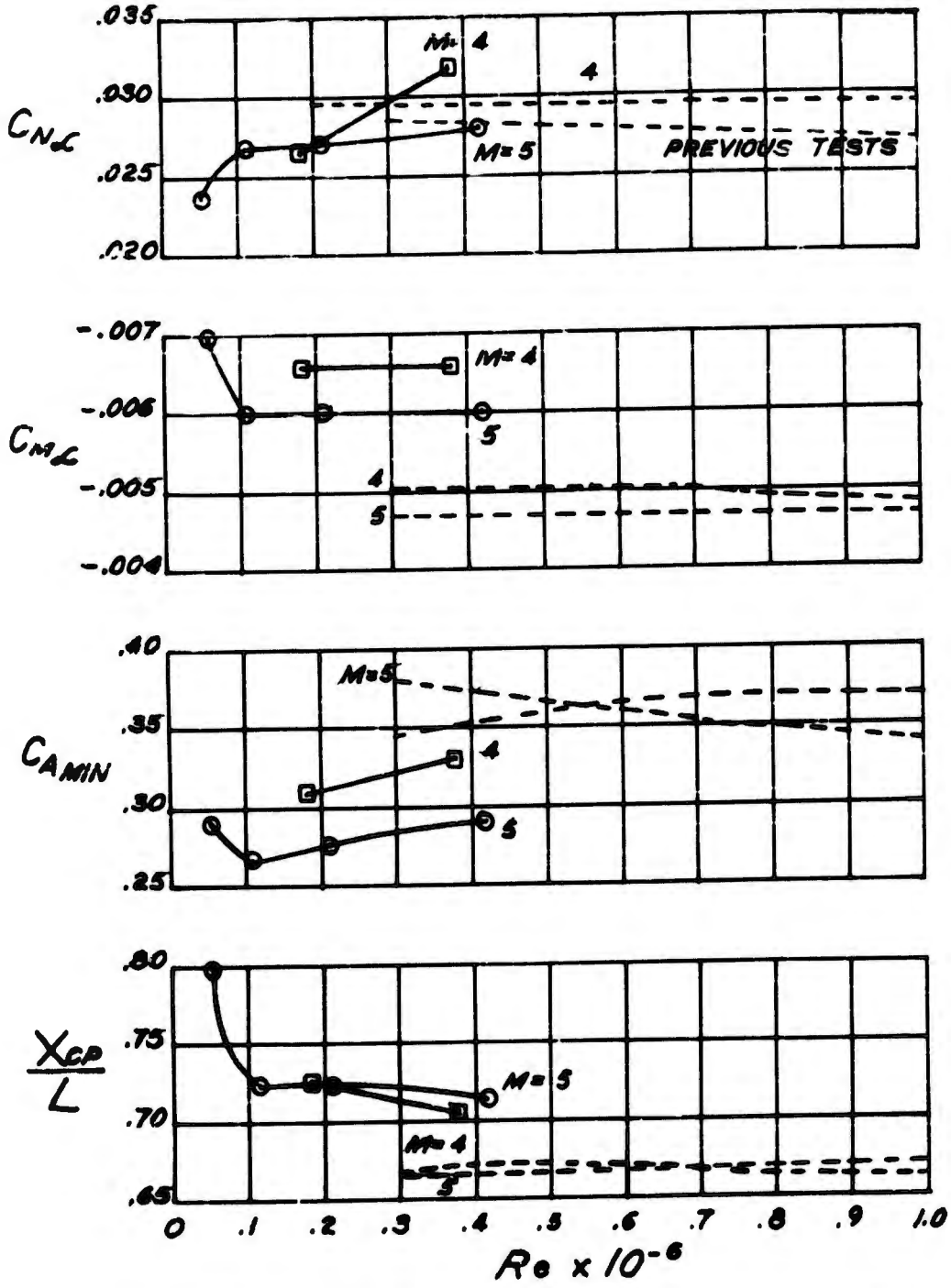

Figure 6h. Free Stream Capsule Characteristics - Force and Stability Parameter Variation with Reynolds Number, and Comparison with Previous Tests of Large Capsule Model

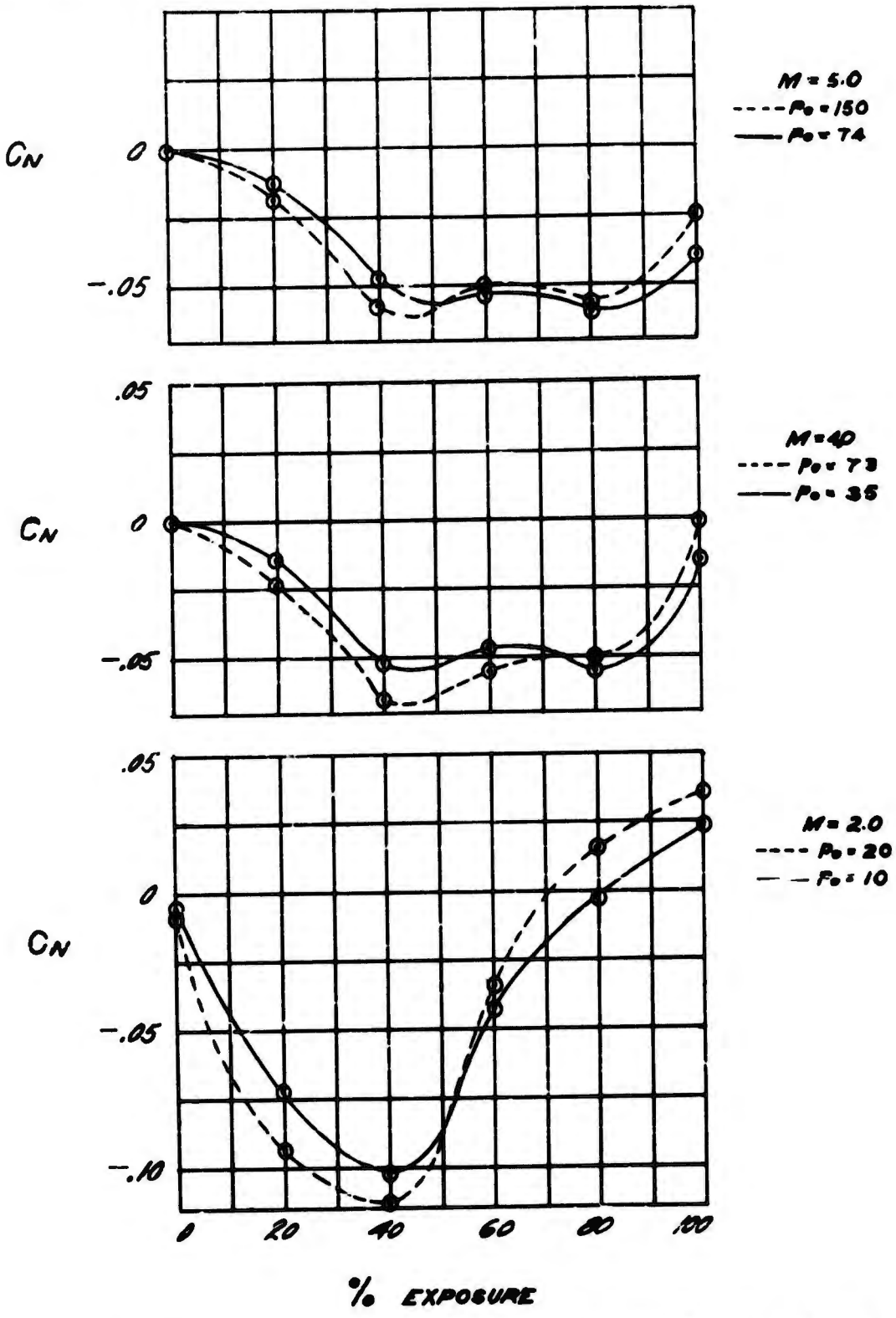

Figure 7a. Partial Exposure Phase - Variation of Normal Force Coefficient with Exposure (α = 0)

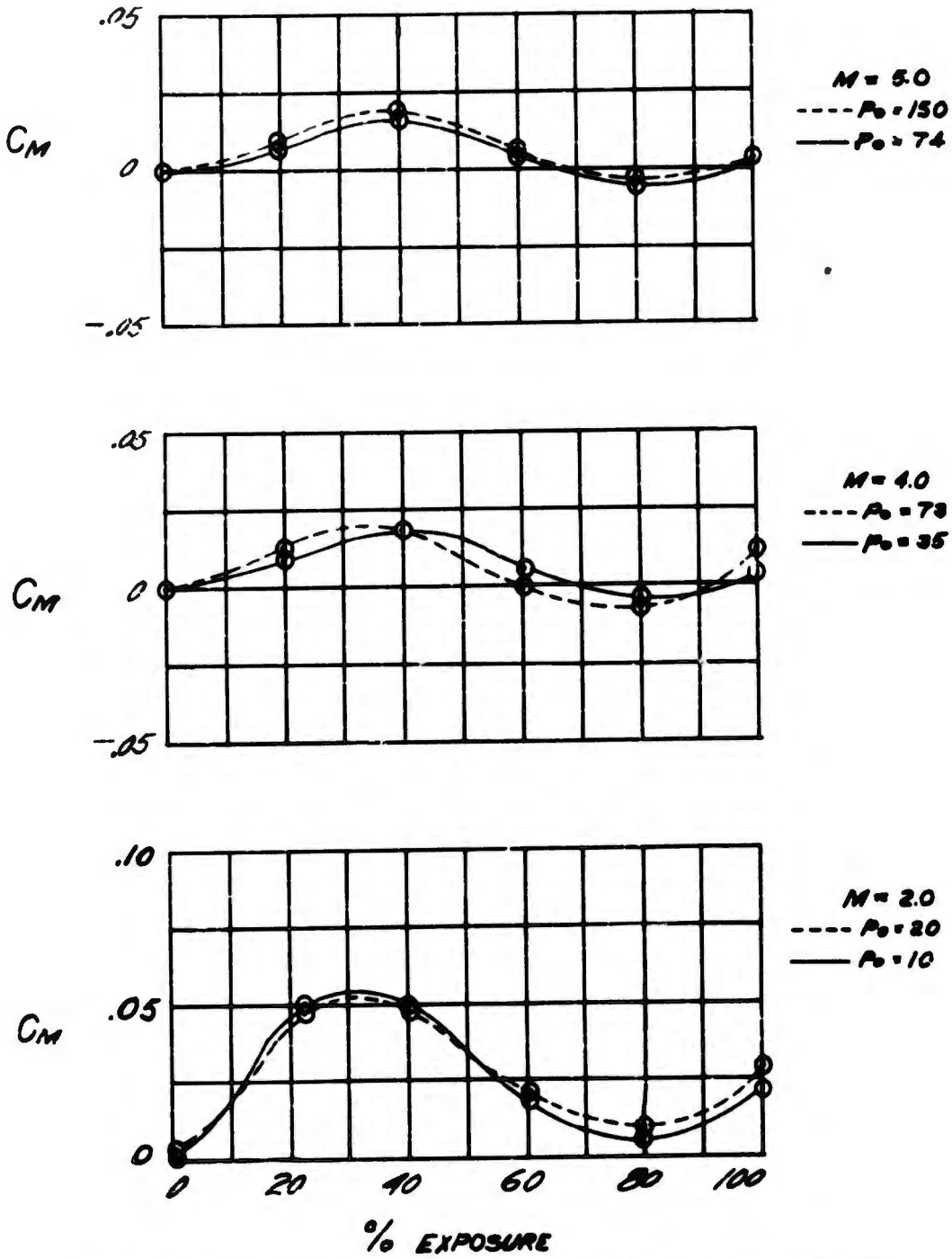

Figure 7b. Partial Exposure Phase - Variation of Pitching Moment Coefficient (α = 0)

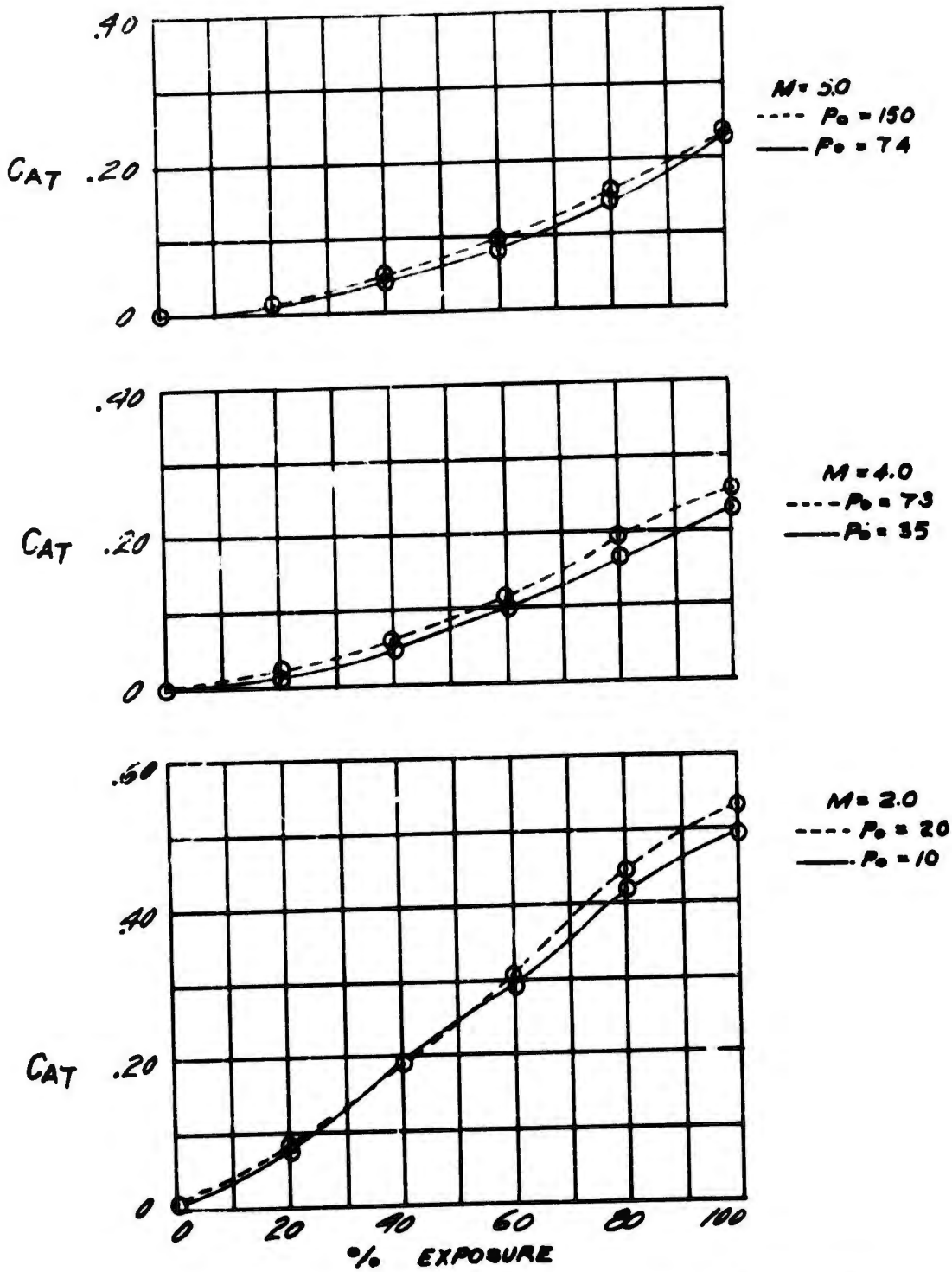

Figure 7c. Partial Exposure Phase - Variation of Total Axial Force Coefficient ($\alpha = 0$)

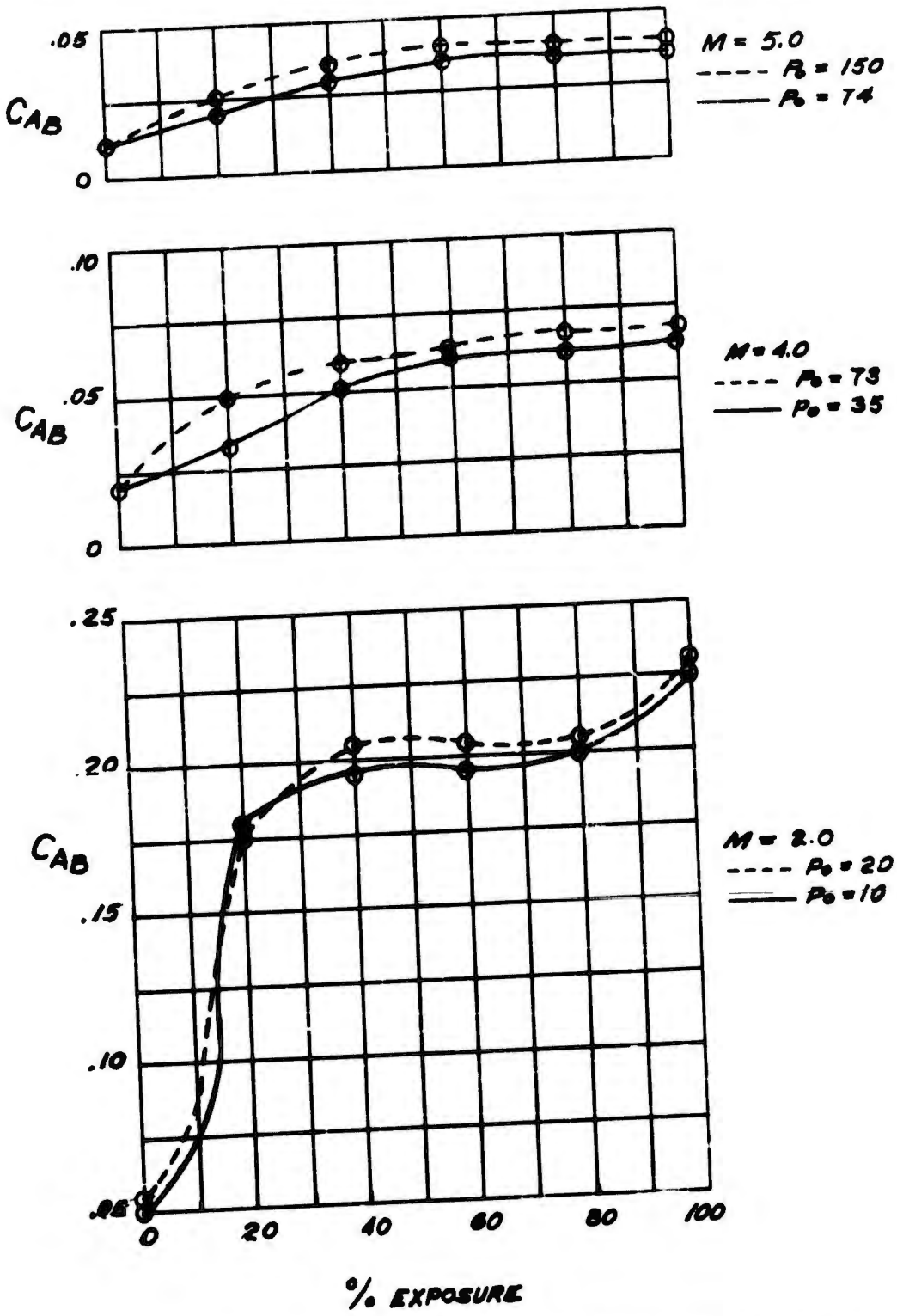

Figure 7d. Partial Exposure Phase - Variation of Base Drag Coefficient ($\alpha = 0$)

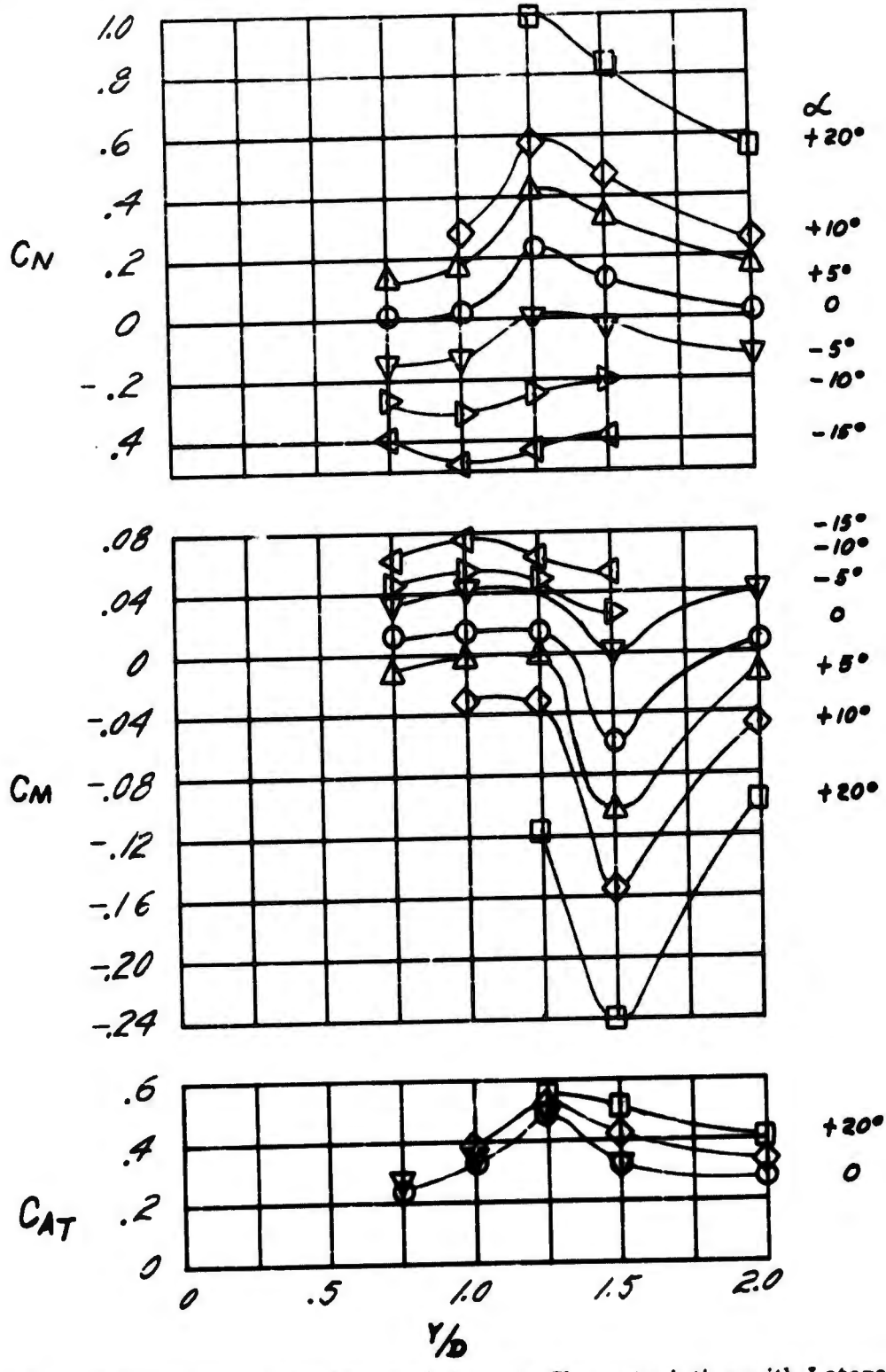

Figure 8a. Close-in Data - Variation of Capsule Characteristics with Lateral Excursion in the Carrier Flow Field - M = 5.0, P_o = 150, Axial Station X/D = 0.5

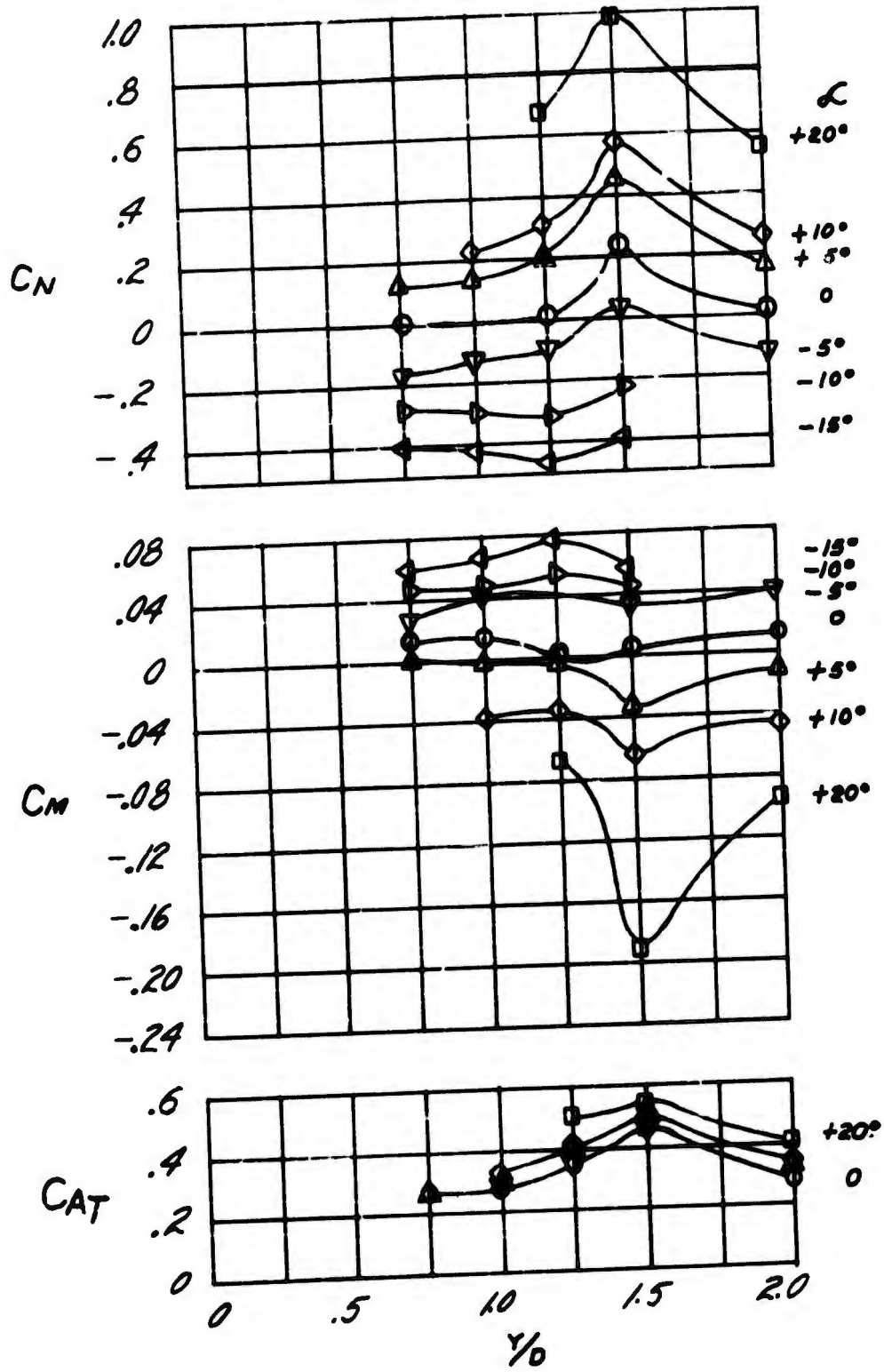

Figure 8b. Close-in Data - Variation of Capsule Characteristics with Lateral Excursion in the Carrier Flow Field - M = 5.0, P_o = 150, Axial Station X/D = 1.25

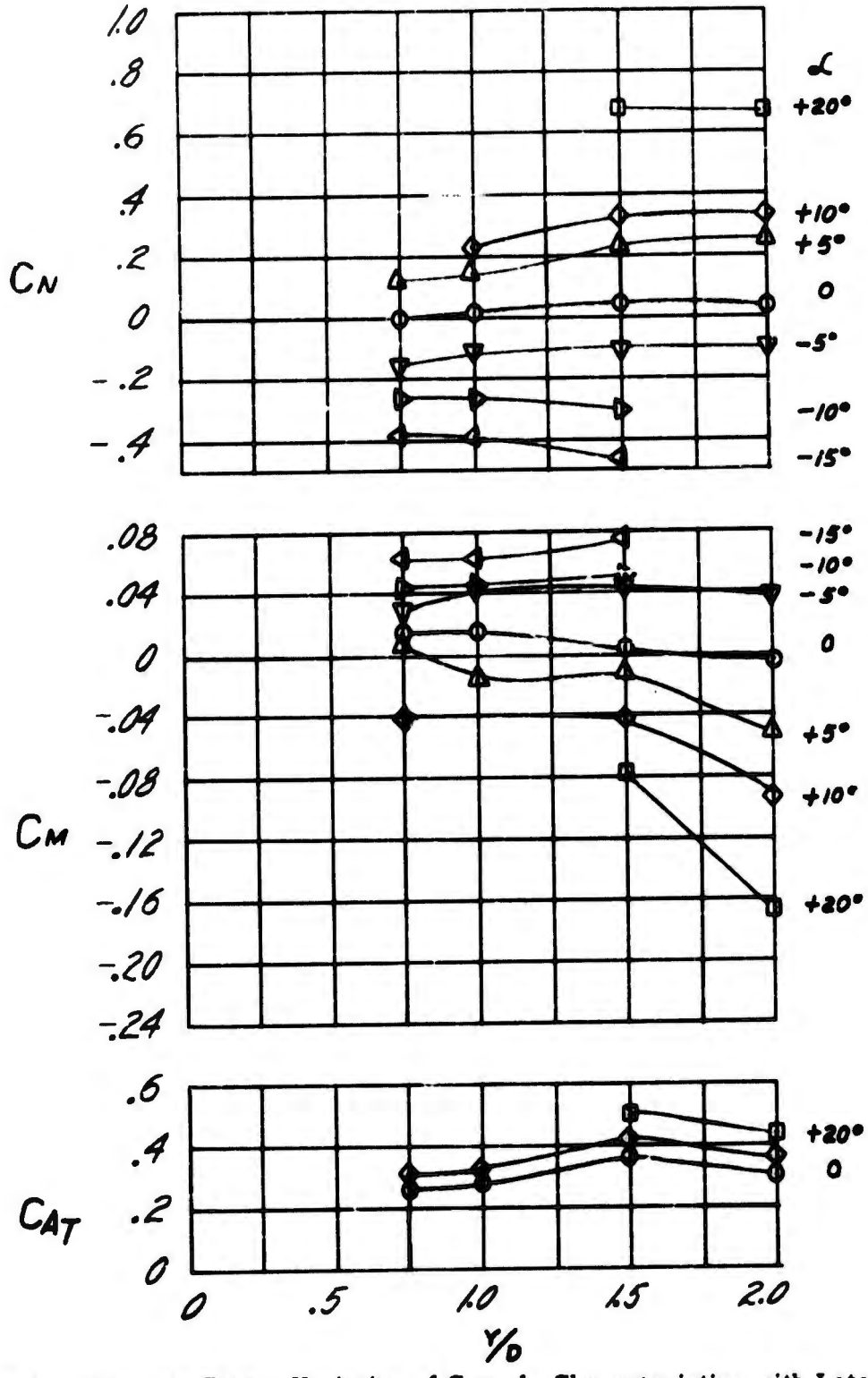

Figure 8c. Close-in Data - Variation of Capsule Characteristics with Lateral Excursion in the Carrier Flow Field - M = 5.0, P_o = 150, Axial Station X/D = 2.25

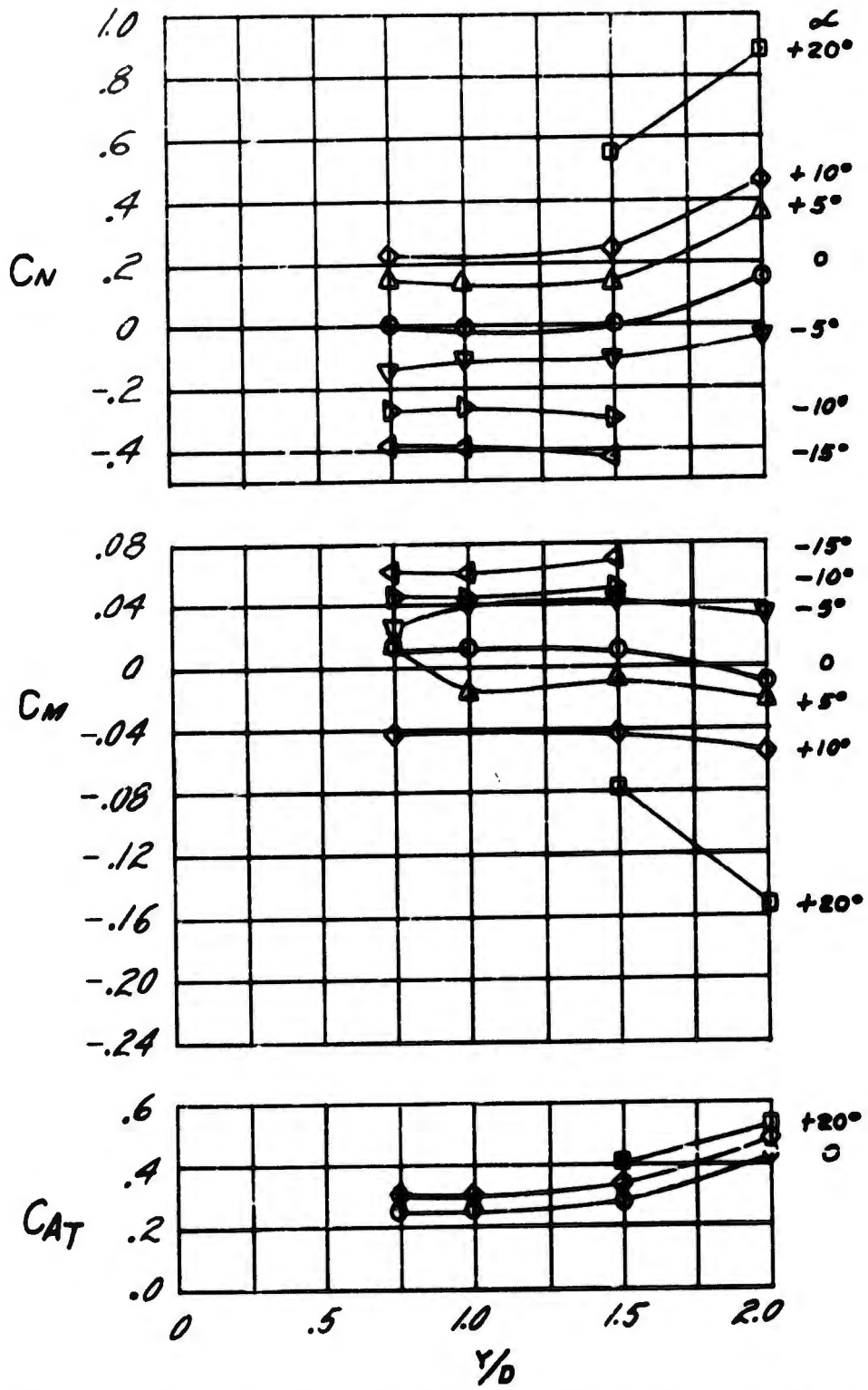

Figure 8d. Close-in Data Variation of Capsule Characteristics with Lateral Excursion in the Carrier Flow Field - M = 5.0, P_o = 150, Axial Station X/D = 3.5

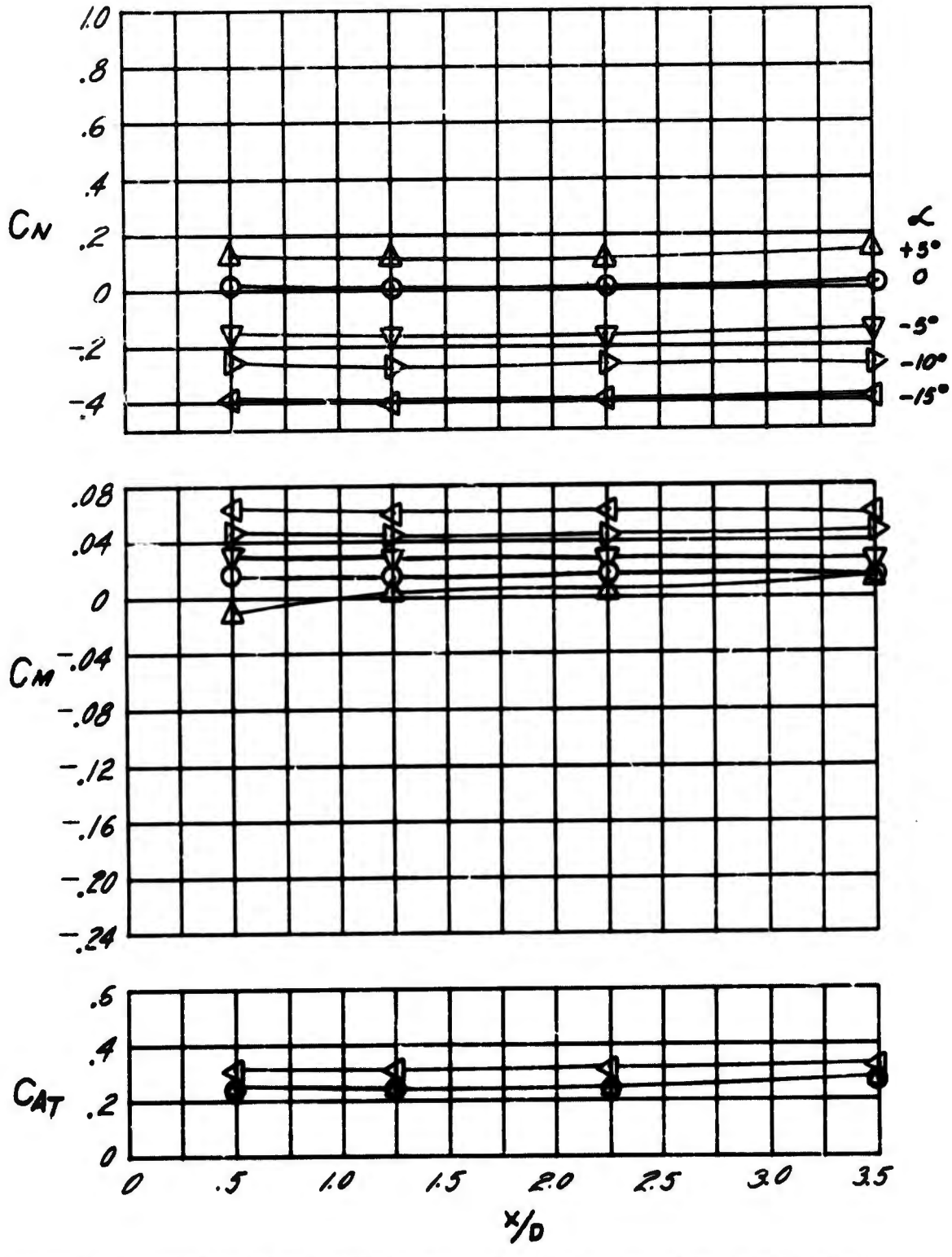

Figure 8e. Close-in Data - Variation of Capsule Characteristics with Axial Excursion in the Carrier Flow Field - M = 5.0, P_o = 150, Lateral Station Y/D = 0.75

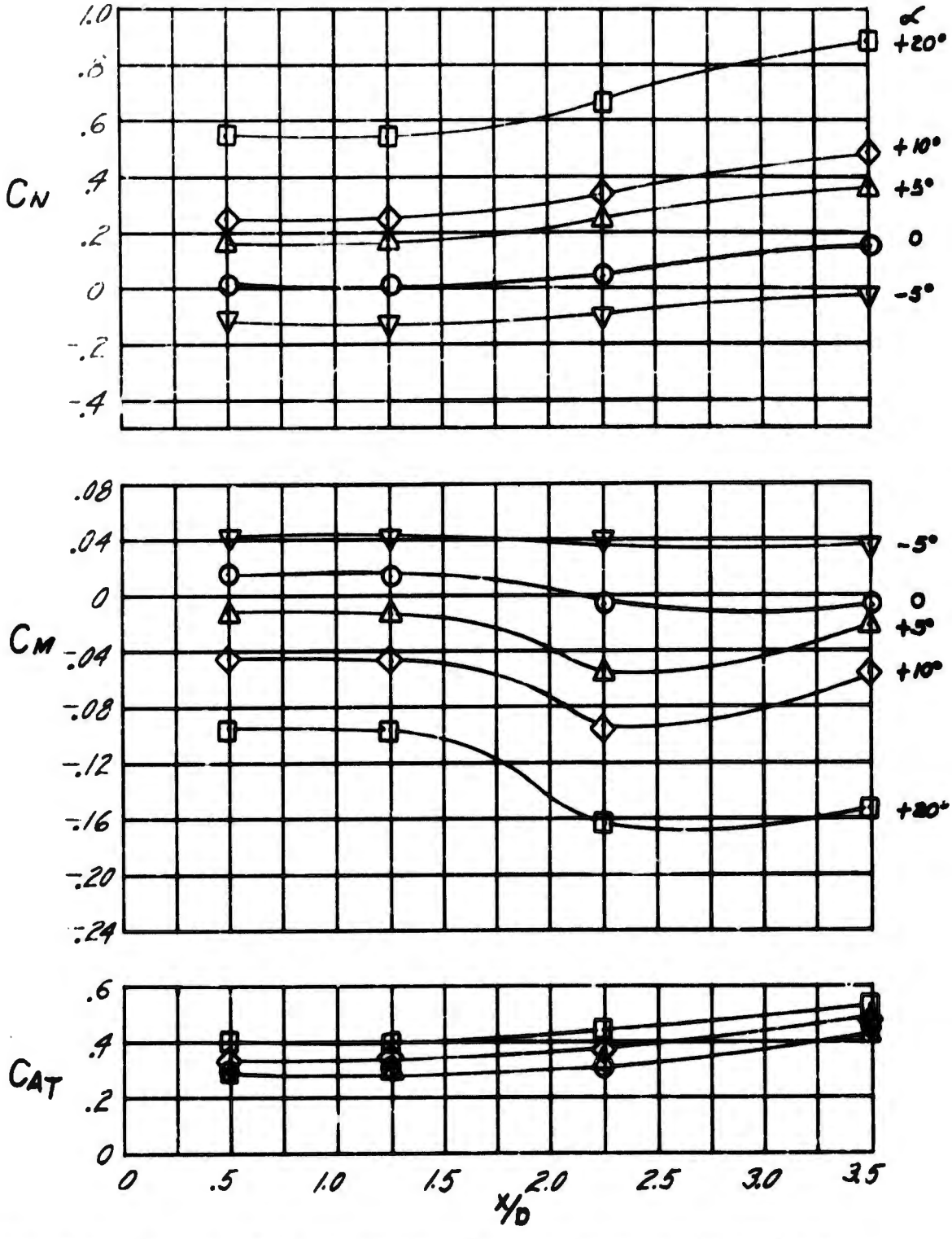

Figure 8f. Close-in Data - Variation of Capsule Characteristics with Axial Excursion in the Carrier Flow Field - M = 5.0, P_o = 150, Lateral Station Y/D = 2.0

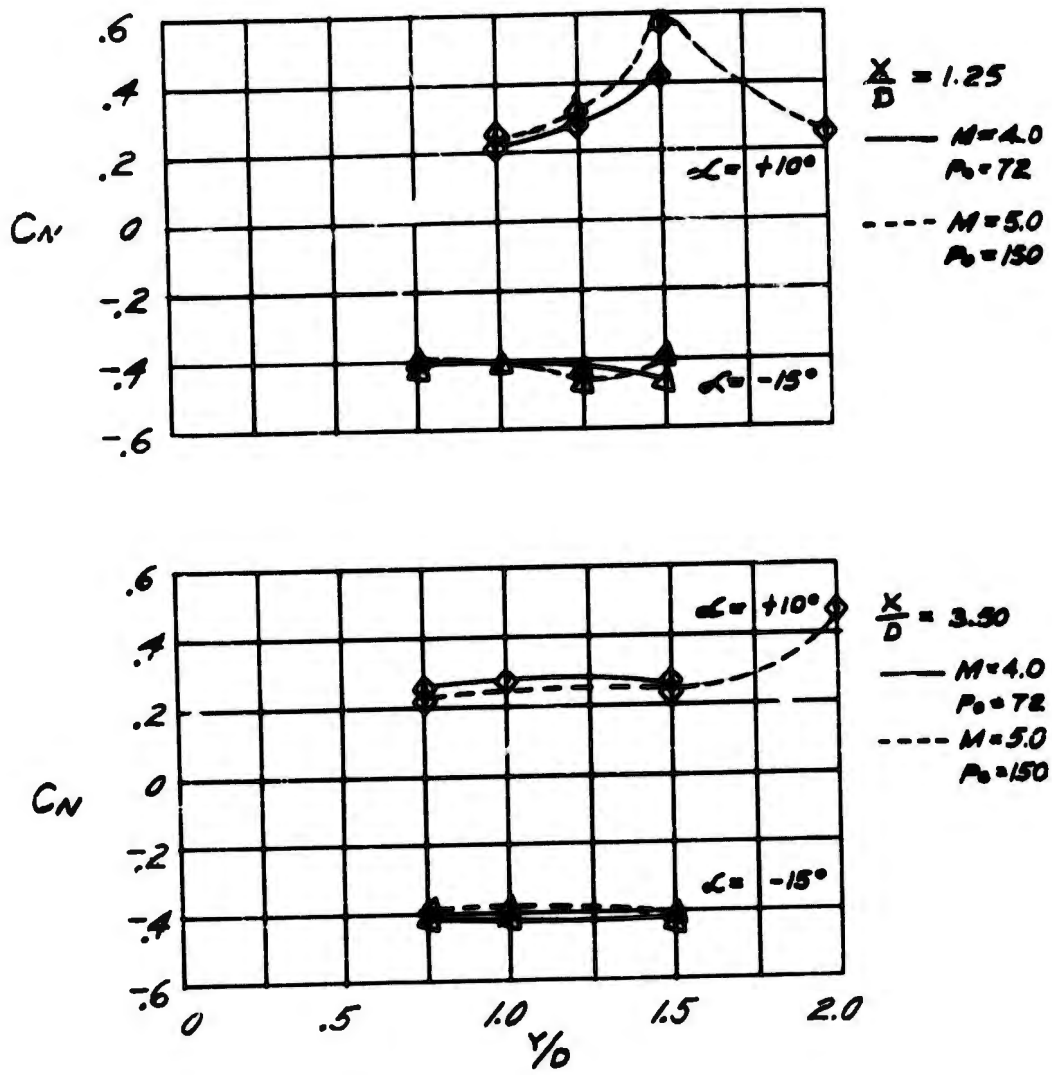

Figure 8g. Close-in Data - Effect of Mach Number on Normal Force Coefficient

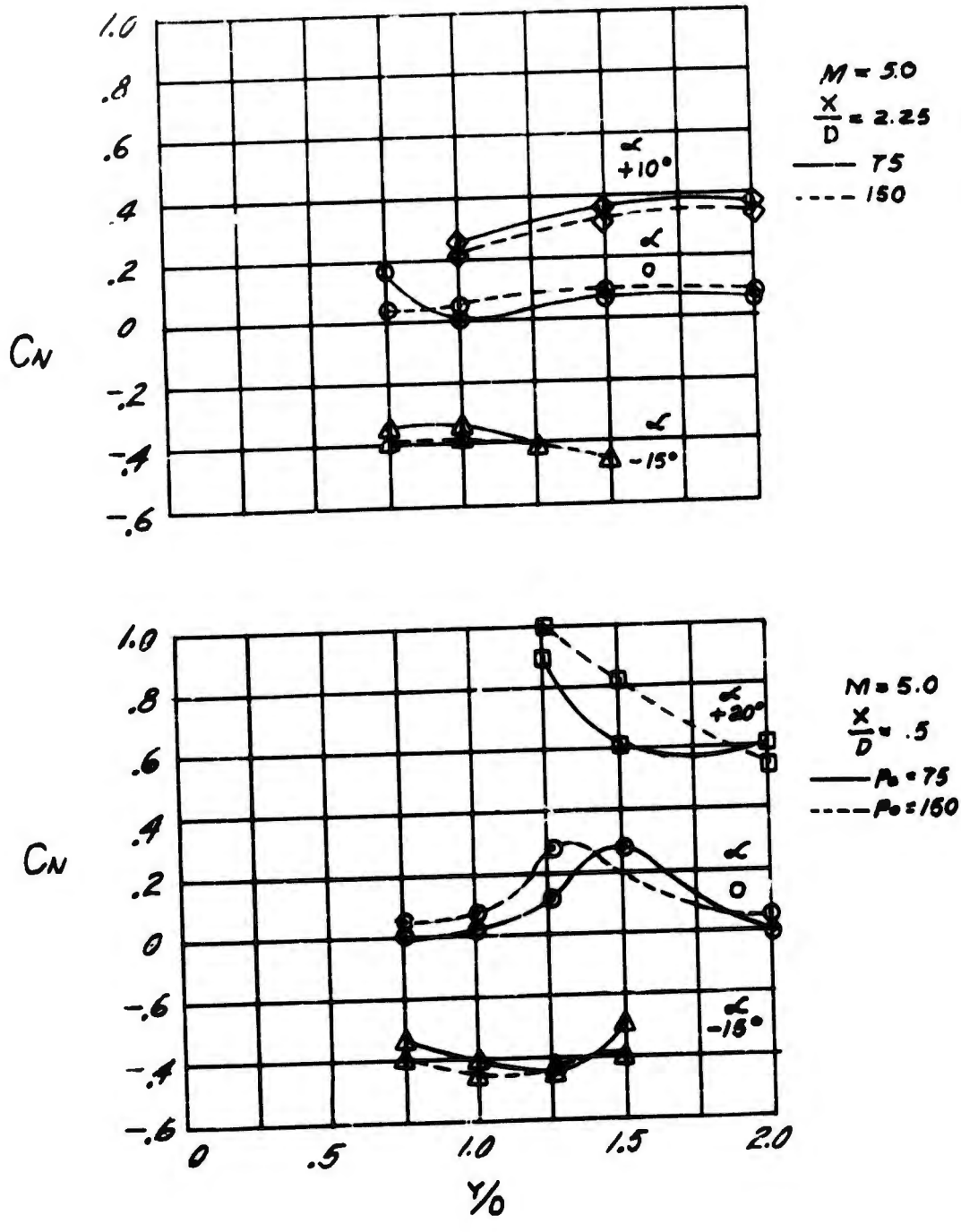

Figure 8h. Close-in Data - Effect of Stagnation Pressure on Normal Force Coefficient at M = 5.0

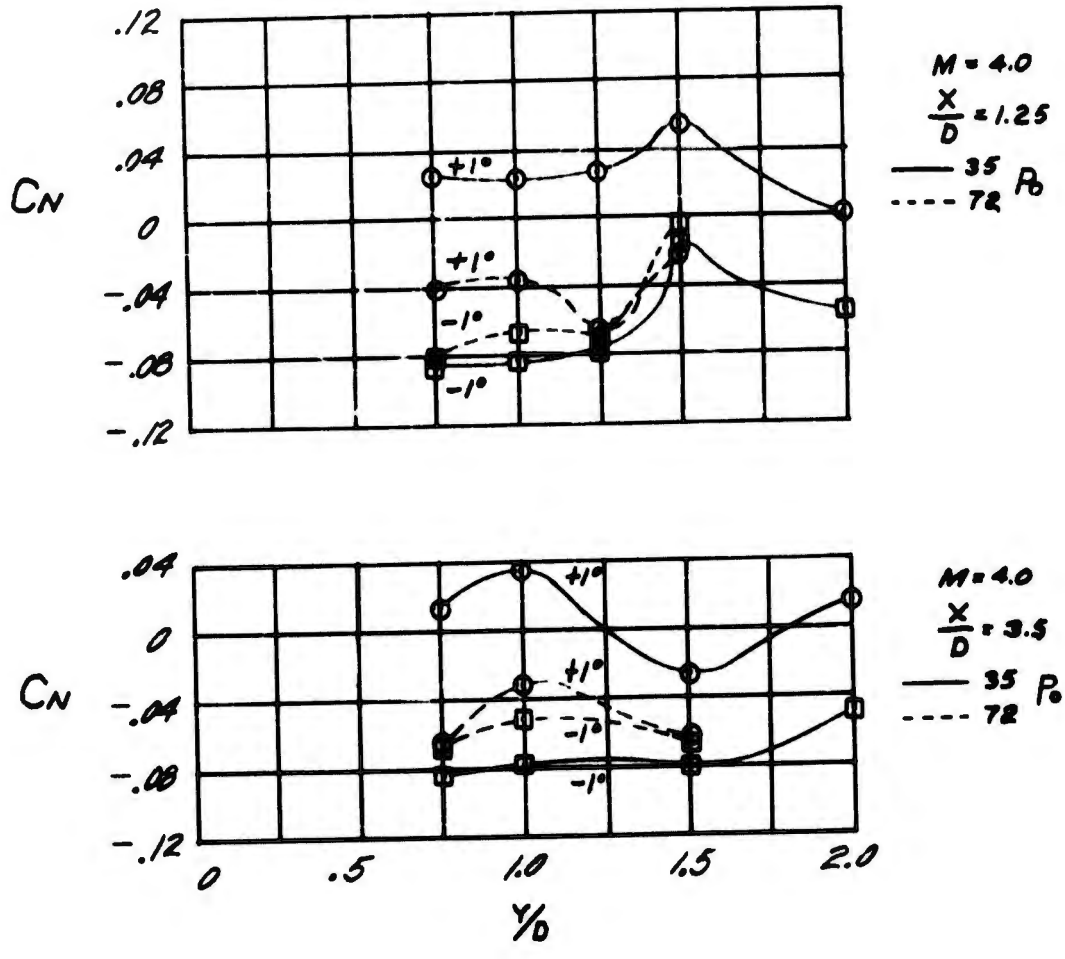

Figure 8i. Close-in Data - Effect of Stagnation Pressure on Normal Force Coefficient at M = 4.0

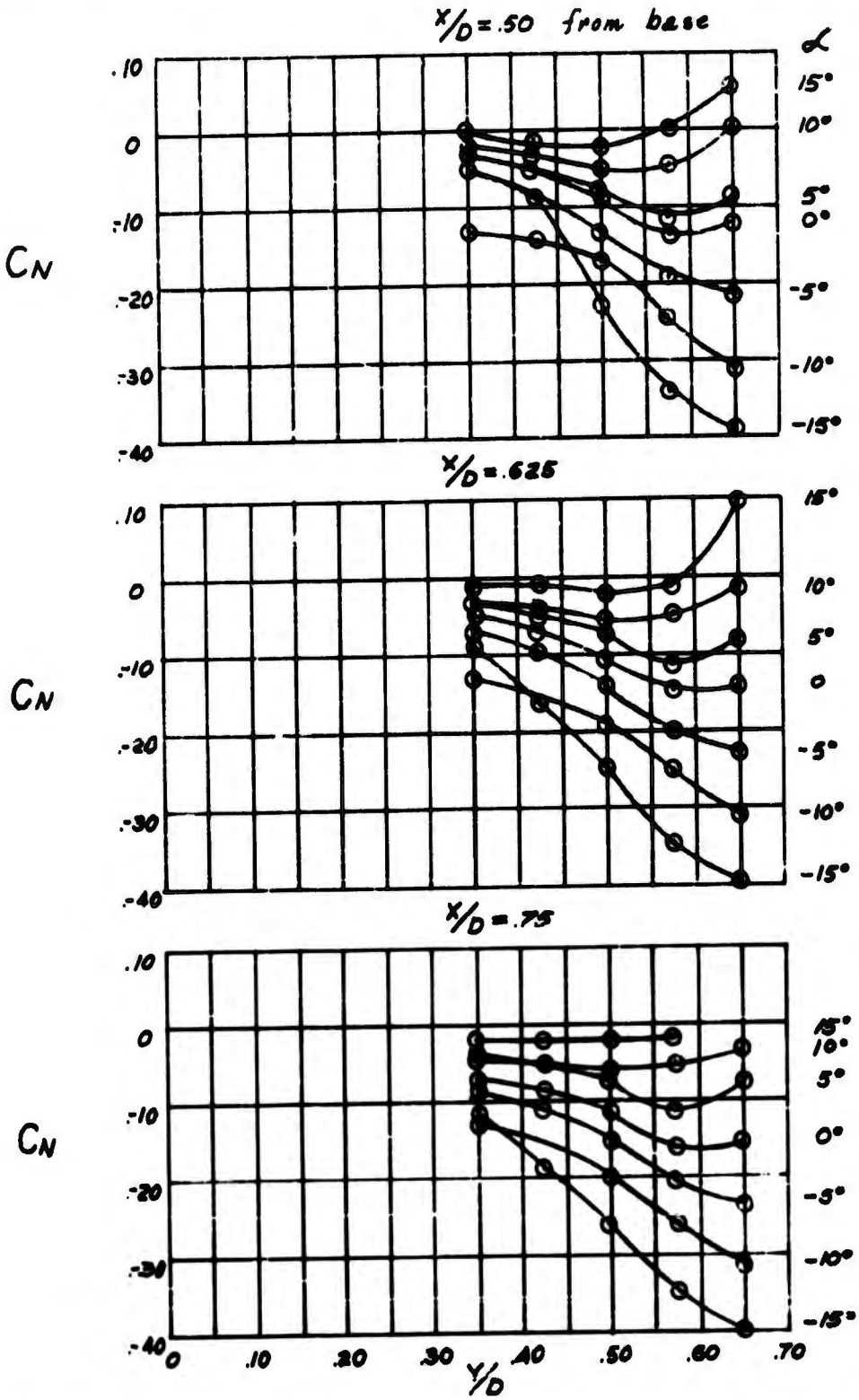

Figure 9a. Wake Penetration Data - Variation of Capsule Normal Force Coefficient with Lateral Traverse across Wake Boundary
M = 5.0, P_o = 150 psia

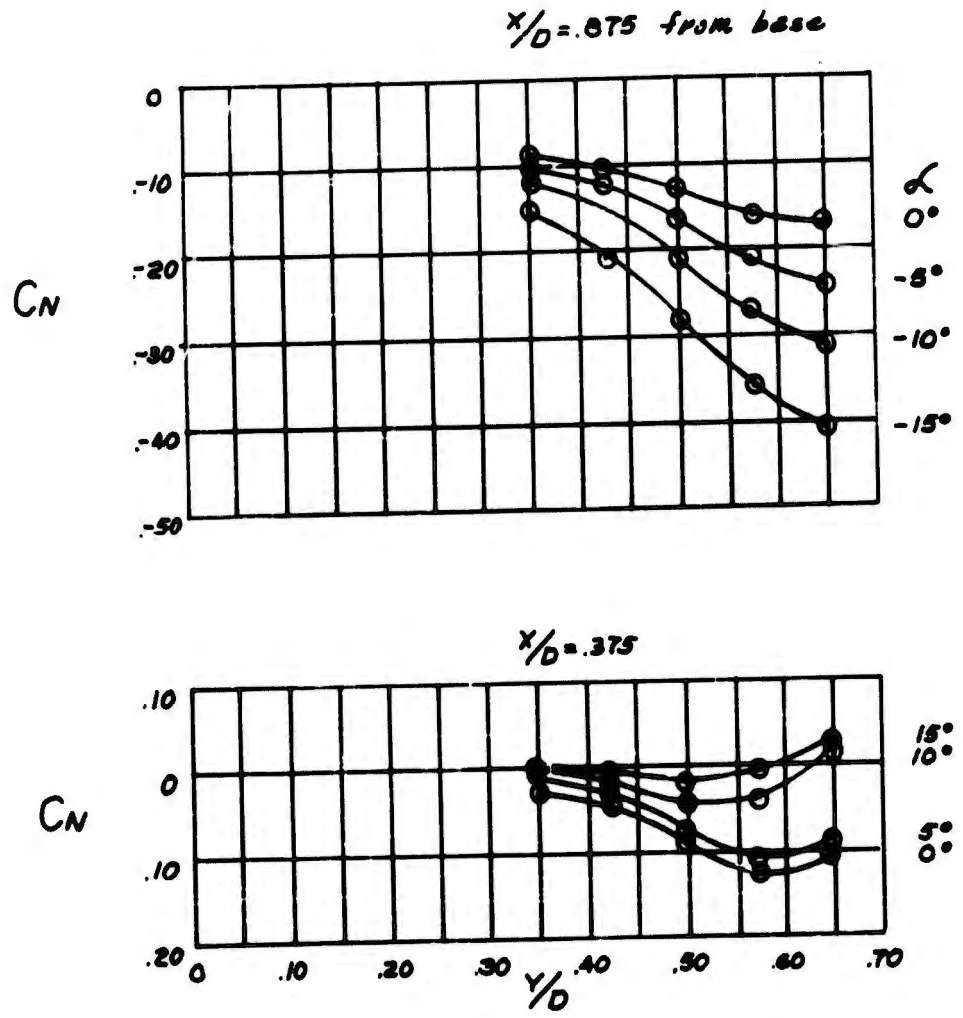

Figure 9b. Wake Penetration Data - Variation of Capsule Normal Force Coefficient with Lateral Traverse across Wake Boundary
$M = 5.0$, $P_o = 150$ psia

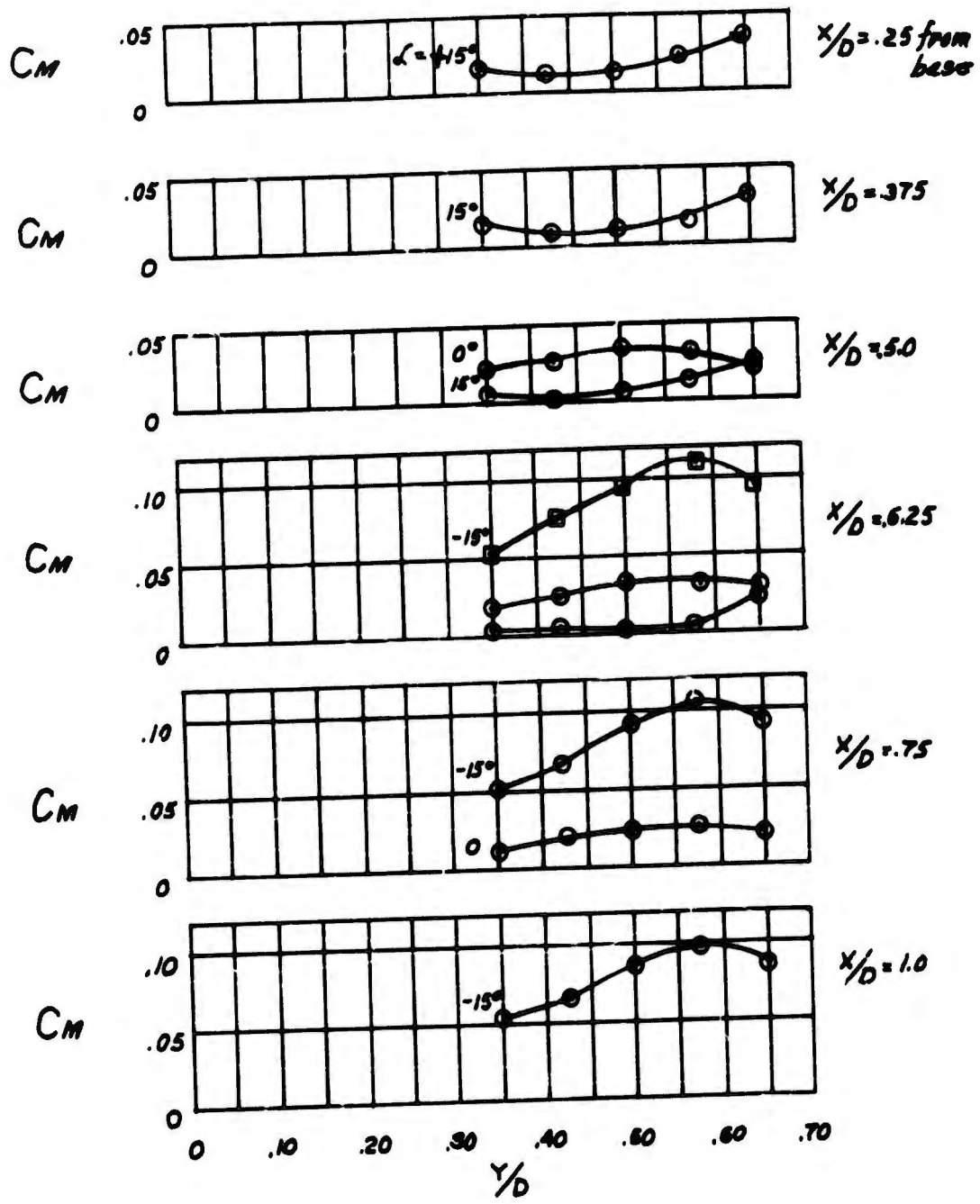

Figure 9c. Wake Penetration Data - Variations of Capsule Pitching Moment Coefficient with Lateral Traverse across Wake Boundary
$M = 5.0$, $P_o = 150$ psia

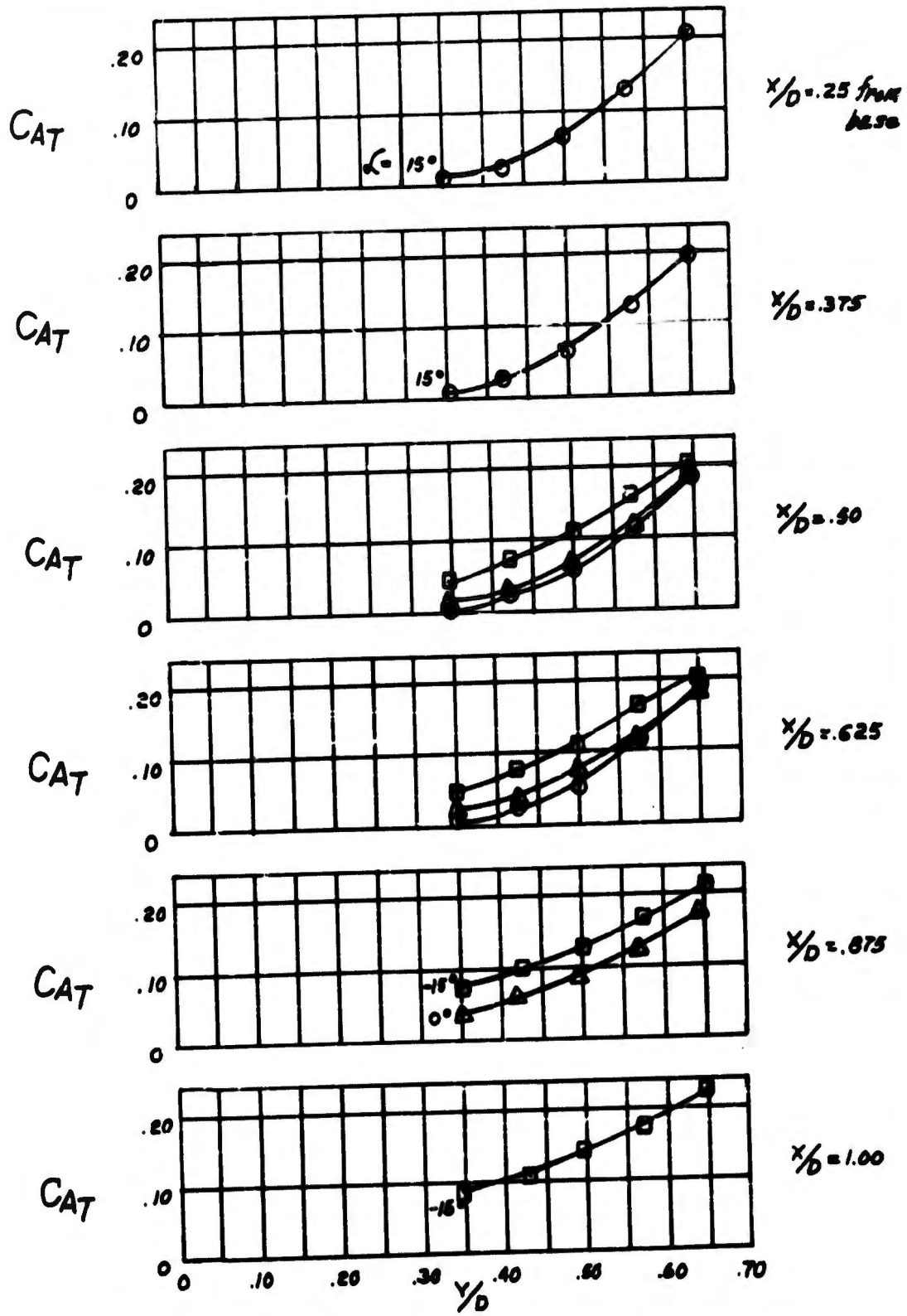

Figure 9d. Wake Penetration Data - Variation of Capsule Axial Force Coefficient with Lateral Traverse across Wake Boundary
M = 5.0, P_o = 150 psia

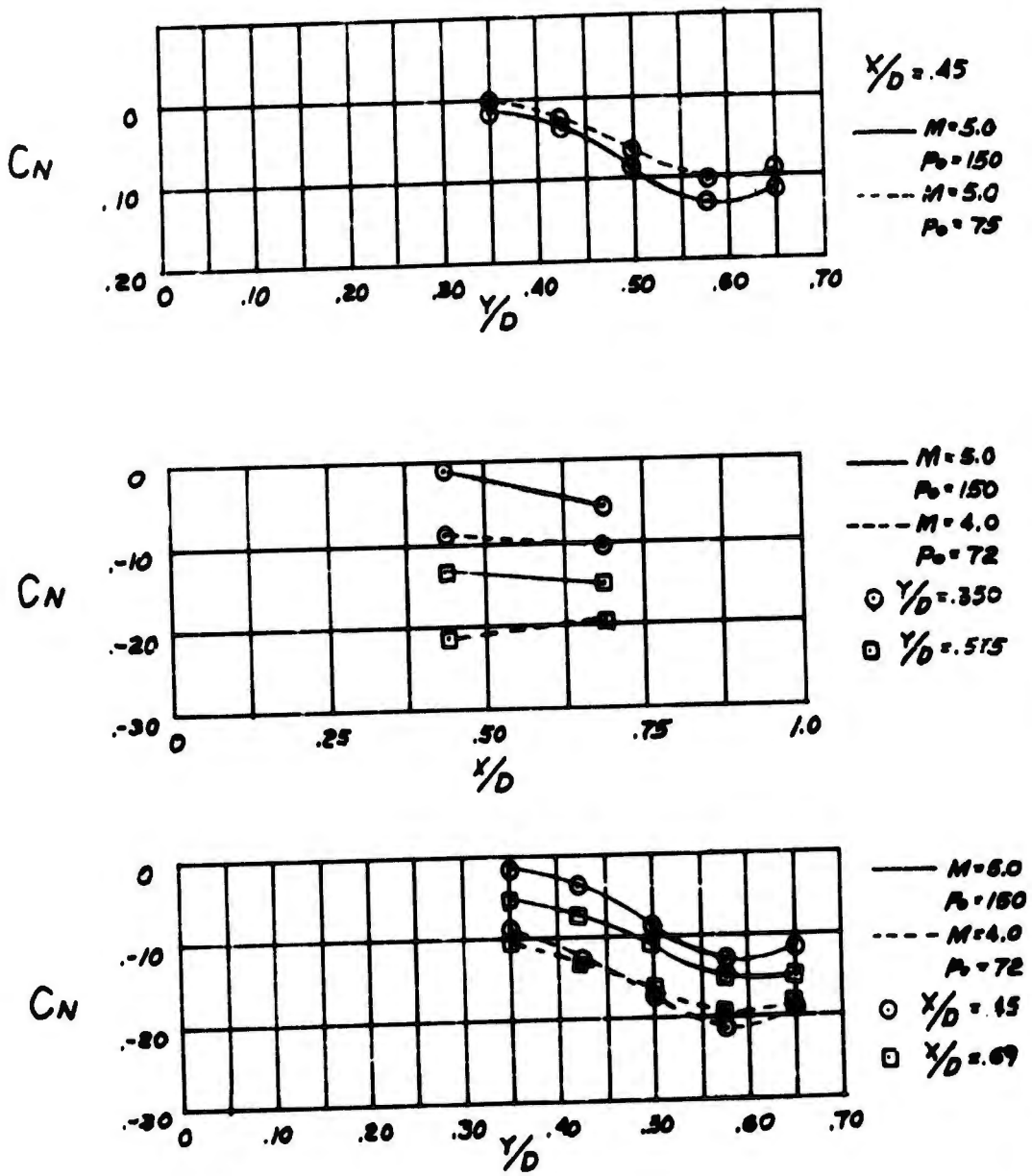

Figure 9e. Wake Penetration Data - Effect of Reynolds and Mach Number on Capsule Normal Force Coefficient

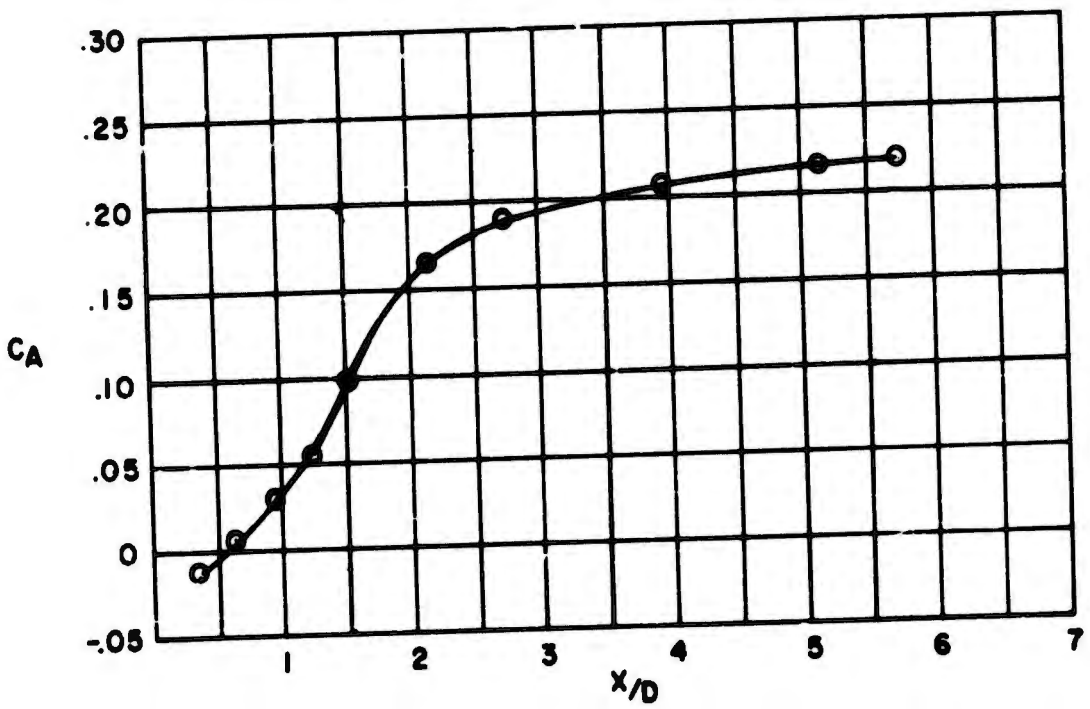

Figure 10. Wake-Capsule Interaction - Variation of Axial Force Coefficient with Wake Centerline Travel Downstream from the Base of the Carrier Vehicle - M = 4.0, P_o = 72

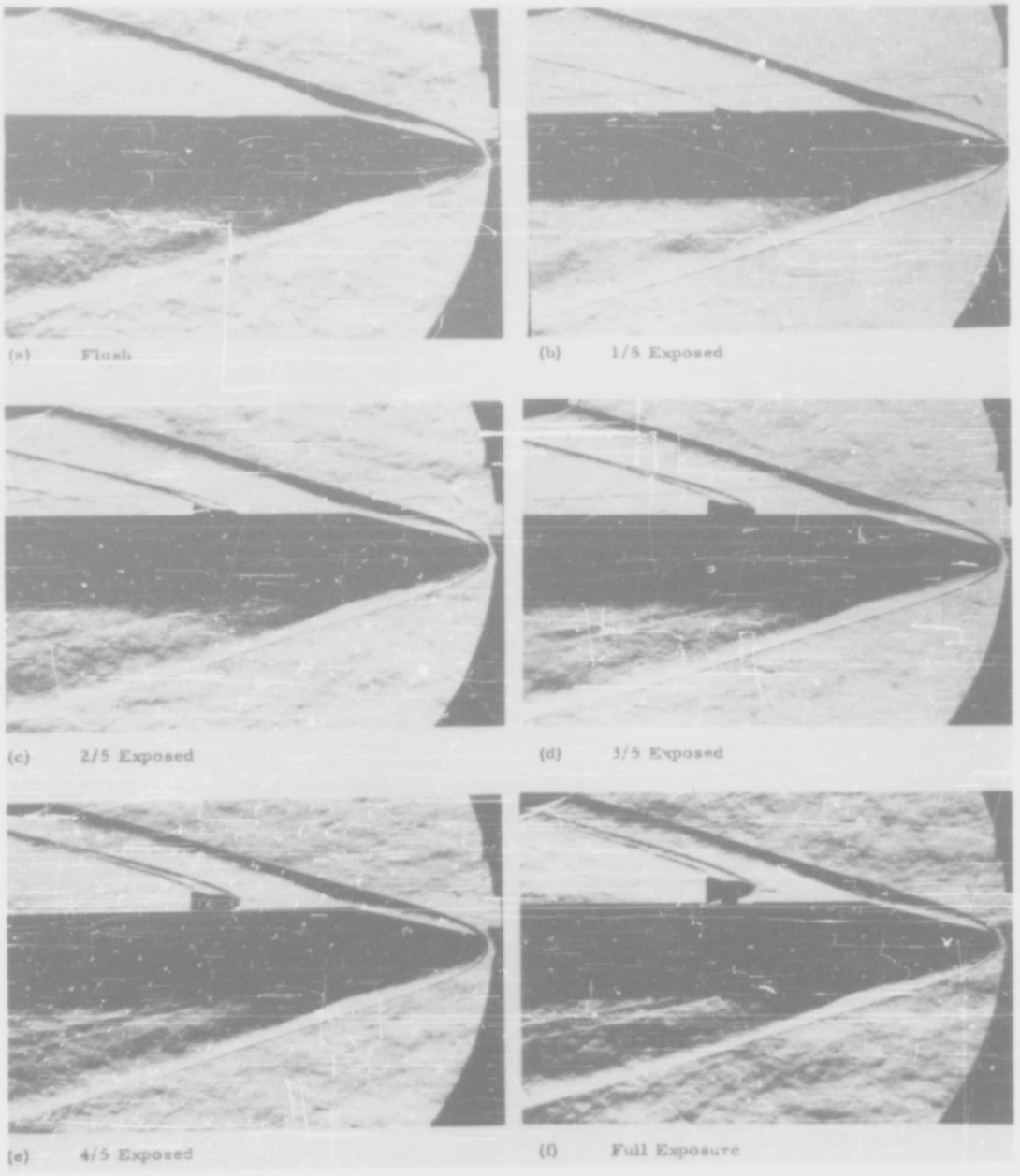

Figure 11. Partial Exposure Phase - Schlieren Sequence Showing Emergence of Capsule - M = 5.0, $\bar{P}_o$ = 150 psia

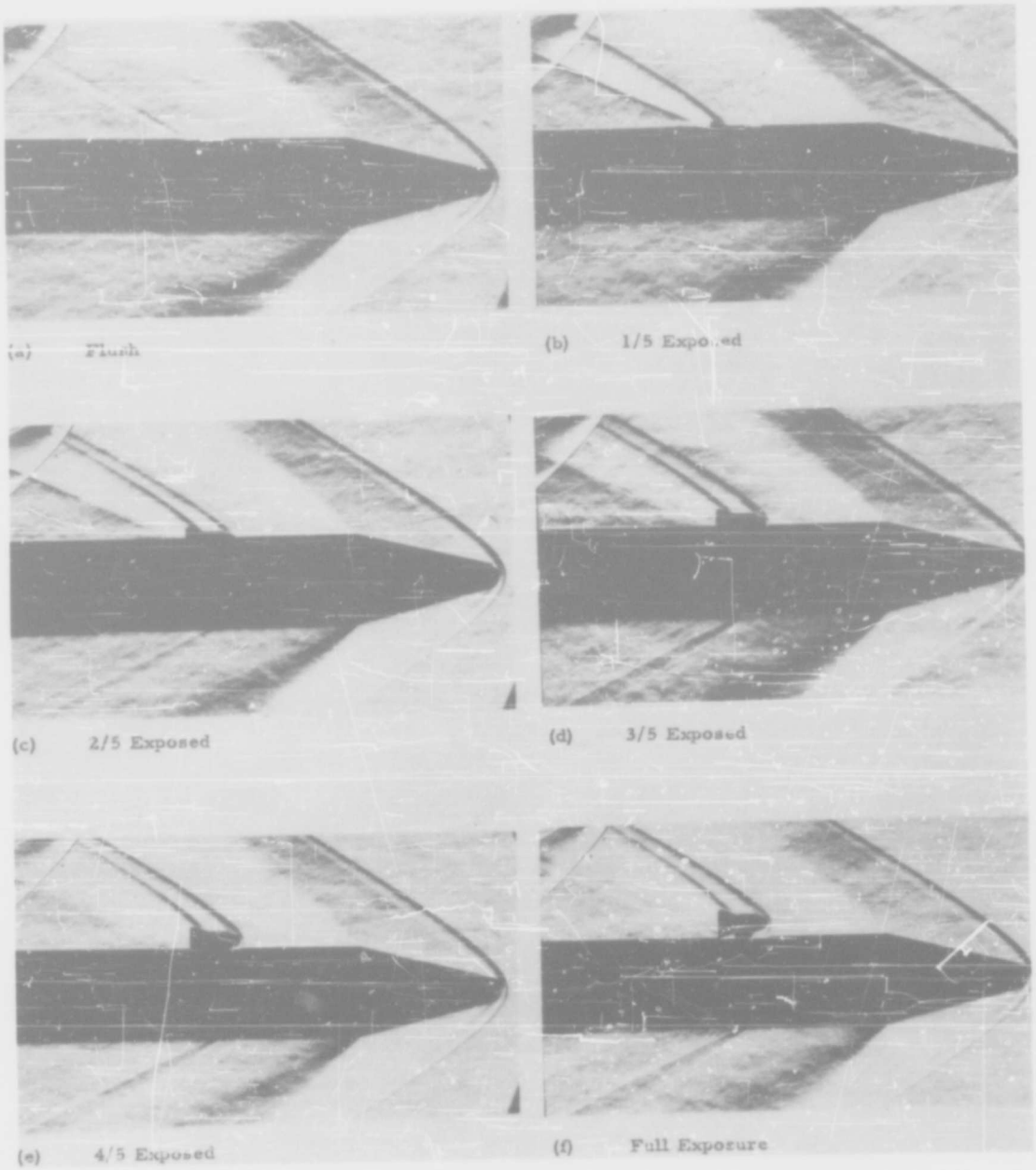

Figure 12. Partial Exposure Phase - Schlieren Sequence Showing Emergence of Capsule - M = 2.0, P_o = 10 psia

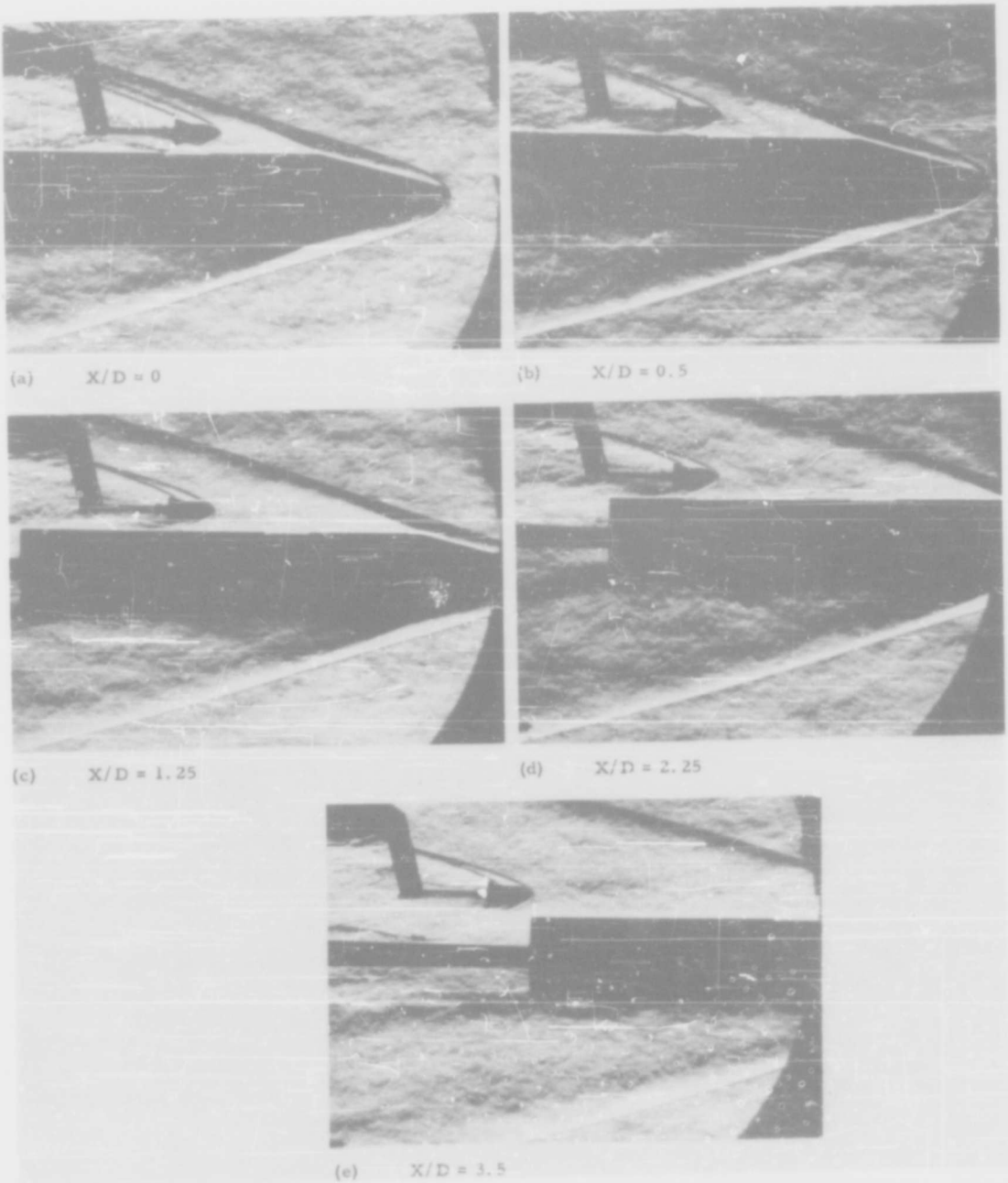

Figure 13. Close-in Phase - Schlieren Sequence Showing Axial Travel of Capsule at Lateral Separation Y/D = 0.5 - M = 5.0, P_c = 75 psia, α = 0

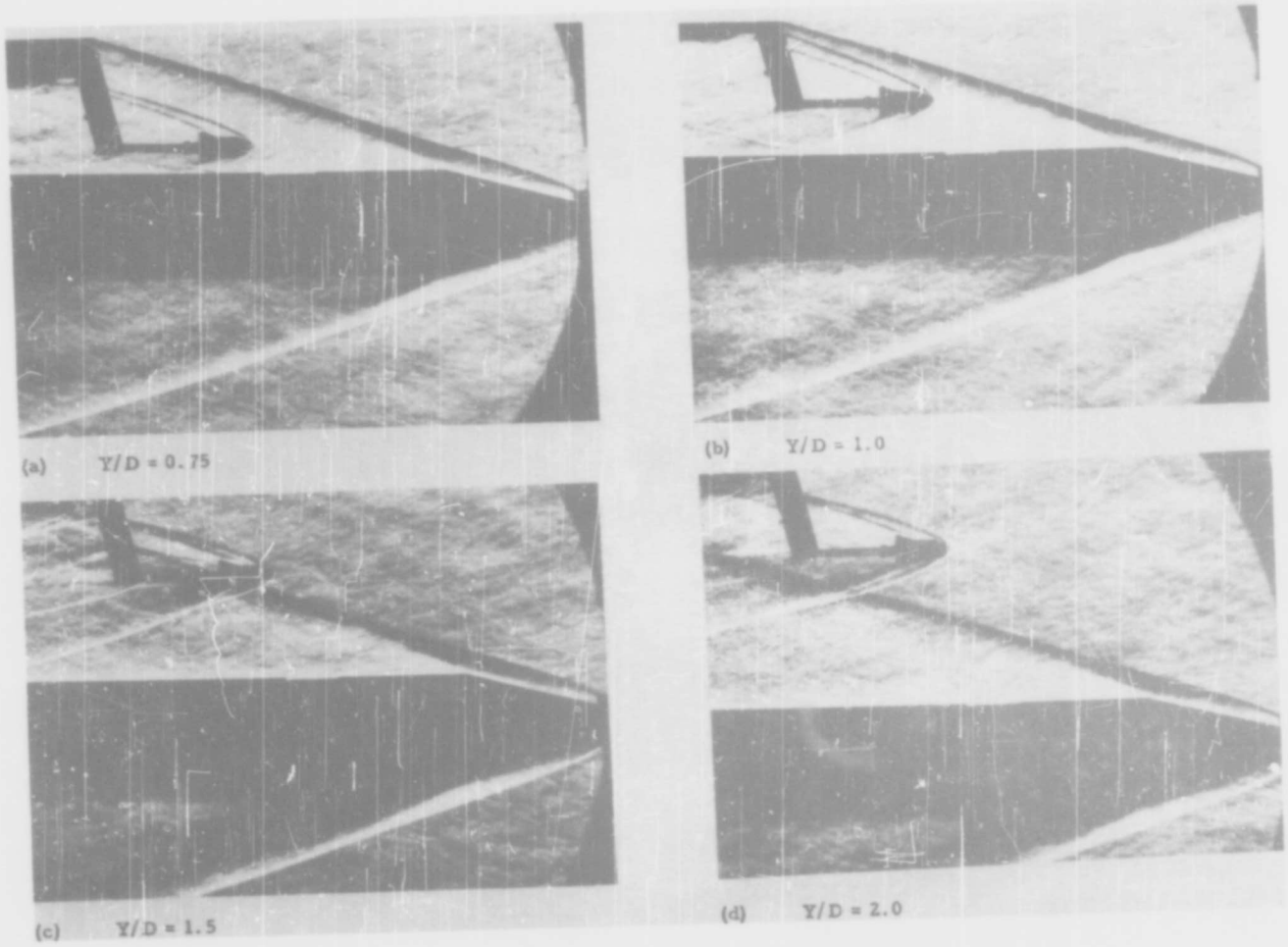

Figure 14. Close-in Phase - Schlieren Sequence Showing Lateral Excursion of Capsule at Axial Station X/D = 0.5 - M = 5.0, P_o = 75 psia. α = 0

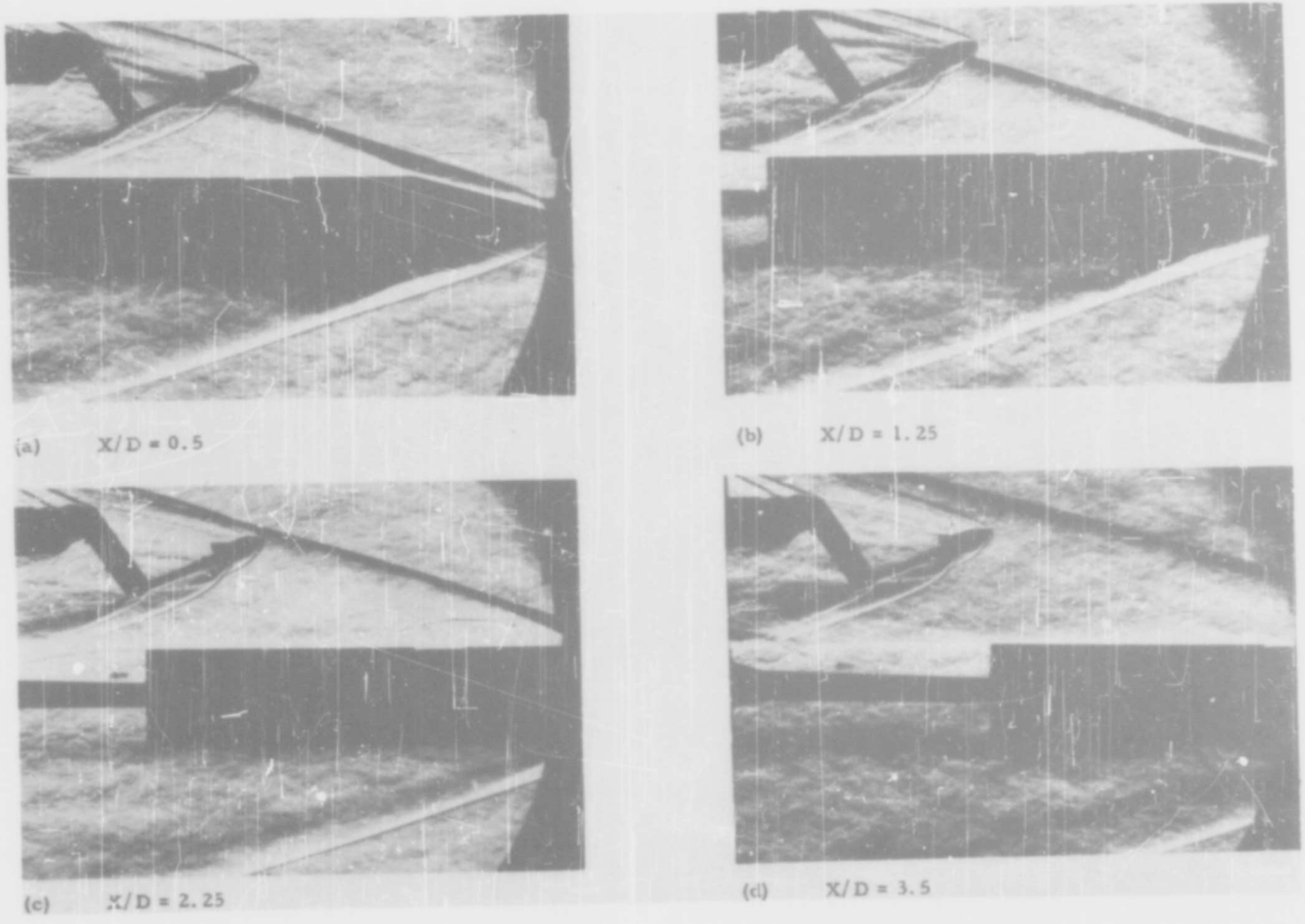

Figure 15. Close-in Phase - Schlieren Sequence Showing Axial Travel of Capsule at Lateral Separation Y/D = 1.25 - M = 5.0, P_o = 150 psia, α = +20°

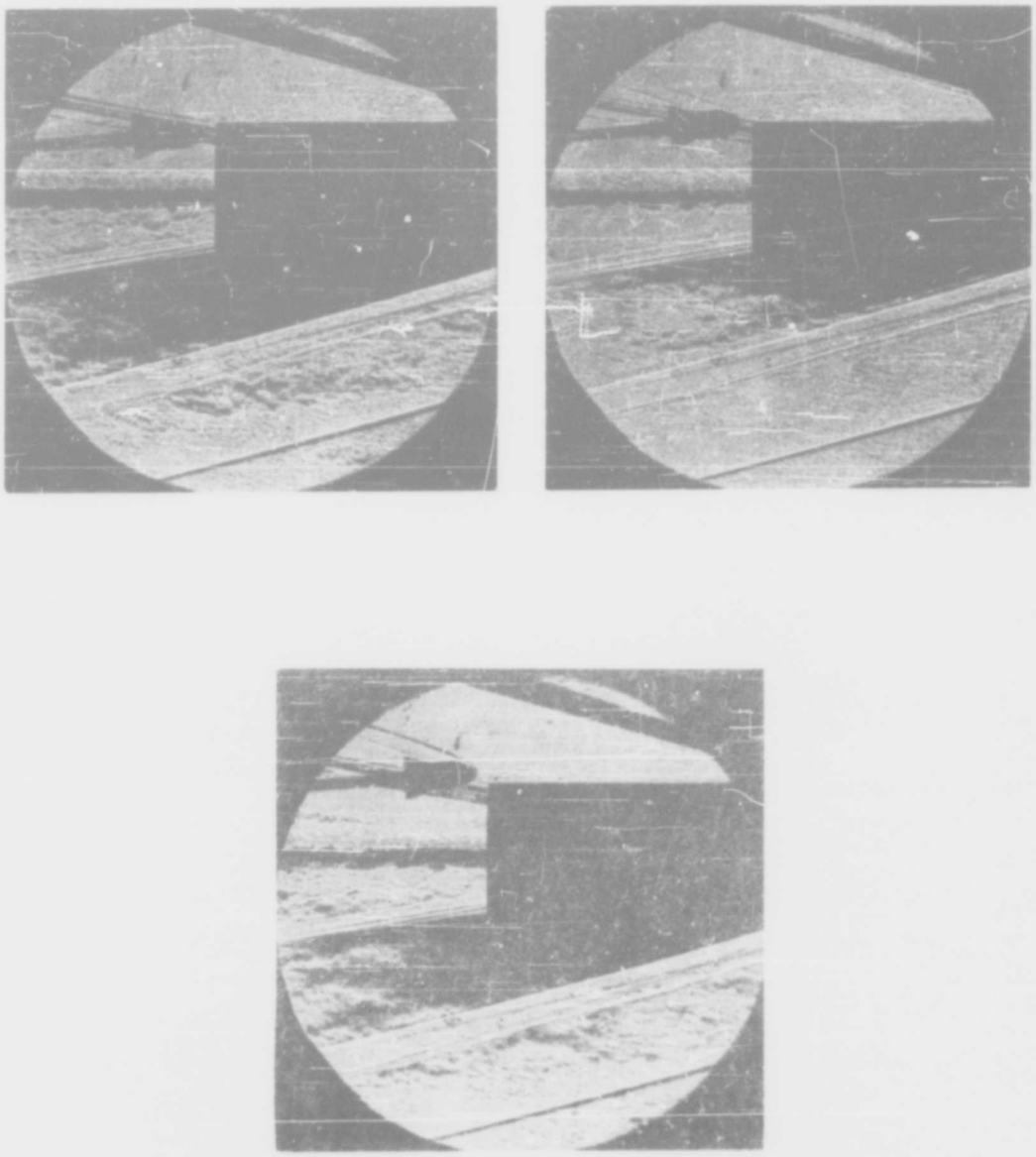

Figure 16. Wake Penetration Phase - Typical Schlieren Sequence Showing Capsule Traversing the Wake Boundary, 0.375 Calibers Behind Base - $\alpha = +5^{o}$

SECTION IV

DATA ANALYSIS

The test data obtained have been studied to determine the trends of variations and the local flow conditions that would be necessary to produce these trends. The data are considered in four main categories: Partial Exposure, Close-in Effects, Wake Penetration, and Wake-Capsule Interaction.

A. Partial Exposure

The partial exposure data shown in Figures 7a through 7d indicate that the force and moment coefficients vary approximately as a function of the exposed areas of the capsule model. For simplicity, the data of these figures are presented as percentage functions of total displacement for complete capsule exposures. The normal force and pitching moment follow the intersection plan area vatiation of the capsule model with exposure, which is defined as the projected area of the nose and flare in the curved plane of intersection of the outer periphery of the carrier with the capsule. (Since the carrier diameter is much greater than the capsule diameter, the curvature of this plane is neglected). When the capsule model is submerged in the carrier model, the projected area is zero. With exposure the plan area increases reaching a maximum at 50 percent displacement when the area is the maximum projected of the nose and flare. Further displacement reduces the projected intersection conical area until full exposure at which time the intersection area, by definition, again becomes zero. The axial force follows the exposed frontal cross-sectional area (or base area) of the capsule model; increasing from zero at the flush position to total base area at the full exposure position.

All of these tests were conducted at an angle of attack of zero (relative to tunnel centerline). The normal coefficient, C_N, curves show a smooth negative increase as the capsule flare emerges, due to the momentum of the impinging airstream. Shortly after the nose cone begins to emerge, the C_N value stabilizes over a fairly long range of exposure; this is probably due to a combination of separation over the flare and increased cavity pressure both being affected by the shock wave cast from the nose cone of the capsule. At approximately 80 percent exposure (percent exposure is defined in Section III of this report), the nose cone is completely exposed and the nose cone and flare bottom begin to feel a lift force negating some of the downward force as shown by the sudden rise in C_N. At full exposure, the C_N curve is rising toward zero indicating the tendency to go positive which would result from the increased pressure on the lower side due to choking between the capsule and carrier models.

The axial force curves in Figure 7c show a smooth increase of C_{A_T} with exposure being a manifestation of the exposed frontal area. The measured base drag coefficients, C_{A_B}, Figure 7d, are essentially constant after 20 percent exposure and the values agree very well with published data for free flight bodies (Hoerner, for example, Ref. 2), indicating little interference effect on base pressure.

The pitching moment coefficients, C_M, vary approximately according to the area exposed. As shown in Figure 7b, C_M increases as the upper portion of the flare and nose cone emerge. The pitching moment then decreases until approximately 80 percent exposure when the nose cone is fully exposed. The nose contribution to moment increases and C_M rises to approximately zero at full capsule exposure.

As the curves show, the effect of Reynolds number on the data is not great and probably due to slight boundary layer changes. The effect of Mach number is much more pronounced as shown by the Mach 2.0 data. The Schlieren photographs indicate the flow at M = 4.0 and 5.0 is parallel to the surface of the carrier whereas at Mach 2.0, the approaching flow turns slightly into the cavity. Data at Mach numbers greater than 5.0 are needed to evaluate the Mach effects in order to determine whether or not the trends from Mach 2.0 to 4.0 and 5.0 continue at higher Mach numbers.

As stated previously, the partial exposure normal and axial force indicate these data to be a function of the projected exposed areas of the capsule. Figure 17 shows how the normalized C_N and C_A curves at M = 4.0 follow fairly well the variations of the projected plan area of the nose cone and flare of the model and the base area exposed. The C_N curve was normalized by the maximum absolute value measured during exposure. The C_A curve was normalized by $C_{A_{max}}$, the value of C_A at full exposure.

The drag of the sloping surfaces of the capsule model was predicted using modified Newtonian pressures applied to the field generated by the carrier body in the vicinity of the cavity. At Mach 2.0, the Newtonian pressures gave reasonable agreement to the C_A variation. However, the predictions at Mach 4.0 and 5.0 were somewhat greater than the measured data.

The Newtonian pressures overpredicted C_N at all Mach numbers indicating the probability of cavity overpressure existing over most of the exposure range. No correlation between the Mach 2.0 data and the Mach 5.0 data was established.

The measured data at Mach 4.0 and 5.0, in general, show relatively small values of the coefficients. The maximum negative value of C_N is less than for a -2 degree angle of attack in the free stream. At full exposure, C_N and C_M are

close to zero. However, the value of the total drag coefficient at full exposure (when the capsule base is tangent to the carrier surface) is just less than when slightly removed from the surface as is shown by the close-in data. Comparing the Mach 5.0 and Mach 2.0 data indicates the forces and moment should decrease with increasing Mach number. Other capsule configurations would no doubt vary greatly but should follow the variations in exposed area. The pressure existing in the ejection cavity would also vary with the configuration.

The predictions of ejection requirements for the capsule shape, may be made using the exposed areas and applying Newtonian pressure data to the area. The wind tunnel test data show that the Newtonian pressures overpredict the lift force resisting capsule emergence and therefore will indicate conservatively high values of ejection velocity required. The wind tunnel data also indicate that static overpressure in the cavity is quite important in reducing the normal force on the capsule. However, when ejection velocities are quite high it is not likely that enough time would elapse during capsule emergency for this cavity pressure to build up to the static values or even increase at all. In this case, the predictions of ejection requirements using data from static wind tunnel tests or estimated with the Newtonian assumption would be less conservative and perhaps even more realistic.

B. Close-in Effects

A study of the close-in data, Figures 8a through 8i, reveals that two distinct areas of consideration exist for a capsule in the side flow field of the carrier vehicle. When the capsule is positioned below the carrier bow wave, excursions in X or Y show little change in forces with positions forward of the expansion flow generated at the base of the carrier. What changes occur are due to a change in dynamic pressure and Mach number from conditions at infinity. Mutual interference, if it exists, is so small that it cannot be evaluated. The normal force curve slopes and axial coefficients differ only slightly from the free stream measured data as would be expected in this region. A slight local effect is apparent when the capsule is very close to the carrier surface and this is due to local interaction between the models.

When the capsule approaches closely - or intersects - the carrier bow wave, very pronounced changes occur; this is a critical region of consideration. Immediately behind the bow wave, the local dynamic pressure is appreciably increased and the local flow turns away from the carrier axis resulting in an induced angle of attack on the capsule. The capsule model, being of finite length, is in a highly nonuniform field because of the rapid field change behing the shock. However, a reasonable approximation to C_N and C_A values at the shock wave may be found by a judicious application of oblique shock data to the free stream capsule characteristics.

In order to determine the changes in aerodynamic characteristics of the capsule in proximity to the bow wave, a region corresponding to the capsule positions used during the wind tunnel tests is selected. This region extends along the bow wave from a forward position over the side ejection port. The curvature of the carrier bow wave in this area has decreased to the extent that the bow wave has become essentially straight. This has been shown by many Schlieren photographs of the carrier model and other cone-cylinder bodies. The relative straightness of the bow wave greatly simplifies the measurement of the wave angle and permits direct determination of flow deflection and pressure, etc., immediately behind the bow wave from oblique shock tables.

Existing data on flow field characteristics such as the data of Clippinger (Ref. 3) show that the decay of pressure and flow deflection angle behind the bow wave aft of the expansion flow from the shoulder are near exponential functions of the axial distance behind the wave. The flow field is determined by the carrier geometry, and physical size introduces only second order effects such as some possible Reynolds number dependency. For the same carrier model, a sufficiently small capsule - when placed near the shock - would experience an effectively uniform field whereas a large capsule would be subject to large field variations along its length. The effects of these gradients must be evaluated over the length of the capsule body in order to reasonably predict the capsule loadings.

Various means of evaluating the effects of flow nonuniformities on the capsule loadings may be used. The simplest method is to determine the flow deflection angle and local dynamic pressure at the midpoint of the capsule and apply these values to the free stream characteristics. A refinement of this is to apply a strip theory where the local characteristics (normal and axial force coefficients) on elemental length sections of the body are computed using local field properties or the slender body approximations of Moskowits (Ref. 1 of Appendix I).

1. Prediction of Capsule Loadings at the Bow Wave

The first example of static data prediction will be made using the local flow angle and dynamic pressure at the midpoint of the capsule body. Normal and axial force coefficients in the flow field are defined as follows:

$$C_{N2} = C_{N_\alpha}(\alpha + \Delta\alpha)\frac{q_2}{q_1}$$

$$C_{A2} = C_{A(\alpha + \Delta\alpha)}\frac{q_2}{q_1}$$

where

C_{N_α} is the free stream normal force curve slope

$\Delta\alpha$ is the local flow inclination angle, = δ

$\frac{q_2}{q_1}$ is the ratio of q behind the oblique shock to q in front of the shock

Considering the Mach 5.0 data, the bow wave angle in the region of the test points, as determined from Schlieren photographs, is approximately 18 degrees. From oblique shock tables for these conditions,

$$\frac{p_2}{p_1} = 2.57$$

$$M_2 = 4.2$$

$$\Delta\alpha_2 = \delta_2 = 8.5^\circ \text{ (flow deflection angle).}$$

The subscript 1 refers to conditions in front of the shock or free stream conditions and the subscript 2 refers to conditions immediately behind the shock wave. The absence of a subscript indicates local flow properties.

As stated previously, the pressure and flow inclination decay rapidly with downstream position and the variation is exponential. From the data of Clippinger (Ref. 3) for a 15-degree cone-cylinder body, at Mach 5.0, the pressure and flow inclination variation was determined to be

$$\frac{\Delta p}{\Delta p_2} \approx e^{-2\,x/D}$$

$$\frac{\Delta\alpha}{\Delta\alpha_2} = \frac{\delta}{\delta_2} \approx e^{-1.4\,x/D}$$

where

$$\frac{\Delta p}{\Delta p_2} = \frac{p - p_1}{p_2 - p_1}$$

x/D = streamwise distance behind bow wave in carrier body calibers.

These expressions are valid for values of x/D at least up to 0.5 which is the capsule length. The variation in dynamic pressure as derived from the static pressure relationship is

$$\frac{q}{q_\infty} = \frac{5}{M_\infty^2} (f P_2) \left[(1 + 0.2M_2^2) \left(\frac{P_2/P_\infty}{f P_2}\right)^{0.286} - 1\right]$$

where

$$f P_2 = 1 + \left(\frac{P_2}{P_\infty} - 1\right) e^{-2 x/D}$$

$$q_\infty = q_1$$

The midpoint of the capsule body with nose touching the bow wave is located at x/D = 0.25.

Solving for q and $\Delta\alpha$ at this position using the oblique shock values previously determined

$$\frac{q}{q_\infty} = 1.53$$

$$\Delta\alpha = 6^\circ.$$

Then

$$C_{N2} = C_{N_\alpha} (\alpha + 6)\, 1.53$$

C_{N_α} measured = 0.027 per degree

and

$$C_{N_2} = 0.0413\ (\alpha + 6)$$

$$C_{A_2} = 1.53\ C_{A_{(\alpha + 6)}}$$

For $\alpha = 0$;

$$C_{N_2} = 0.248$$

$$C_{A_2} = 0.49$$

For $\alpha = -5^{\circ}$;

$$C_{N_2} = 0.041$$

$$C_{A_2} = 0.445$$

These values compare very well with the measured data at (X/D = 1.25, Y/D = 1.5) and (X/D = 0.5, Y/D = 1.25) both positions being where the capsule nose is touching the shock wave as was determined from Schlieren photographs of the test points. Referring to Figures 8a and 8b, the agreement in C_N and C_A is seen to be within 0.03, for both angles of attack and both positions.

The second example of static force coefficient prediction is the prediction of C_A by parts or strip theory. For the case of the capsule model the important contributions to drag are generated by the nose, the flare, and the base pressure. In this case, the dynamic pressures used were those at approximately the midpoint of the nose cone and the midpoint of the flare. For base drag estimation, the flare dynamic pressure was used. This computation was carried out for a -5 degree angle of attack which made the effects of angle of attack very small and these were neglected because of

the relative insensitivity of C_A to α. The effects of static pressure were calculated and found to be negligible, thus

$$C_{A_T} = C_{A_{nose}} \frac{q_N}{q_\infty} + C_{A_{flare}} \frac{q_F}{q_\infty} + C_{A_{base}} \frac{q_F}{q_\infty}$$

$C_{A_{nose}}$ is the drag of the nose, for the local Mach number, corrected to the capsule base area

$C_{A_{flare}}$ is the average flare pressure coefficient as determined from wind tunnel tests, corrected to capsule base area

$C_{A_{base}}$ is the base pressure coefficient from test.

These values are,

$$C_{A_N} = 0.193$$

$$C_{A_F} = 0.067$$

$$C_{A_B} = 0.040.$$

Local q ratios as computed from the derived expression for $\frac{q}{q_\infty}$ at the nose and flare midpoints are,

$$\frac{q_N}{q_\infty} = 1.73 \text{ and}$$

$$\frac{q_F}{q_\infty} = 1.37$$

Then

$$C_{A_T} = 1.93\,(1.73) + 0.067\,(1.37) + 0.04\,(1.37) = 0.481$$

which agrees with the test data and Figures 8a and 8b.

2. Comparison of Calculated and Experimental Capsule Model Data for a Lateral Excursion through the Flow Field

The approximation to the capsule characteristics in the region below the shock wave is made by applying local flow field conditions to the capsule free stream characteristics. Flow field parameters for a cone-cylinder body with cone half angle of 15 degrees at M = 5.0, as reported by Clippinger (Ref. 3), were used to obtain the following flow field conditions at X/D = 1.25.

Y/D	$\frac{p}{p_\infty}$	$\frac{\rho}{\rho_\infty}$	$\Delta\alpha$
0.7	0.84	0.88	-0.5°
1.0	0.77	0.83	+1.0°

Solving for $\frac{q}{q_\infty}$ from the expression,

$$\frac{q}{q_\infty} = \frac{5}{M_\infty^2}\left[\frac{\rho}{\rho_\infty}\left(1 + 0.2M_\infty^2\right) - \frac{p}{p_\infty}\right]$$

and using the relationships

$$C_N = C_{N_\alpha}\,(\alpha + \Delta\alpha)\,\frac{q}{q_\infty}$$

$$C_A = C_{A(\alpha + \Delta\alpha)}\,\frac{q}{q_\infty}$$

the following field point characteristics, at Y/D = 0.7 and 1.0, were calculated for the angle of attack of +5°, X/D = 1.25, M = 5.0.

Y/D	$\frac{q}{q_\infty}$	C_N	C_A
0.7	0.888	0.108	0.275
1.0	0.842	0.136	0.270
1.5		0.455	0.520

The Y/D = 1.5 values were calculated for bow wave conditions as described previously. Comparison of the above values with the curves for α = +5 degrees in Figure 8b shows good agreement with the measured data. The predicted values fall within the accuracy of the measured data. Figure 18 shows the comparison of the calculated and measured data. In the figure, the predicted points at Y/D = 2.0 are free stream values.

The comparisons of the results with these simple means of calculation indicate that once the character of the flow is known, rather simple considerations can predict the forces within acceptable limits. The method of characteristics can be used for developing the flow field.

In order to determine separation requirements and proximity trajectories, the equations of motion summarized in Appendix I must be employed in conjunction with the aerodynamic data. The correlation of the data from static wind tunnel tests supplies the basis for obtaining some of the aerodynamic coefficients needed. The equations of motion have been written so that local field properties and instantaneous capsule velocities are used in determining capsule dynamic pressure and angles of attack. Thus, these equations apply to situations where flow disturbances generated by the carrier and/or instantaneous velocities of the capsule relative to the carrier are significant functions of the carrier velocity.

Dynamic derivatives such as C_{m_q} (pitch damping due to body angle rate), $C_{m_{\dot{\alpha}}}$ (pitch damping due to rate of change of body angle of attack - vertical acceleration), etc., are naturally not determinable from a static series of wind tunnel tests, nor are the effects of relative motion between the capsule and carrier.

The effects of dynamic derivatives during the short interval of proximity may be anticipated to be small relative to the effects of the static terms. Consequently, until such data are available, it is necessary and quite probably adequate to use estimates of these derivatives from uniform flow characteristics of the capsule multiplied by local values of dynamic pressure in the equations of motion.

By far, the largest uncertainty in determining separation characteristics is the effect of relative motion on the flow field generated by the carrier. This effect may be expected to be particularly significant in the partial exposure phase of side separation and in wake core and penetration ejections. The extent to which relative motion will produce flow conditions and consequently capsule aerodynamic coefficients intermediate to effectively unmodified flow configurations (infinite ejection velocities) and the conditions established in static wind tunnel tests (zero ejection velocity) can be established only after conduct of dynamic ejection tests.

C. Wake Penetration

The data obtained from the Mach 5.0 wake penetration tests are presented in Figures 9a through 9e. The curves of the aerodynamic coefficients vs positions crossing the wake boundary show relatively continuous characteristics.

Examination of the normal force coefficient variation presented in Figures 9a and 9b indicates flow deflections of the order of 15 degrees with reference to free stream direction are experienced along the wake boundary. This flow deflection is in reasonable agreement with the wake angle (12.8) predicted by Love (Ref. 4) for a carrier vehicle of this configuration at a free stream Mach number of 5.0. Due to this flow deflection, the capsule normal force coefficient was negative for all angles of attack investigated except for the +15 degree angle of attack cases at the large Y/D locations. These trends in normal force coefficient variation are what would be expected in this region of the carrier flow field.

In Figure 9a it is seen that for the -15 degree case, the normal force coefficient increases rapidly as the capsule is positioned closer to the wake centerline (Y/D decreasing). This trend is greatest at stations close behind the carrier base (X/D = 0.50). As a result, the C_N values at low Y/D for the -15 degree angle are greater than for the -10 degree angle. The curves cross at approximately Y/D = 0.46 at the X/D = 0.5 station. This effect is the result of the opening of the wake, in the region of the capsule model, due to the interference of the capsule body on the carrier base pressure. The opening of the wake decreases the capsule area exposed to the high energy stream outside the wake edge resulting in a decrease in C_N. At angles of attack close to zero, the wake appears to be relatively undisturbed by the presence of the capsule model. As the capsule is turned more broadside to the stream (more negative angle of attack), the flare pressure increases until enough flow and pressure has been propagated forward — along the upstream side of the capsule body — into the recirculation region to locally increase the base pressure to a value preventing normal expansion around the base corner. The wake, then, opens locally in the region directly in front of the capsule model.

The axial force coefficients indicate the effective dynamic pressure is sizeably reduced even with the capsule at Y/D's equal to 0.65. The axial force coefficient was used to obtain a measure of the flow field dynamic pressure since this coefficient is relatively insensitive to small angle of attack variations. Ratioing the axial force coefficient measured to the Mach 5.0 free stream value (0.295) at Y/D equal to 0.65 indicates a dynamic pressure ratio of approximately 60 percent. As Y/D is reduced, this effective drag ratio reduces to nearly zero at Y/D equal to 0.35 and X/D values of 0.25.

The moment data given in Figure 9c show the aerodynamic moment is positive for all caliber locations and angles of attack less than 15 degrees. Hence,

during a free flight ejection a favorable pitching moment would be attained which would increase the capsule angle of attack and cause it to fly clear of the wake boundary.

Figure 9e gives the variation of C_N for various Y/D and X/D locations at Mach numbers of 4.0 and 5.0. It can be seen that similar trends are exhibited for both Mach numbers. The Mach 4.0 data, however, are considerably lower than the Mach 5.0 values. Presented in the same figure is the variation of C_N as a function of wind tunnel total pressure (i.e., Reynolds number) for a Mach number of 5.0. Results of these tests indicate that Reynolds number has little effect for Y/D less than 0.5. For Y/D values greater than 0.5, some slight increase in C_N is noted for the lower Reynolds number.

The data from the wake penetration tests indicate that a reasonable prediction of capsule coefficients can be made in this region by using local flow field conditions with techniques similar to those developed for the characteristics of shock wave interaction with the dead air space behind the carrier base.

D. Wake-Capsule Interaction

Figure 10 shows the variation of drag coefficients based on free stream dynamic pressure and flare base area as measured for various caliber locations behind the carrier vehicle. The reference point on the capsule used for distance measurements was 50 percent of the capsule length. All capsule drag measurements were performed with the capsule's longitudinal axis parallel to and aligned with the carrier vehicle-axis. The Mach number and tunnel total pressure for which these data were obtained was 4.0 and 72 pounds per square inch absolute, respectively.

The variation of drag coefficient as shown in Figure 10 can be attributed to the variation in Mach number, dynamic pressure, and in close-in positions to the existence of static pressure gradients. Obtaining a quantitative description of the forces applied to a body in the wake would require theoretical methods which are capable of describing the velocity, Mach number, pressure, and temperature variations both longitudinally and transversely, as well as of considering the interaction the body has with the undisturbed wake characteristics. Since such theoretical methods are unavailable, recourse to empirical methods which may apply over limited ranges and conditions should be considered as possible means of attaining estimates of engineering value. Such empirical methods can be obtained by employing results from subsonic turbulent wake analyses for basic functional variations in wake properties with longitudinal and transverse distances where certain needed empirical constants are obtained by comparing these variations with wake characteristics measured at supersonic speeds. Following this procedure, the velocity depression in the wake as a function of the transverse

distance as given by Schlichting (Ref. 5, page 493) is,

$$\frac{U}{U_{max}} = \left[1 - \left(\frac{r}{r_o}\right)^{3/2}\right]^2$$

and (from Ref. 5, page 488) the variation in centerline velocity with longitudinal distance is,

$$\frac{V_w}{V_\infty} \sim \left(\frac{X}{D}\right)^{-2/3}$$

for axially symmetric cases. By employing these two variations and comparing with the measurement at Mach 1.33 given by Howarth (Ref. 6), the following empirical relationship results:

$$\frac{V_w}{V_\infty} = 1 - \frac{0.684}{\left(\frac{X}{D} - \frac{X_A}{D}\right)^{2/3}} \frac{U}{U_{max}}$$

where

$$\frac{X_A}{D} = \frac{X_t}{D} - (0.684)^{3/2}$$

and X_t/D is the distance from the carrier base to the position of minimum wake diameter (Ref. 4). At distances which are large compared to X_t/D, the static pressure approaches uniformity at the free stream value and the wake dynamic pressure becomes large; thus, the effect of a static pressure gradient on static forces becomes relatively less important. Since the variation in static pressure is unknown, it is assumed that reasonable estimates can be obtained by taking the static pressure equal to the free stream value. This, with the further assumption that the stagnation temperature remains equal to the free stream stagnation temperature enables the calculations of density and Mach number, which combined with the empirical velocity variation, yields an estimation of the dynamic pressure.

Using the above relations, the average dynamic pressure and average Mach number across the positions of the wake occupied were computed ignoring possible

capsule wake interaction and longitudinal gradients. The drag coefficients used for the capsule were the free stream values tabulated below.

Mach No.	C_D
1.0	0.820
2.0	0.592
3.0	0.435
4.0	0.330
5.0	0.294

These were obtained from wind tunnel tests in a uniform flow except for Mach number 1.0 which was extrapolated. The average Mach number at the midpoint of the body was used to enter this table. The comparison of the calculated with the measured values is shown in Figure 18 as ratios of the local drag coefficient to the free stream value at Mach number 4.0 (i.e., $C_D = 0.33$). The agreement between the measured and estimated values is reasonably good. The maximum deviation of 0.05 or approximately 10 percent occurs at 2.5 calibers. At this distance, gradients in Mach number and dynamic pressure as well as static pressure do exist which have not been taken into account and probably account for a substantial part of the disagreement. Moreover, this is a region of reduced wake diameter where capsule wake interference would be expected to be more pronounced.

In the close-in position, Figure 19, negative drags are indicated by the data. In this region, solid and dashed curves are shown for the estimated value. The dashed curve was obtained under the assumption of a "dead air" space existing in the converging portion of the wake. The solid curve is based on an extrapolation of data presented in References 4 and 6 which show the existence of an increasing static pressure with distance behind an axially symmetric body. The improved agreement with the measured values indicates that negative drag values associated with this capsule (having significant length) in this region are attributed to positive static pressure gradients.

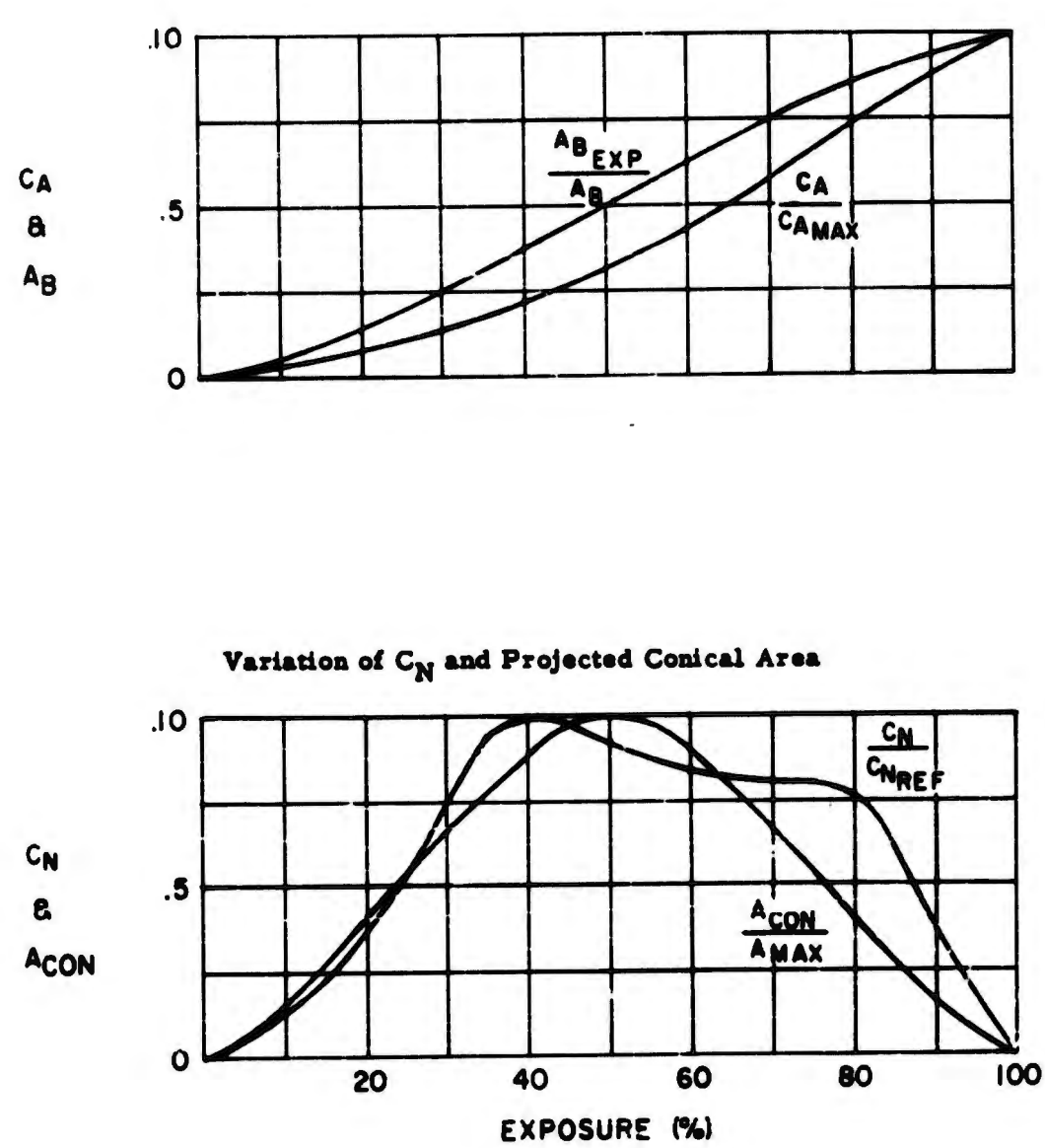

Figure 17. Partial Exposure - Comparison of Capsule Projected Areas and Measured Force Data with Capsule Exposure

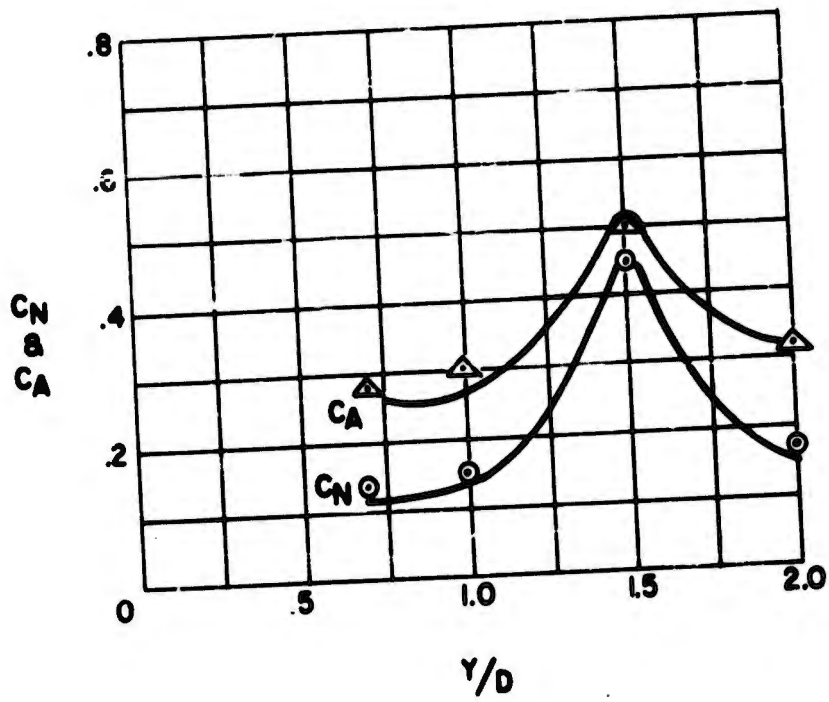

△ ⊙ = MEASURED DATA

——— = CALCULATED DATA

Figure 18. Comparison of Calculated and Experimental Capsule Model Data for Close-in Phase - X/D = 1.25, α = +5°, M = 5.0

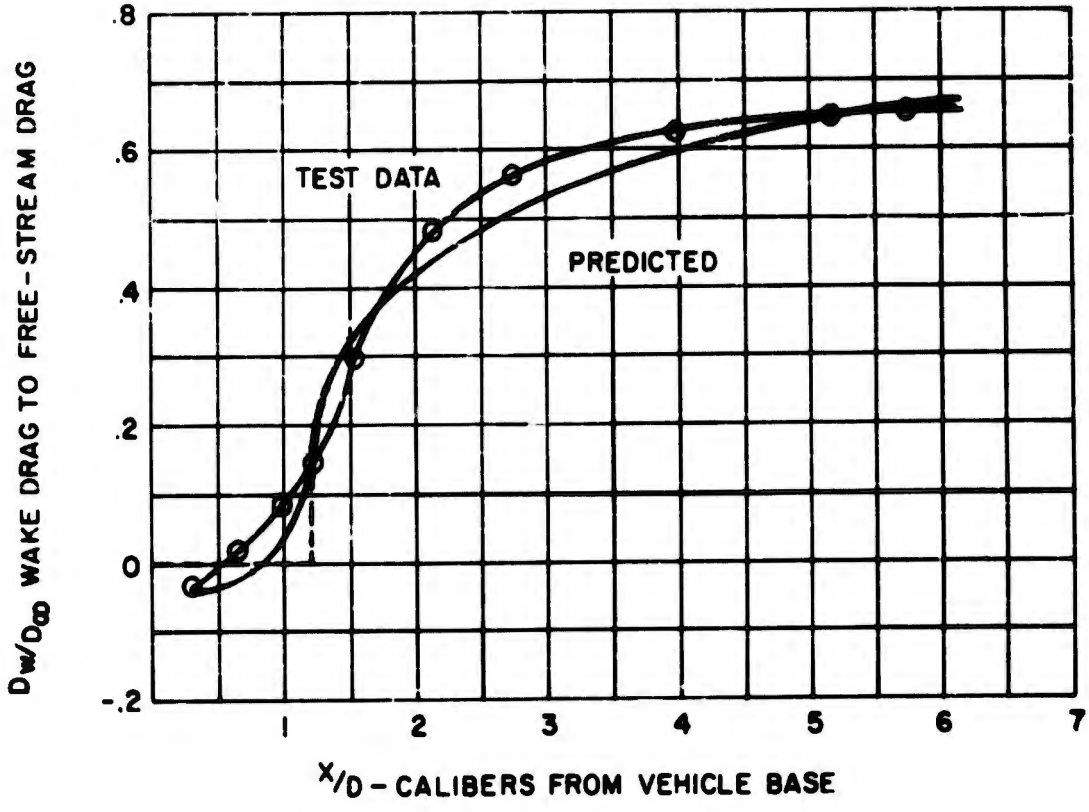

Figure 19. Comparison of Predicted and Experimental Data for Wake Core Drag Ratio

SECTION V

APPLICABILITY OF DATA

The data obtained from these wind tunnel tests are applicable to the determination of separation and trajectories for capsule bodies of identical shape to the capsule model of test. In applying these data to other capsules and carriers, or conditions, consideration must be given to:

(1) The effects of scale, i.e., Reynolds number

(2) The relative size of the capsule to the carrier vehicle

(3) The specific shapes of the capsule and carrier.

The results of comparing the measured aerodynamic coefficients with free stream characteristics show that the differences are almost entirely accounted for by simply applying local flow characteristics to free stream coefficients or by simple geometric consideration. Consequently it is anticipated that a similar procedure may be used for other capsule and carrier shapes employing the flow fields generated by the specific carrier. The effects of scale and relative size are discussed in the following sections.

A. Scale-Effect

All of the test conducted, with the exception of the wake core survey were conducted at more than one Reynolds number. The variation of the data with Reynolds number, for the most part, was small; often within the accuracy of measurement or the scatter of the data. It is believed that the data taken at the highest Reynolds numbers can be used and considered constant at Reynolds numbers greater than the test maxima. Some free stream data were taken at Mach 5.0 at Reynolds numbers appreciably lower than in the other phases of testing in order to extend this range downward to give some insight into the scale-effect on the free stream capsule characteristics. At the lower values, strong variations are seen to occur as shown in Figure 6h. At the higher values, however, the variation is relatively slight and observation of the tests of the large capsule model, which greatly extend the Reynolds number range, indicate an approach to constancy.

It is not believed that the carrier vehicle influence on the capsule will be affected by increasing Reynolds number for the close-in phase. The partial exposure phase and wake penetration phase may be influenced by changes in the carrier vehicle boundary layer, the character of which is determined by the

Reynolds number. The local Reynolds number on the carrier vehicle at the forward edge of the exit port, based on the distance from the nose, is approximately 14 times as great as the capsule's based on its centerbody diameter or, for the maximum test conditions, about 5.9 millions. At these Reynolds numbers, the boundary layers should be turbulent and an increase in Reynolds number would result only in boundary layer thickness variation which would at most produce only second order influences on the capsule.

Based on all of these considerations, at Reynolds numbers greater than those of these tests the maximum Reynolds number data are applicable. For the range of Reynolds numbers of the tests the test data, of course, are directly applicable. For Reynolds numbers below the test values the data must be used with reservation and only to indicate relative trends or magnitudes, as in this region the scale-effects become pronounced and unpredictable.

Figures 20 and 21 show the range of test Reynolds numbers converted to an altitude vs capsule centerbody diameter variation. These figures indicate the altitude limits of data applicability for the test Mach numbers. The relationship between Reynolds number and altitude is based on the ARDC 1959 model atmosphere. The free stream data (Figure 20) include tests of both the small (2 inch long) and the large (15 inch long) capsule model. Since the Reynolds numbers of the tests of these two models overlap, the region of direct applicability is continuous.

In the high altitude region above the upper limits of data applicability, the dynamic pressures, at these Mach numbers, are very low. Therefore, the capsule loads are small; approaching insignificance as the altitude increases. Thus, at very high altitudes, the decreased reliability of the data is not of great significance. Under these conditions, the mass and inertia of the capsule body and the initial conditions of separation are the most important parameters in trajectory calculations.

B. Relative Size of Capsule and Carrier Vehicle

For the proximity tests conducted, only one size of capsule and carrier model was tested and the data are directly applicable for this ratio of diameters only. However, this ratio was chosen to represent a relatively large capsule and capsule to carrier diameter ratios higher than these would not be likely in practice. The comparison of predicted to measured values for the close inphase show that local flow conditions applied to the capsule characteristics at the capsule reference center give reasonable predictions, thereby indicating that, except at the shock wave, a nearly uniform local flow is felt by the capsule. The data should then be applicable to relatively smaller capsules. In the influence of the shock wave predictions of capsule characteristics may be made as discussed in

Section IV and the accuracy of prediction should improve as the capsule size reduces because this size reduction results, again, in a relative improvement in the uniformity of the local flow around the capsule body.

To apply the measured data to a relatively larger capsule than tested would probably yield erroneous results as the actual capsule would be immersed in a relatively more variable flow field than was the test capsule model. The flow field variation over the larger capsule is due not only to the increased length but also to the increased diameter. For a larger capsule, the circles of influence around the carrier vehicle which would intersect the test capsule centerline, intersect the capsule body appreciably below the capsule centerline (longitudinal axis).

C. Calculation of Separation Characteristics and Trajectories

The wind tunnel data may be used directly to predict static loading on the capsule body at any position in the flow field. A comparison of the proximity data with the free stream data modified by local flow field characteristics, for the close-in phase, indicates that the field characteristics of the capsule model may be determined at Mach numbers other than the test values once the flow field characteristics at these Mach numbers have been determined. However, in predicting capsule separation trajectories, consideration must be given to the relative velocity between the capsule and carrier, and the resulting field disturbance, which will modify the capsule forces.

The equations of motion discussed in Section III of Appendix I describe the dynamics of the capsule body taking into account the flow field disturbance due to the relative velocity of the capsule body and should be used for trajectory computation.

For those cases where the disturbances from free stream conditions are large, the equations of Appendix I should be employed. In instances where the disturbances are small, the simpler equations described in Reference 7 may be used to determine the separation characteristics and trajectories.

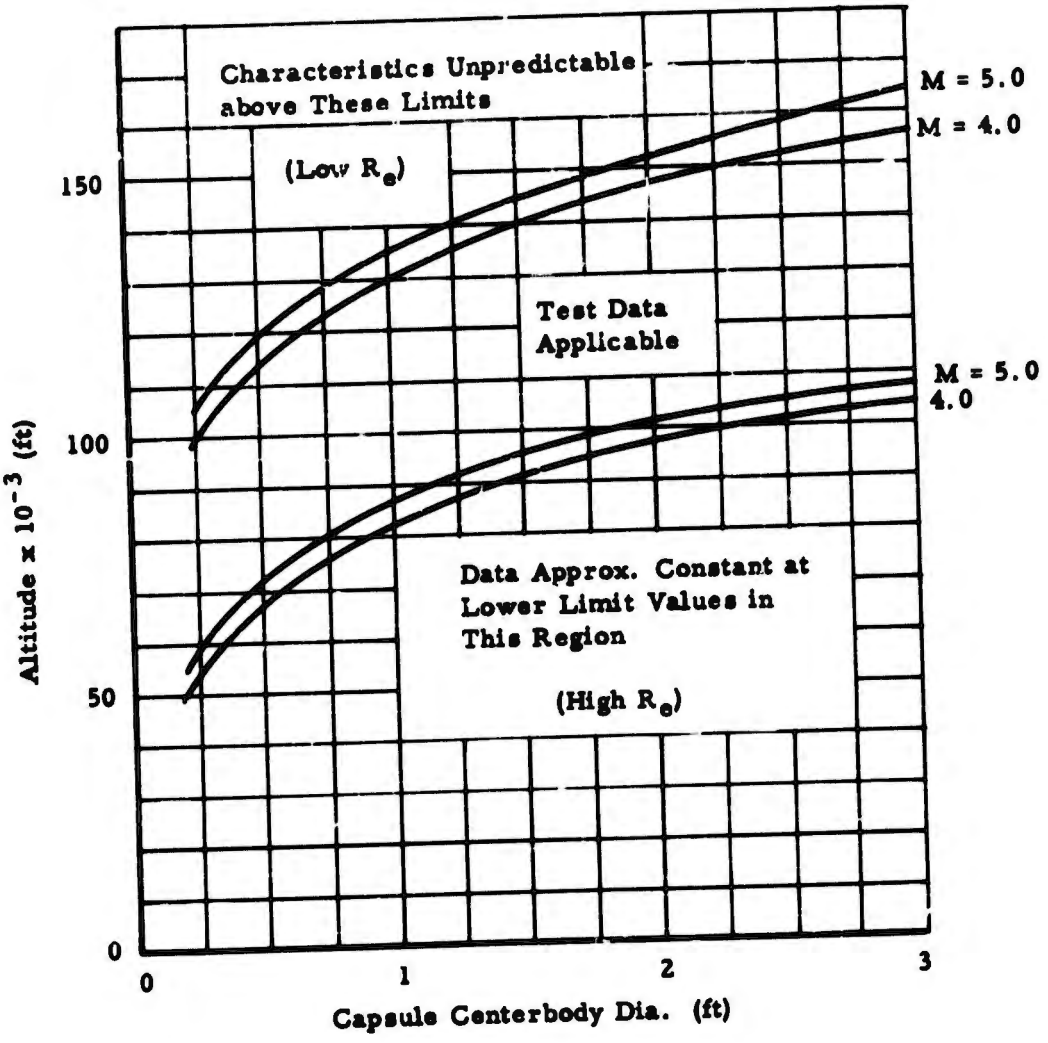

Figure 20. Altitude Limits Corresponding to Reynolds Numbers of Test - Variation with Capsule Centerbody Diameter to Show Limits of Applicability of Data. Free Stream Data Only. M = 4.0 and 5.0

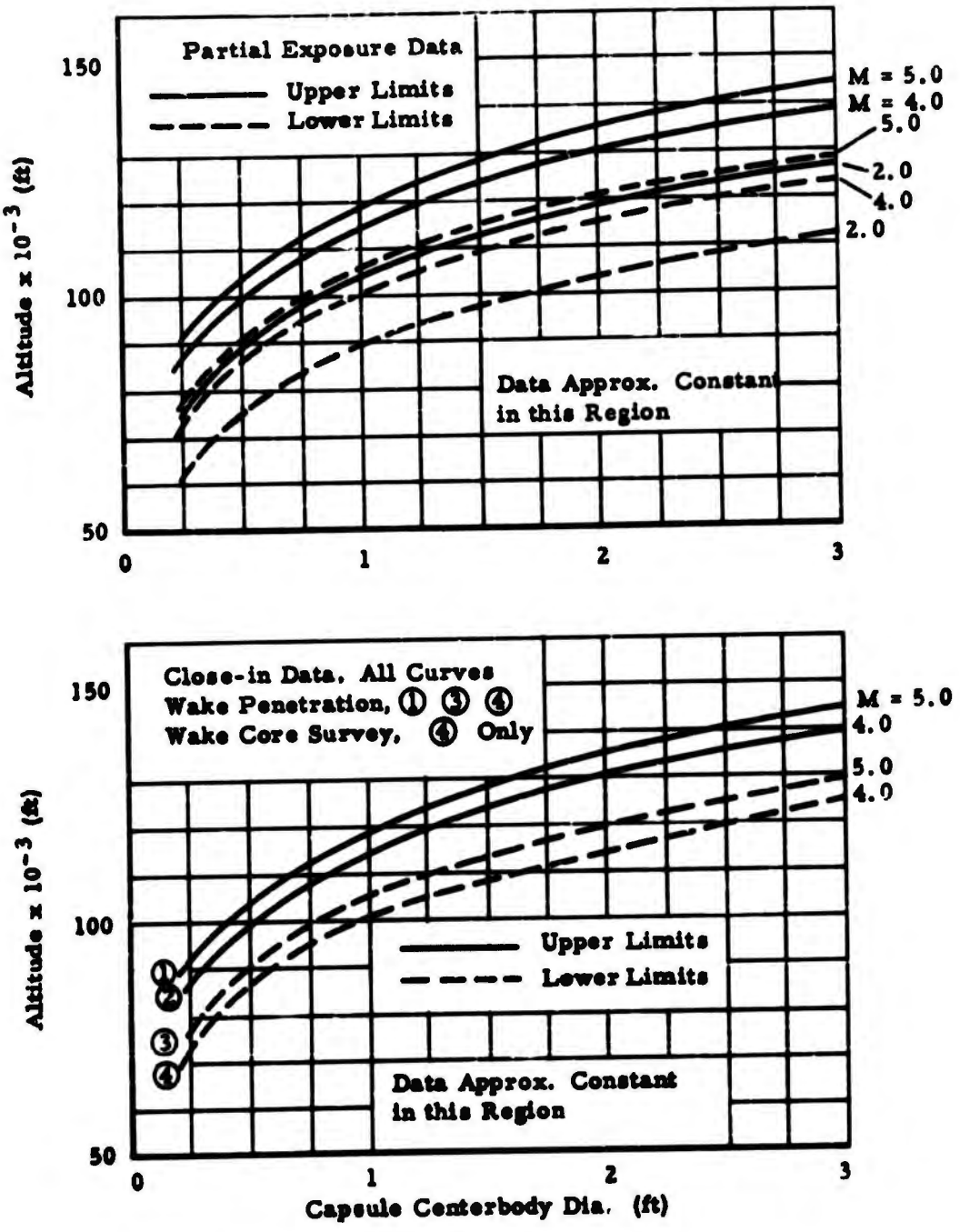

Figure 21. Altitude Limits of Data Applicability Based on Reynolds Number of Test - Variation with Capsule Size

SECTION VI

CONCLUSIONS

The analysis of the wind tunnel data has indicated that reasonable agreement is obtained between these data and values estimated by employing free stream capsule characteristics and correcting these with the local flow inclination, Mach number, and dynamic pressure of the field generated by the carrier vehicle. Consequently capsule characteristics in the vicinity of a vehicle can be obtained with the relatively simple expedient of generating a flow field, such as by the Method of Characteristics or other means, and by obtaining free flight characteristics of the capsule.

Reasonable agreement of axial force coefficients in the wake core are obtained at distances beyond the wake closure by considering the effect of dynamic pressure and Mach number as dominating effects. Improvements can be made in the estimation of axial force coefficients by estimating the effect of gradients in the axial direction. However, in the cases considered, such corrections would produce refinements of a relatively insignificant magnitude.

At positions close to the base static pressure buoyancy corrections, which can be obtained from treatments such as Love (Ref. 4), reasonably predict the negative drag forces obtained.

For capsules that are relatively smaller than those of the current tests, similar techniques should yield satisfactory results. For relatively larger sized capsules, interactions with the carrier vehicle will be increased. Such interactions may be expected to produce changes in the flow field which will reduce the accuracy with which the aerodynamic coefficients may be estimated.

REFERENCES

1. Gray, J. Don, Force Measurements on a Data Capsule in Proximity to a Carrier Vehicle at Supersonic Speeds, AEDC TN-60-46, March 1960

2. Hoerner, S. F., Aerodynamic Drag, Otterbein Press, Ohio, 1951

3. Clippinger, R. F., Geise, J. H., and Carter, W. C., Tables of Supersonic Flows about Cone-Cylinders, Part II, Complete Flows, BRL Report No. 730, August 1950

4. Love, E. S., Base Pressure at Supersonic Speeds on Two-Dimensional Airfoils and on Bodies of Revolution with and without Fins Having Turbulent Boundary Layers, NACA TN-3819

5. Schlichting, H., Boundary Layer Theory, Pergamon Press, New York, 1955

6. Howarth, L., Editor, "Modern Developments in Fluid Dynamics," High Speed Flow, Vol. II, Oxford at the Clarendon Press, 1953

7. Smith, N. F., and Carlson, H. W., Measurement of Static Forces on Internally Carried Bombs of Three Fineness Ratios in Flow Field of a Swept Wing Fighter Bomber Configuration at a Mach Number of 1.61 with Illustrative Drop Path Calculations, NACA RM L56I18, 1957

APPENDIX I

DYNAMICS OF SEPARATION

CONDENSATION OF INTERIM SUMMARY REPORT
(The List of Symbols is at the end of this Appendix)

SECTION I

INTRODUCTION

This study is concerned with the prediction of separation characteristics of capsule bodies ejected from the side and base areas of high performance rocket vehicles in various stages of flight.

The increasing use of large impulse rocket-powered vehicles for scientific experiments in the region of the earth's upper atmosphere and beyond has indicated the desirability of ejecting various types of capsules at intermediate stages of the carrier vehicle's flight. The types of capsules of immediate interest are data capsules, camera packages, and biocapsules. Capsules may vary greatly in shape and size. In addition, the regime of flight required at separation can also vary widely. Hence, many configurations and separation conditions can be envisioned. In this study, two possible areas of separation have been considered, viz (1) ejection of a capsule from the side of a carrier vehicle and (2) ejection of a capsule from the base of the carrier vehicle.

A survey of all available literature in the area of capsule ejection has indicated that relatively little work has been accomplished in the specific field of capsule ejection. A number of sled tests have been conducted on pilot ejection seats. These tests unfortunately reflect aircraft types of configuration and are restricted to relatively low Mach numbers. A similar difficulty exists with the results of investigations in connection with store separation from aircraft. Moskowitz (Ref. 1) has developed expressions for calculation of the lift of combinations of bodies. These expressions have been used in this study to compute the part of the interference lift of bodies of revolution due to the upwash field generated by the capsule and carrier vehicle on each other.

The final objective of this investigation is the determination of force or velocity requirements necessary for satisfactory separation of capsules. This is accomplished by calculation of capsule separation trajectories. Preliminary to performing any such calculations, work in two broad areas is required. These are, (1) determination of pertinent aerodynamic characteristics and (2) formulation of motion equations representing both dynamic and aerodynamic effects. An interaction of these two areas also occurs since the flow field into which the capsule is ejected is in general nonuniform. These nonuniformities and their effects must be incorporated in the formulation of motion equations.

These aerodynamic considerations and the equations of motion are discussed and presented in this appendix.

SECTION II

AERODYNAMIC CHARACTERISTICS

In order to determine the requirements for satisfactorily separating capsules from a carrier vehicle, it is necessary to determine aerodynamic characteristics in three general areas. These are:

(1) The characteristics of the flow field caused by the presence of the carrier

(2) The aerodynamic characteristics of the separating capsule

(3) The effects of interference between the carrier vehicle and separating capsule.

Investigation in the second area above is straightforward and hence is not considered here. It is sufficient to remark that the capsule configurations employed in dynamic calculations were a sphere, a right circular cylinder and a composite nose-cylinder configuration with a base flare.

A. Flow Field about Sides of Carrier

The carrier flow field parameters that must be evaluated are flow velocity and direction, Mach number, pressure, and density. Where ejection is to take place from the side of the carrier vehicle, the flow field about the carrier from the point of ejection aft must be known. Where ejection takes place from the base of the carrier, the flow field in the wake of the carrier vehicle is of importance. In both cases, interference effects are of importance. These topics are now discussed briefly.

The carrier flow field parameters for bodies with attached shock waves may be determined with varying degrees of accuracy by one of several methods. The Method of Characteristics is equally applicable in irrotational and rotational flow and provides the ultimate in rigor in inviscid flow calculations. Real gas effects can be considered using the method of Gravalos (Ref. 2). For blunt bodies, over which a part of the flow field is subsonic, relaxation techniques such as those described by Gravalos may be used to determine the flow field in the subsonic regions. In the high Mach number case, real gas effects become extremely significant and must be incorporated into the calculations. An appreciation of the characteristics of the flow fields about the carrier vehicle can be obtained by considering the results of computations.

The variations of flow field parameters about a 10-degree half angle cone-cylinder at a free stream Mach number of 2.075 obtained from results of Liepmann (Ref. 3) are shown in Figure A-1. From this figure, it is apparent that essentially free stream conditions prevail in the flow aft of a position five to six body diameters aft of the nose.

At higher Mach numbers, more significant effects are encountered. For example, Figure A-2 shows flow field parameters about a 15-degree half angle cone-cylinder at a free stream Mach number of 7.0. These data are deduced from data of Clippinger (Ref. 4) and show flow field parameters as a function of axial distance from the nose for three transverse distances. Velocity variation is not illustrated since throughout the majority of the flow field the velocity is within 95 percent of the free stream value. From this figure, it is apparent that aft of four to five calibers from the nose, the flow parameters shown do not vary rapidly as a function of axial or transverse distance. However, it should be noted that a reduced Mach number will exist throughout the field corresponding to the total pressure loss through the shock wave.

As indicated above, calculation of the flow field about a blunt-nosed body involves obtaining the subsonic and transonic portions of the flow field before the Method of Characteristics can be employed to obtain the supersonic flow field. The flow field over a cone-cylinder carrier with a spherical nose at 85,000 feet altitude with a free stream Mach number of 15 has been computed. The subsonic and transonic portion is obtained using the method of Gravalos and the supersonic portion using the Method of Characteristics. Pertinent results of this computation are shown in Figures A-3a and A-3b. The relationships employed to derive these results were programmed on a digital computer to expedite the computations. Of particular interest is the large deviation of density from the free stream value in that portion of the field aft of five to six calibers. Variations in the flow field parameters are relatively small as functions of positions aft of this station. Also of interest are the relatively low Mach numbers throughout the flow field. Velocity variation is not shown since it is within 10 percent of the free stream value throughout the majority of the flow field.

B. Flow Field in Wake of Carrier

Analysis of the flow field structure behind a high speed body is made difficult because the wake region involves simultaneous interaction of an external inviscid flow with an internal dissipative core. Furthermore, the case of most practical application, the turbulent wake, involves a time dependent transport mechanism about which very little is known.

At the present time, then, wake characteristics must be determined primarily in an empirical manner. However, considerable progress towards

description of the wake has been accomplished as a result of efforts to correlate and explain base pressure data.

The general features of the wake are depicted in Figure A-4. As shown here, the inviscid portion of the flow ahead of the base expands around the corner and separates from the surface at the corner. A weak lip shock terminates the corner centered expansion fan. Entrainment of air from the region behind the base by the jet pump action of this stream lowers the pressure behind the base. The resulting pressure difference across the stream causes it to be deflected inward toward the axis of the body. Upon reaching the axis, the stream must again be deflected (and hence, recompressed) back to the longitudinal direction. An equilibrium state is reached wherein the flow expands at an angle such that the dissipative flow can negotiate the resulting recompression.

It is readily seen that the region of flow recompression, or the wake throat, is the critical region which controls both the upstream and downstream wake structure. An analogy between the critical region and shock wave, separated boundary layers is also apparent; either represents a case of a dissipative flow negotiating an adverse pressure gradient. The throat serves to divide the separated flow region from the spreading downstream wake.

Figure A-5 shows the separated flow region ahead of the throat. The boundary layer (of thickness AB) formed on the surface of the body spreads into the region behind the base. Entrainment of air from the "dead air" region increases the thickness of this separated mixing layer. At the point where streamlines from opposite sides of the body converge, one of the streamlines must stagnate at point D. Streamlines having a total pressure greater than that of BD will pass downstream while those of lesser total pressure are reversed and recirculated in the "dead air" region. For steady flow, no mass flow is added to or removed from the "dead air" region. The streamline BD is therefore a dividing streamline.

Between points B and C, the process is one of viscous mixing or air entrainment. However, between C and D there must occur a pressure rise of magnitude sufficient to destroy the momentum of the entrained air. The line CD is therefore curved and a series of compression waves are set up which coalesce to form the trailing shock.

In principle, then, it is possible to calculate the wake separation angle and thus determine the wake geometry by equating the total pressure on the dividing streamline to the pressure after recompression. The dividing streamline conditions can be obtained from solutions to the classical problem of parallel-stream mixing. This procedure, in fact, gives good results for two-dimensional wakes where the approaching boundary layer has a negligible effect (Ref. 5).

In general, however, the boundary layer must be considered precluding a simple solution to the mixing problem. Further, the boundary layer itself depends in a complicated way on such factors as the Mach number, Reynolds number, heat transfer history, body surface condition and upstream body geometry.

An additional analytical difficulty is presented by the fact that the pressure along the separated region is not constant in three-dimensional flow (as it is in two-dimensional flow). No simple function such as the two-dimensional Prandtl-Meyer relationship relates flow properties to streamline direction. Thus, a characteristics or equivalent type of calculation must be used to define the recompression pressure for three-dimensional flow.

Fortunately, Love (Ref. 6) noted that the measured three-dimensional wake angle (for bodies of revolution with turbulent boundary layers) can be empirically correlated with the two-dimensional angle for a given base pressure. The calculations reported here thus use Love's data to determine the axisymmetric wake convergence angle.

Referring to Figure A-6, it is seen that the balance between scavenged mass and reversed mass calls for a vortex-like flow in the separated or "dead air" region – better called the recirculation zone. Although the mixing-induced velocities average only a few percent of the free stream velocity, the streamline just below the dividing streamline has a total pressure almost equal to the recompression pressure. It is stagnated near the end of the recompression zone and accelerated back towards the base. Thus, a portion of the flow near the body centerline is capable of attaining a relatively high reverse flow velocity.

Conversely, the air entrained just before point C of Figure A-5 has a total pressure just above the base pressure. It is stagnated at the beginning of the recompression zone and attains essentially no reverse flow velocity.

The reverse flow is of particular importance for small objects ejected down the wake centerline. A rough idea of its characteristics can be obtained from Figure A-6 which was calculated by assuming isentropic flow from the recompression point back to the base pressure. As shown here, the importance of the reverse flow diminishes (because of the low dynamic pressures relative to free stream dynamic pressures) at high Mach numbers.

It may be noted here that, although the reverse flow is of most importance for relatively small objects, the buoyancy forces associated with the recompression pressure gradients are of considerable importance for larger bodies as well.

However, at high upstream Mach numbers, both the reverse flow and the pressure gradients are minimized in relative magnitude. The pressure, as

observed in the three-dimensional case, can be closely approximated by a two-dimensional or Prandtl-Meyer type of analysis. The pressure overshoot (above free stream) found for three-dimensional flow at low supersonic speeds disappears. For these reasons, calculations of separation dynamics at high Mach numbers can employ some simplifications by neglecting the above mentioned effects.

Once past the throat or critical region, the wake-ejected object is immersed in the dissipative (usually turbulent) spreading wake core. Simple dimensional analysis dictates how the wake width and centerline velocities vary with distance behind the body. An asymptotic solution of the momentum equation, using Prandtl's turbulent mising length hypothesis, gives the form of velocity variation across the wake core.

Two empirically determined constants are required: one associated with the rate of spreading of the wake and the other with the effective origin of coordinates. These constants were determined from Reference 7 and assumed to be independent of Mach number. In addition, the thickness of the wake core at the throat was required; this was determined from the compilation of Chapman (Ref. 8).

Empirical equations for the velocity distribution in the wake downstream of the minimum wake diameter and the procedure for determining other wake properties are given in Section IV. D of the main body of the report.

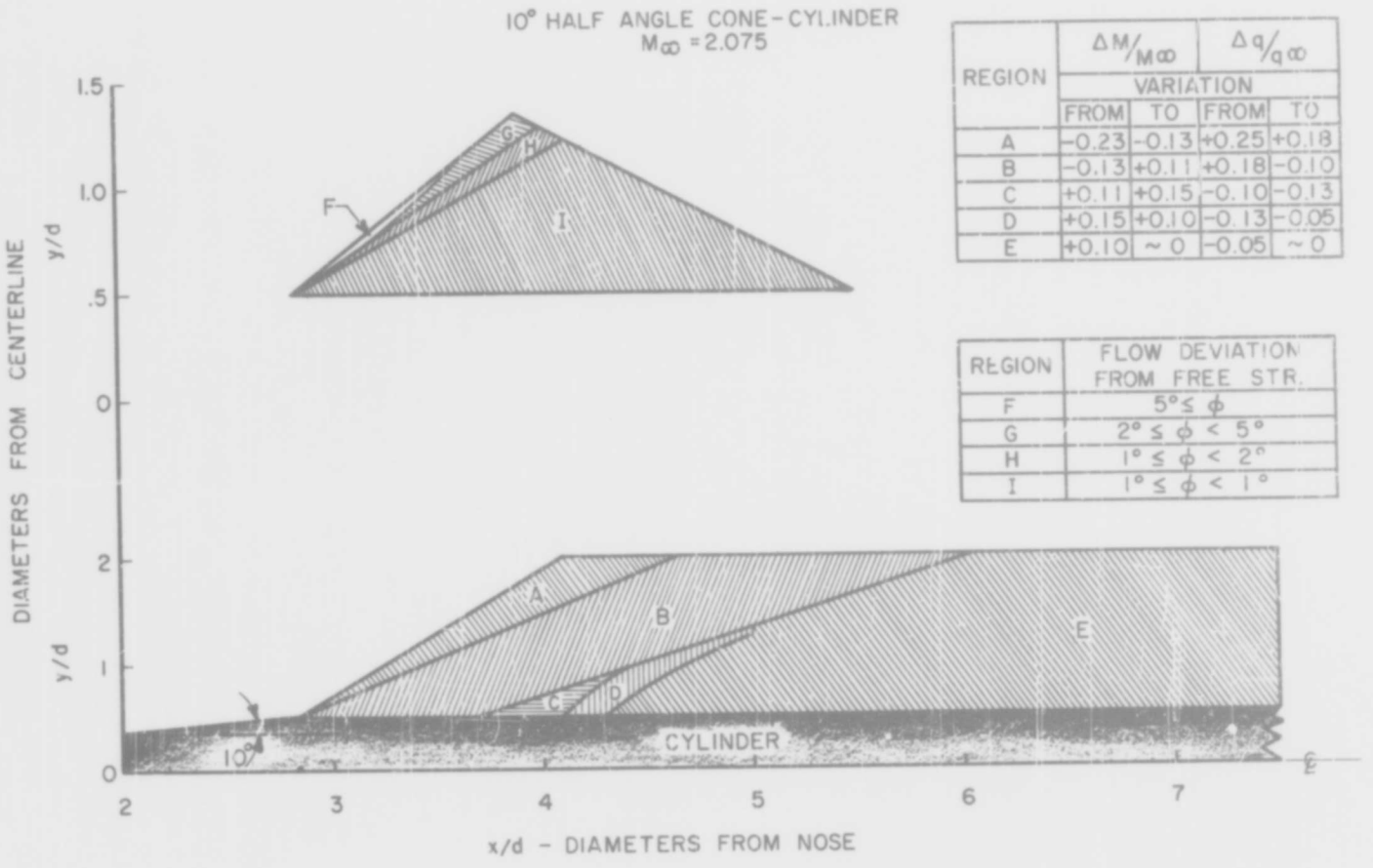

REGION	$\Delta M/M_\infty$ VARIATION		$\Delta q/q_\infty$ VARIATION	
	FROM	TO	FROM	TO
A	-0.23	-0.13	+0.25	+0.18
B	-0.13	+0.11	+0.18	-0.10
C	+0.11	+0.15	-0.10	-0.13
D	+0.15	+0.10	-0.13	-0.05
E	+0.10	~ 0	-0.05	~ 0

REGION	FLOW DEVIATION FROM FREE STR.
F	$5° \leq \phi$
G	$2° \leq \phi < 5°$
H	$1° \leq \phi < 2°$
I	$1° \leq \phi < 1°$

Figure A-1. Flow Deviation Angle, Mach Number, and Dynamic Pressure for Body Slide Flow Field

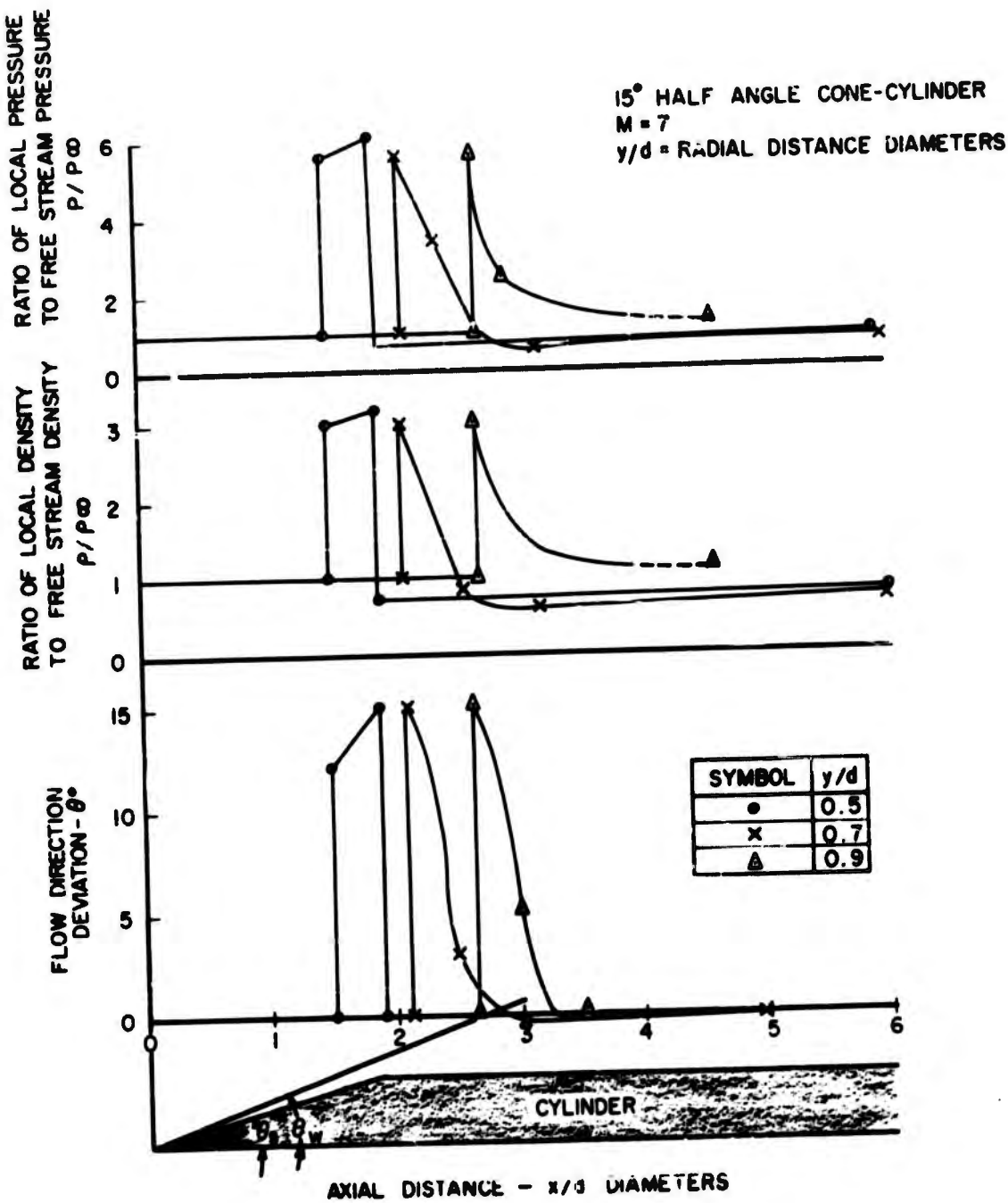

Figure A-2. Flow Density, Pressure, and Deviation Body Side Flow Field

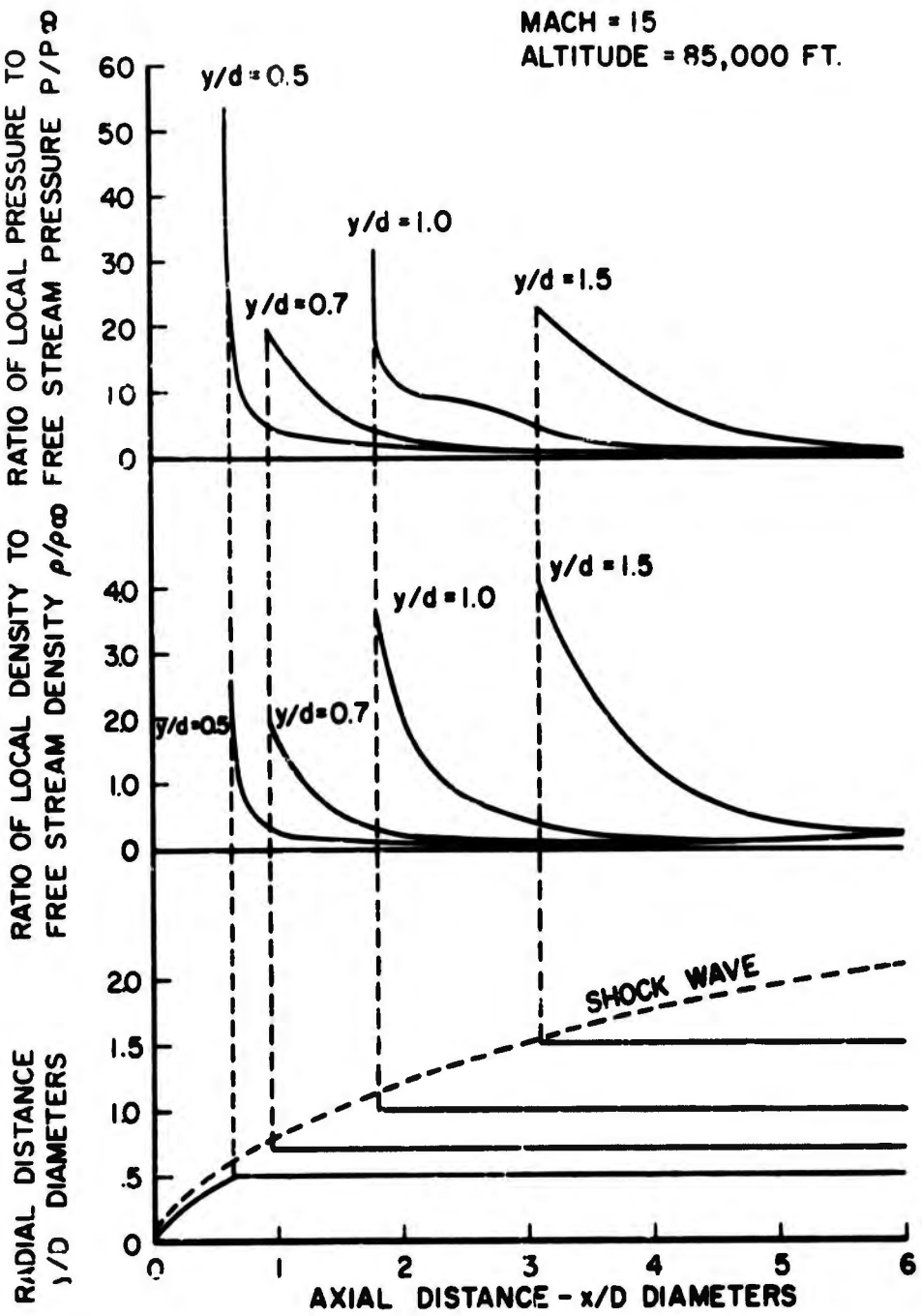

Figure A-3a. Density and Pressure Ratios-Body Side Flow Field for Real Gas

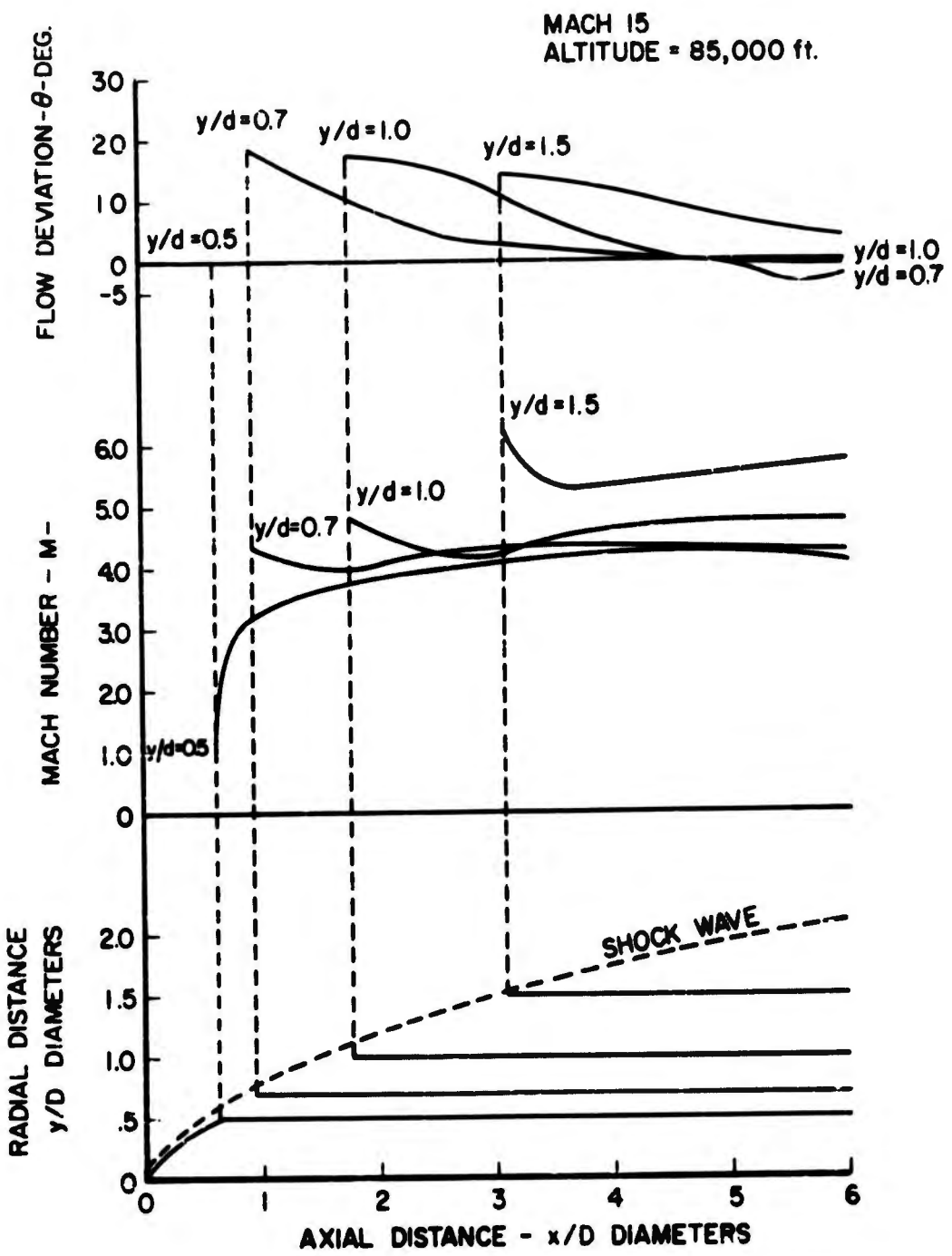

Figure A-3b. Local Flow Deviation and Mach Number-Body Side Flow Field for Real Gas

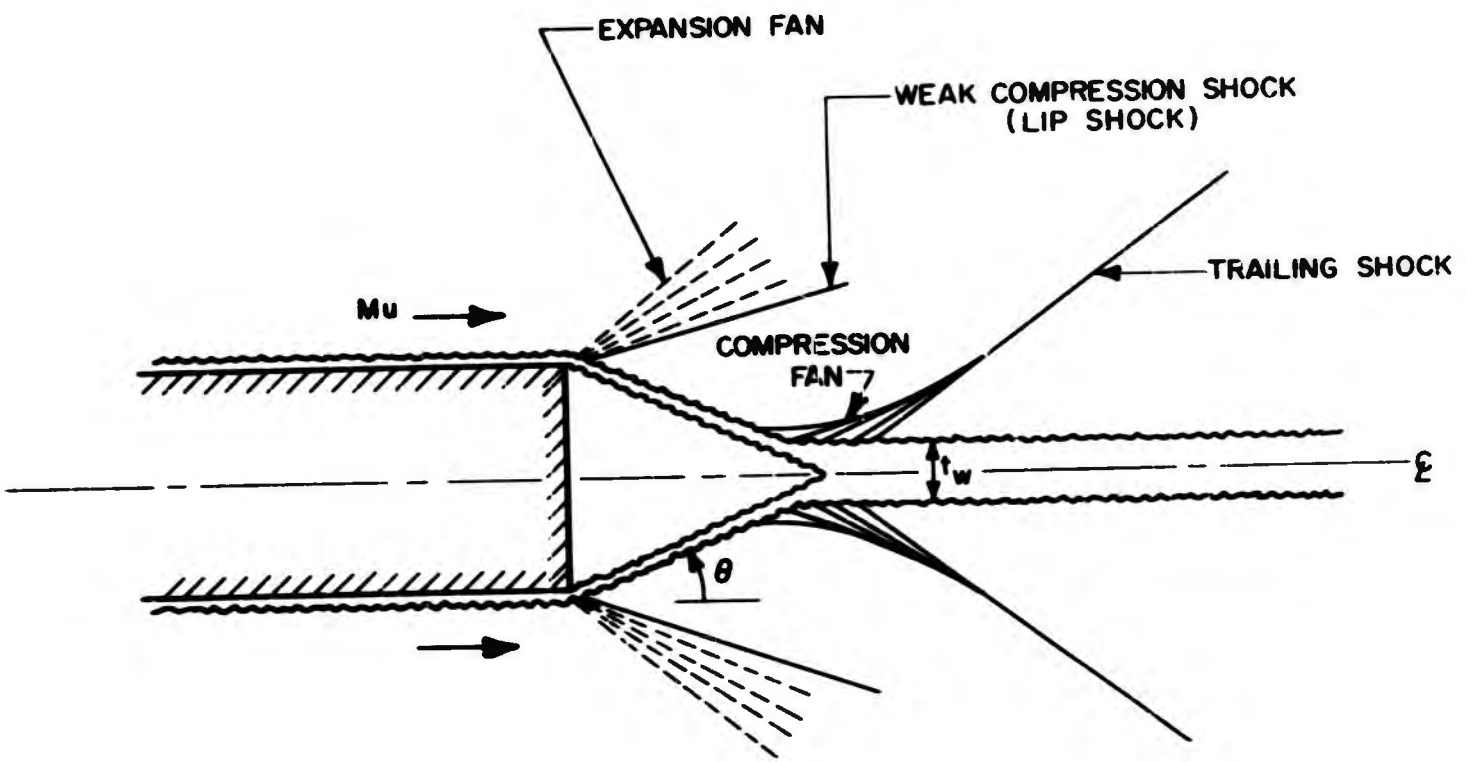

Figure A-4. Schematic Diagram of the Flow Past a Blunt Base

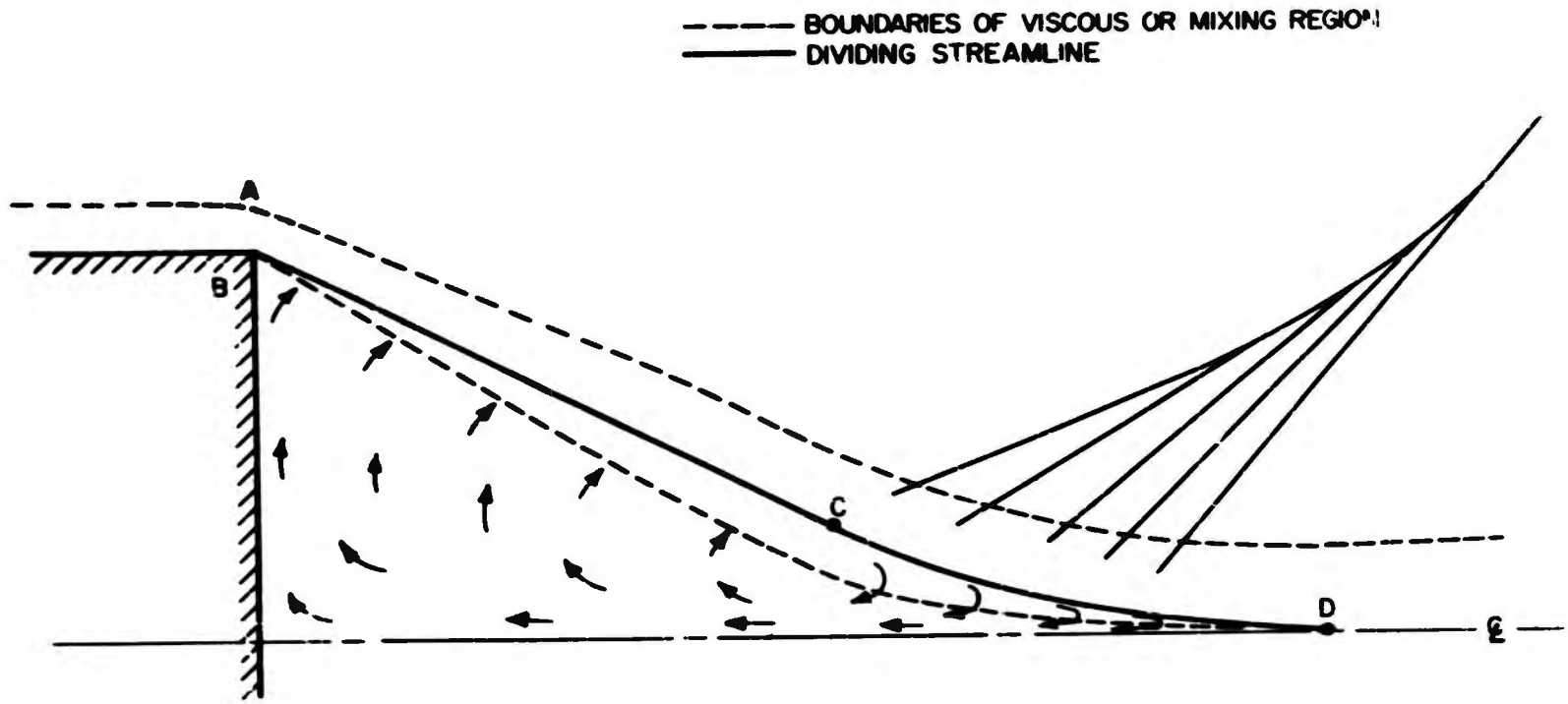

Figure A-5. The Region Behind a Blunt Base

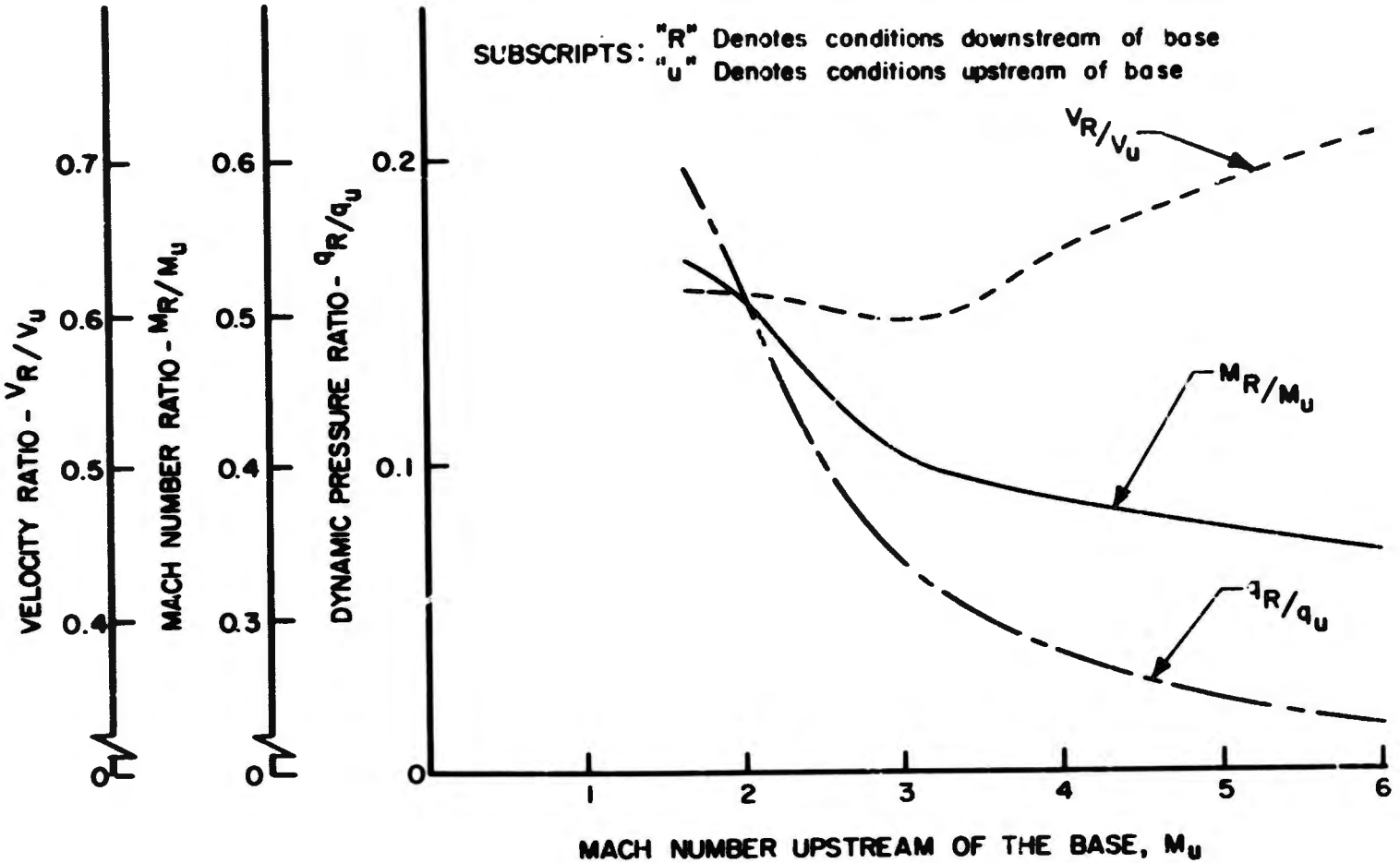

Figure A-6. Maximum Reverse Flow Conditions (Highest Energy Reverse Flow Stream Tube Near the Wake Centerline)

SECTION III

EQUATIONS OF MOTION

The separation conditions and trajectories studied under this program are sufficiently different from conventional conditions to have necessitated the development of motion equations of several types. Particular problems have been created by the nature of the flow fields into which the separating body must be ejected and through which it must pass. This is reflected both in interference effects and pressure variations. In certain of the cases on the other hand, unusual restraints must be placed on the separating body. These requirements have made necessary the formulation of motion equations in all but one of the cases. The following is a discussion of these formulations to indicate the considerations that were required. The following discussion considers each of the particular sets of equations in turn.

A. Base Separation Equations

1. Discussion

Base separation may be obtained in either of two manners. One of these is to eject the separating body in the direction of the longitudinal axis; the other method is to eject at an angle to the longitudinal axis. In the former procedure, the separating body is deployed down the wake core through the low energy portions of the wake. In the latter procedure, the deployment angle is such that the separating body contacts the wake boundary between the vehicle base and the wake throat. The attempt in this case is to penetrate the wake boundary. Since these two methods of deployment are considerably different, two different sets of equations were derived and programmed. These two sets are discussed separately below.

a. Wake Core Ejection

This type of ejection has been studied with a set of equations representing one-dimensional linear motion. The equations in this case were purposely made general in order to provide for various combinations of ejected bodies.

These equations are written for two (or possibly more) ejected bodies with the possibility of elastic interconnection between these bodies. In addition, provision has been made for elastic connection between the ejected body and the carrier vehicle. In cases where no interconnection exists, the spring constant associated with the

elastic connection is taken as zero. Where only a single body is ejected, the differential equation for the second body is suppressed.

Of particular importance in the computations in this case are the wake flow static pressure and density variation. The variation of wake velocity, static pressure and density with position relative to the vehicle base is represented by algebraic expressions. In the process of the computation, the density, static pressure and wake velocity are computed as a function of body position. The dynamic pressure is then obtained as a combination of these quantities and the body absolute velocity.

The wake characteristics employed in these calculations are discussed elsewhere.

b. Wake-Penetration

The physical condition that is to be represented in these equations is that of a cylindrical capsule ejected rearward from the base of the vehicle. It penetrates the wake boundary and possibly passes into free stream conditions.

As the capsule encounters the wake boundary, the dynamic and static pressures to which it is exposed change. In particular, the principal resistance to penetration of the wake boundary results from the large static and dynamic pressures on those portions of the capsule which are external to the wake boundary. Hence, in the motion equations it is important to obtain accurately the areas exposed to these high pressure fields. In addition, it is necessary to represent accurately the wake density, velocity components, and static pressure as functions of position relative to the carrier vehicle base. This variation is represented in terms of distance aft of the vehicle base and distance above or below the vehicle longitudinal axis. The area exposed to the high pressure region is obtained by computing the coordinates of the points at which the capsule crosses the wake boundary. From these coordinates the projected area of the capsule faces, both interior and exterior to the wake, is computed. In addition, the centroids of these areas are also computed for purposes of moment calculations.

As the separating cylinder emerges from the low energy region of the wake, large moments will be imposed upon it Consequently, large angular accelerations may be anticipated. These large angular accelerations can seriously affect the relative velocity of air with

respect to the faces of the separating body, depending of course on the exposure time and the moment of inertia of the body. This is considered in the formulation of the computation procedures. Eight faces of the body are considered, and the total relative velocity of these faces with respect to the air computed as the vector sum of the velocity of the center of gravity of the capsule, the linear velocity of the face induced by rotation, and the wake velocity at the centroid of the face.

2. Formulation

a. One-Dimensional Wake Core Ejection

The motion of the carrier vehicle, and all ejected bodies is assumed to be along a line making a constant angle θ_o with the horizontal. The origin for the x axis is taken to be the point at which separation begins. The equations of motion are now considered.

The equation for the carrier vehicle is

$$m_v\ddot{x} = -(C_DA)_v\frac{\rho_\infty}{2}\dot{x}_v^2 + m_v g \sin\theta_o - K_p(x_v - x_p - \lambda_p)\left(1 + \frac{\dot{x}_v - \dot{x}_p}{k_p}\right)$$

$$-K_c(x_v - x_c - \lambda_c)\left(1 + \frac{\dot{x}_v - \dot{x}_c}{k_c}\right)$$

where

K_p is used if a pilot device is attached by lines to the vehicle,
K_c is used if the capsule is attached by lines to the vehicle.

These tension terms are zero except during line stretch, i.e., the interconnecting line cannot supply force to separate the bodies. The damping is taken proportional to both the separation velocity and the line tension.

The equation of motion for an ejected pilot device which is attached to a capsule is given by

$$\left[m_p + \rho_p(x - x_p)\right]\ddot{x}_p = -(C_DA)_p\frac{\rho_w}{2}(\dot{x}_p - W)^2$$

$$+\left[m_p + \rho_p(x - x_p)\right] g \sin\theta_o + K_p(x - x_p - \lambda_p)$$

where

$x = x_v$ when the vehicle is at the opposite end of the line and
$x = x_c$ when the capsule is at the end of the line.

When lines are employed, the mass term $\rho_p(x - x_p)$ is fixed as $\rho_p\lambda_p$ after the time when full extension of the unstretched length occurs. However, during the period of line stretch, the effective mass of the lines is taken as $1/2\ \rho_p\lambda_p$. It should be noted that during the time of line extension the derivative

$$\frac{d}{d_t}\left[m_p + \rho_p (x_v - x_p)\right] \dot{x}_p$$

has been taken as

$$\left[m_p + \rho_p (x_v - x_p)\right] \ddot{x}_p$$

since the lines are pulled out of the pack rather than being pushed out by a reaction force. The term $K_p (x_v - x_p - \lambda_p)$ is zero unless $x_v - x_p - \lambda_p > 0$.

If the pilot device is to increase its effective drag area, as for example with a small parachute or balloon, this increase in drag area can be initiated either at a predetermined time or at a predetermined distance aft of the carrier vehicle. The increase in drag or effectiveness can be made instantaneously or at a prescribed rate.

When this pilot device is employed to extract a capsule, the motion equation of the capsule is written:

$$\left[m_c + \rho_c (x_v - x_c)\right] \ddot{x}_c = -(C_D A)_c \frac{\rho w}{2} (\dot{x}_c - W)^2$$

$$+ \left[m_c + \rho_c (x_v - x_c)\right] g \sin\theta_o - K_p (x_c - x_p - \lambda_p)\left(1 + \frac{\dot{x}_c - \dot{x}_p}{k_p}\right)$$

$$+ K_c (x_v - x_c - \lambda_c)\left(1 + \frac{\dot{x}_v - \dot{x}_c}{k_c}\right)$$

The terms $\rho_c (x_v - x_c)$ and $K_2(x_v - x_c - \lambda_c)$ are inserted to permit attachment of the capsule to the carrier vehicle or to a second capsule if desired. Considerations similar to those mentioned above apply to these terms.

It should be mentioned that the terms representing tension forces in the connecting lines provide for a linear variation of tension with elongation. This can be varied to provide a quadratic variation during unloading thus representing a hysteresis loop in the connecting line material such as is common with nylon.

b. Three Degree of Freedom Equations for Wake-Penetration

The equations representing three degree of freedom motion of a capsule in the wake of a carrier vehicle are of themselves relatively straightforward. However, the representation of forces and moments on such a capsule is complex.

The notation used is similar to that given above. In addition, the angles θ represents the angle between the longitudinal axis and the space fixed x axis. As before, the carrier vehicle motion is assumed to take place along a straight line, the x axis; Figure A-7 shows the axis system

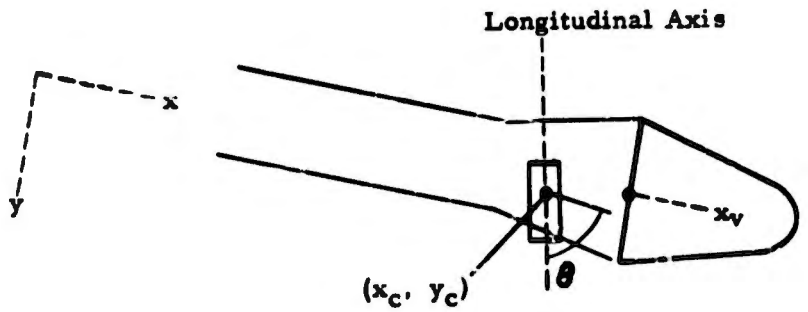

Figure A-7

The equations of motion then become:

For the vehicle

$$m_v \ddot{x}_v = - (C_D A)_v \frac{\rho_\infty}{2} \dot{x}_v^2 + m_v g \sin \gamma_o$$

For the capsule

$$m_c \ddot{x}_c = F_x + m_c g \sin \gamma_o$$

$$m_c \ddot{y}_c = F_y$$

$$I_c \ddot{\theta} = M$$

As mentioned above, considerable complexity occurs in representing the forces and moments on the capsule during wake-penetration. Preliminary calculations indicate that high angular velocities of the capsule are to be anticipated during wake-penetration. Hence in computing the linear velocity of each face of the capsule, account must be taken of the velocity induced by rotation. This rotationally induced velocity will vary appreciably across a face. In the representation of forces and moments, this variation in velocity is accounted for by dividing the surface of the capsule into eight half faces. These half faces are determined by a plane which includes the longitudinal axis and a second plane at right angles and passing through the capsule center of gravity. The velocity of each half face is taken to be the velocity of the centroid of the half face. The angle of attack of each half face is the angle of attack at the centroid.

This involves then, determining at each step of the calculation eight attitude angles, eight velocities and at least eight angles of attack. Faces are designated 0, 1, 2, 3 and half faces by a plus or minus. In this notation, the absolute velocity of the centroid of half face j^+ or j^- is given by

$$\dot{x}_j = \dot{x}_c - B_j \dot{\theta} \sin (\theta + \tau_j)$$

$$\dot{y}_j = \dot{y}_c + B_j \dot{\theta} \cos (\theta + \tau_j) \qquad (j = 0, 1, 2, 3)$$

where B_j is the distance from the centroid of the half face to the capsule center of gravity and τ_j is the angle between the longitudinal axis and the line from the center of gravity to the centroid of half face j^+ or j^-.

The air flow angle as seen at the centroidal points will vary depending upon whether the point is inside or outside the wake. Hnece it is necessary to compute these flow angles and angles of attack for conditions both inside designated by a subscript w and external to the wake, designated by a subscript E. Thus, for half face j^+ or j^-, the air flow angle, γa_j, is given outside the wake by

$$\tan \gamma a_{j_E} = \frac{\dot{y}_j - W_y}{\dot{x}_j - W_x} \qquad (j = 0, 1, 2, 3)$$

and inside the wake by (assuming that transverse wake velocities are negligible)

$$\tan \gamma a_{j_w} = \frac{\dot{y}_j}{\dot{x}_j - W} \qquad (j = 0, 1, 2, 3)$$

Here W_x and W_y are velocity components of the air outside the wake at the centroid and W is the wake velocity along x at the centroid. These velocities, determined by a study of the wake structure, are programmed into the computation as functions of Mach number, distances, aft of the parent vehicle and distance from the wake boundary. Similar variations in P_{s_E} and ρ were employed. The angles of attack of face j^+ or j^- are given by

$$\alpha_{j_E} = \gamma a_{j_E} - (\theta + j\,\pi/2)$$

$$(j = 0, 1, 2, 3)$$

$$\alpha_{j_w} = \gamma a_{j_w} - (\theta + j\,\pi/2)$$

The forces of each half face are obtained as the product of area, the component of pressure normal to the half face, and a pressure coefficient. Flow parallel to a face is assumed to contribute no force. Thus, the net forces along x and along y are composed of eight

parts.

$$F_x = F_{x_{0^+}} + F_{x_{0^-}} + F_{x_{1^+}} + \text{etc.}$$

$$F_y = F_{y_{0^+}} + F_{y_{0^-}} + F_{y_{1^+}} + \text{etc.}$$

For face j^+ or j^-

$$F_{x_j} = -\left[\begin{Bmatrix} P_{B_{j_E}} \\ P_{F_{j_E}} \end{Bmatrix} A_{j_E} + \begin{Bmatrix} P_{B_{j_w}} \\ P_{F_{j_w}} \end{Bmatrix} (A_j - A_{j_E})\right] \cos(\theta + j\,\pi/2)$$

$$\equiv \left[B_{j_E} + B_{j_w}\right] \cos(\theta + j\,\pi/2)$$

$$F_{y_j} = -\left[B_{j_E} + B_{j_w}\right] \sin(\theta + j\,\pi/2) \qquad (j = 0,\ 1,\ 2,\ 3)$$

The term $P_{B_{j_E}}$ is used if $\pi/2 < \alpha_{j_E} < 3\,\pi/2$. $P_{F_{j_E}}$ is used otherwise. This change is associated with the use of base or frontal surface pressure coefficients associated with the appropriate type of surface, i.e., whether the surface is flat or curved.

Similarly α_{j_w} is associated with $P_{B_{j_w}}$ and $P_{F_{j_w}}$. A_j is the total area of the half face and A_{j_E} is the area of the half face which is external to the wake boundary.

The terms P_B and P_F are defined as follows:

$$P_{B_{j_E}} = C_{D_B} \frac{\rho_E}{2} Va_{j_E}^2 \cos^2 \alpha_{j_E} + P_{s_E}$$

$$P_{F_{j_E}} = C_{D_F} \frac{\rho_E}{2} Va_{j_E}^2 \cos^2 \alpha_{j_E} + P_{s_E}$$

$$P_{B_{j_w}} = C_{D_B} \frac{\rho_w}{2} Va_{j_w}^2 \cos^2 \alpha_{j_w} + P_{s_w}$$

$$P_{F_{j_w}} = C_{D_F} \frac{\rho_w}{2} Va_{j_w}^2 \cos^2 \alpha_{j_w} + P_{s_w} \qquad (j = 0,\ 1,\ 2,\ 3)$$

where P_{s_E} and P_{s_W} are static pressures at the centroid. The velocities employed above are given by

$$Va_{j_E} = \left[(\dot{x}_j - W_x)^2 + (\dot{y}_j - W_y)^2 \right]^{1/2}$$

$$Va_{j_W} = \left[(\dot{x}_j - W)^2 + \dot{y}_j{}^2 \right]^{1/2}$$

In terms of the above notations, the moments are simply obtained:

$$M = M_{o+} + M_{o-} + M_{1+} \text{ etc.}$$

$$M_{j^-} = B_{j_{E^-}} \cdot a_{j_{E^-}} - B_{j_{W^-}} \cdot a_{j_W}$$

$$M_{j^+} = B_{j^+_E} \cdot a_{j^+_W} + B_{j^+_W} \cdot a_{j^+_W} \qquad (j = 0, 1, 2, 3)$$

where a_{j_E} is the moment arm of the centroid of the exposed portion of half face j^- and a_{j_W} is the moment arm to the centroid of the portion of half face j^- within the wake. A similar statement applies to half face j^+.

The details of the computation of the quantities a_{j_E} and a_{j_W} are not given here. The areas associated with partial exposure of the flat faces of the cylinder are determined as part of a circle cut by a chord, while the appropriate centroid of this area is computed to obtain the center of pressure. The projected area of the curved faces when partially across the wake boundary is obtained by approximating this area as a trapezoid. The centroid of the trapezoid is obtained for the moment calculations.

B. Side Ejection Equations

1. Discussion

The equations employed in this case are used to represent two conditions. The first of these is associated with forces and moments on the ejected body as it emerges from the carrier vehicle and is only partially exposed to

the air stream. This set of equations is employed until the body is entirely free; a second set of equations is employed to describe the motion. The initial conditions for this set of calculations are obtained from the final conditions of the computations associated with the partial exposure during ejection.

In the case of the equations associated with capsule emergence, particular attention is required in representing the areas and effective forces of the parts of the separating body which are exposed to the air stream in the vicinity of the carrier vehicle. The forces are obtained in terms of pressure coefficients and exposed areas. The exposed area is obtained by computing the position at which the axis of the emerging capsule that is normal to the air stream crosses the carrier vehicle surface. From this coordinate and the geometry of the capsule, it is possible to compute both the exposed area and the center of pressure for this area. During the initial phase of the emergence, the capsule is assumed restrained. In the computations this restraint is released at different levels of exposure. The moments on the capsule which exist during the restraint phase of emergence are calculated to determine structural requirements on this restraint and to determine frictional forces opposing ejection.

The second phase of the separation trajectory involves the motion of the capsule in the vicinity of the carrier vehicle while under the influence of the flow field about the carrier vehicle. The equations employed in this part of the analysis represent three-dimensional motion of the capsule. These equations are conventional in form.

The problem occurs in the representation of the aerodynamic forces on the capsule as it separates from the carrier vehicle. Three sources of difficulty occur. They are: the presence of a nonuniform flow field in the free stream direction; the presence of a shock front with which the separating capsule may come in contact as it emerges thus causing a discontinuity in the force on the capsule; and, finally, interference on the capsule due to an "upwash" effect caused by the flow field of the carrier vehicle.

The variations in flow intensity in the free stream direction are accounted for by inserting the flow field velocity as a function of position with respect to the vehicle in the computer program and computing flow velocity as a function of capsule position with respect to the carrier.

In the process of the computation, the equation of the shock front in coordinates attached to the carrier vehicle is programmed into the computation. The coordinates of the separating body are compared with the equation of the shock front at each step of the computation to determine

if the separating body was in contact with the front. At time of contact with the shock front, the body area lying on the shock front is computed. This is employed in the force and moment equations along with the pressure differential across this area. Interference effects are obtained by a similar procedure. The interference field is represented in carrier vehicle body fixed coordinates. The coordinates of the separating body are also represented in the same axis system and the interference flow at points on the separating body obtained. This flow is used with a formulation of interference effects on the separating body to obtain the associated forces.

2. Formulation of Equations

a. Partial Exposure Phase

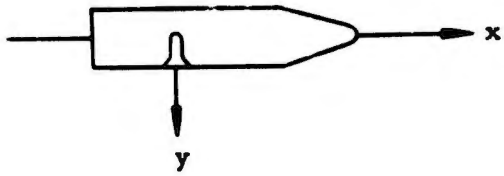

Figure A-8

The carrier vehicle is assumed to be initially traveling on a straight line path which is the x axis. Its acceleration, ng, is assumed constant. The origin is taken at the initial center of gravity of the separating body, and the coordinate system is space fixed. The separating body is restrained during a portion of the ejection phase so that rotation and differential motion with respect to the carrier longitudinal axis are not possible. This restraint is released when the differential y coordinate of the separating body is equal to some value less than or equal to that corresponding to total exposure of the separating body. Then during the period of restraint

$$\ddot{x}_c = ng$$

$$\ddot{\theta} = 0$$

$$m_c \ddot{y}_c = - \mu f_a F_{a_x} - \mu f_m m_c ng - F_{a_y} + F(y, t)$$

where μ is the coefficient of friction, F_a's are the aerodynamic forces and $F(y, t)$ is the force imparted by the ejection mechanism.

The f's are determinable from the geometry of the capsule-carrier restraint system. The subscripts a and m are used to take into account the fact that the centers of aerodynamic loads and mass will in general be different.

The quantities F_{a_x} and F_{a_y} are obtained by summing the products of pressure and projected areas of the capsule. The pressures over the parts of the capsule exposed to the air stream may be approximated with modified Newtonian coefficient times the local dynamic pressure experienced by the capsule.

In order to exclude the mathematical possibility of the frictional force aiding the ejection of the capsule in the equations of motion (i.e., the friction force acting in the desired direction of motion), the terms contributing to this force must be properly identified by sign. Thus, when the magnitude of frictional resistance due to inertial forces exceeds that due to F_{a_x}, and the carrier is decelerating, the absolute magnitude of the friction force must be employed with a negative sign in the lateral displacement equation of motion. In all other cases, since F_{a_x} is considered acting in the "drag" direction, the pure algebraic values can be used to achieve the proper vector direction of the net friction force.

When the restraint is released, the separating body is free to both rotate and translate relative to the carrier vehicle. The equations for this part of the ejection phase are as follows:

$$m_c \ddot{y}_c = - F_{a_y} + F(y, t)$$

$$m_c \ddot{x}_c = - F_{a_x} + m_c g \sin \Gamma_o$$

$$I_c \ddot{\theta}_c = F_{a_x} \bar{y} + F_{a_y} \bar{x}$$

where $\bar{x}$ and $\bar{y}$ are the axial and normal moment arms from the center of pressure of the exposed portion of the capsule to the capsule center of gravity.

The areas exposed and centroids of these areas are computed from the geometry of the particular body and the instantaneous extent of emergence.

In some cases the longitudinal axis of the separating body is at right angles to the longitudinal axis of the carrier vehicle. In other cases, the two longitudinal axes are parallel. In the case of a sphere, the orientation is immaterial.

b. Side Separation Proximity Phase

These equations are employed to calculate separation trajectories during the phase while the separating body is free of the carrier vehicle and in the flow field altered by the parent body. The carrier vehicle is assumed to be accelerating along a straight line path, the x axis. The y axis is obtained by a counterclockwise rotation. The carrier vehicle is accelerating at a rate of n g's. The x and y coordinate system is attached to the carrier vehicle nose. The interference effects are denoted by a subscript i. The equations of motion are:

$$m_c(\ddot{x}_c + ng) = - C_A(\alpha)\, QA \cos\theta - C_N(\alpha)\, QA \sin\theta$$

$$- mg \sin\Gamma_o - C_{L_i}\, QA \sin\gamma - C_{D_i}\, QA \cos\gamma$$

$$m_c\ddot{y}_c = - C_A(\alpha)\, QA \sin\theta + C_N(\alpha)\, QA \cos\theta$$

$$+ C_{L_i}\, QA \cos\gamma - C_{D_i}\, QA \sin\gamma$$

$$I_c\, \ddot{\theta}_c = C_m(\alpha)\, QAd + C_{m_q} \frac{\dot{\theta}\, d}{2V}\, QAd$$

$$+ C_{m_i}\, QAd$$

where

$$\alpha = \theta - \tan^{-1} \frac{u_y - w_y}{u_\infty + u_x - w_x}$$

$$Q = 1/2\, \rho_1\, V_1^2,$$

$$V_1^2 = (u_\infty + u_x - w_x)^2 + (u_y - w_y)^2,$$

u_∞ is the carrier velocity, a function of time, $= u_{o_\infty} + ng(t - t_o)$

u_x and u_y are the x and y components of the relative velocity of capsule to carrier

w_x and w_y are the local velocities imparted to the medium by the passage of the carrier.

C_{L_i} and C_{D_i} are the force increments normal and parallel to the mean stream direction due to continuous stream gradients and curvature. C_{L_i} and C_{m_i}, as well as the other coefficients, are referred to the capsule reference area and the local average dynamic pressure.

The values of C_A, C_N, C_m, and C_{m_q} to be used in these equations are those appropriate to the capsule in a uniform flow field at an effective Mach number generated locally by the carrier.

This effective Mach number may be taken as the average of the Mach number existing over the length of the capsule when flow variations are within the limits of the linear approximations of Moskowitz (Ref. 1). In this case, the additional terms C_{L_i} and C_{m_i}, due to stream curvature and gradients, are determinable by integrations of the velocity potential functions (Ref. 1) and are obtained in terms of longitudinal and lateral velocity variations from the mean condition.

For blunt capsule configurations or for areas of flow where large gradients exist, the strip theory described in Section IV of the main body of the report avoids the restrictions of linearization. The correlation of the method with wind tunnel data indicates satisfactory prediction of aerodynamic coefficients is achievable. When strip theory is used, the effect of gradients and curvature are more conveniently included in single coefficients such as $C_{A'}$ and $C_{N'}$ with the deletion of the incremental nonuniformity terms, i.e., C_{L_i} and C_{m_i}, from the equations of motion.

The effects of flow discontinuities generated by the intersection of a shock wave with the capsule are not obtainable from the linearized approximation and must be determined by the strip method of calculation.

Morkovin, et al (Ref. 9) presents some pressure data on oblique intersection of shock waves and cylinders, yielding, therefore, data on diffracted shock induced pressures which are supplementary to the force data presented in this report.

Geometric relations are employed to compute the coordinates of the outermost points on the base and nose of the separating capsule. At each step of the computation, these are compared to the coordinates of the side of the carrier vehicle to determine if the capsule has collided with the carrier vehicle. If collision occurs, the computation is stopped.

LIST OF SYMBOLS FOR APPENDIX I

A	Cross sectional area, ft^2
B	Distance from center of gravity, ft
C	Force coefficient, dimensionless
F	Force, lbs
I	Moment of inertia, slug ft^2
K	Spring rate of attachment lines, lb/ft
M	Moment, ft-lb
P	Force, lbs
Q	Dynamic pressure, lb/ft^2
V	Velocity, fps
W	Interference velocity, fps
d	Diameter, ft
f	Restraint geometry function for partial exposure phase
g	Gravitational acceleration, fps
k	Damping constant associated with lines
l	Length, dimensionless
m	Mass, slugs
n	Acceleration, gravity units
t	Time, seconds
(x, y, z)	Coordinates along trajectory, ft
$(\dot{x}, \dot{y}, \dot{z})$	Velocity components along trajectory, fps

$(\ddot{x}, \ddot{y}, \ddot{z})$	Acceleration components along axes, fps^2
Γ_o	Initial path angle, radians
θ	Attitude angle, radians
θ_o	Initial attitude angle, radians
α	Angle of attack, radians
γ	Path angle, radians
λ	Unstretched length of attachment lines, ft
μ	Friction coefficient, dimensionless
ρ	Mass density, $slugs/ft^3$ - or linear mass density, slugs/ft
τ	Position angle with respect to body axes, radians
$(\dot{\cdot})$	First derivative with respect to time
$(\ddot{\cdot})$	Second derivative with respect to time

LIST OF SUBSCRIPTS FOR APPENDIX I

A	Axial direction, axial force
B	Base
D	Drag force
E	Exterior to wake or dimensions and conditions of exposed portion of capsule during partial exposure phase
F	Frontal
L	Lift force
N	Normal direction, normal force
c	With respect to capsule
cg	With respect to center of gravity
i	Interference terms
l	Local conditions
m	Moment
o	Initial conditions
p	With respect to pilot device
q	With respect to pitching velocity
s	With respect to afterbody shoulder
v	With respect to carrier vehicle
w	With respect to wake conditions
∞	With respect to free stream conditions
1, 2, 3	Along coordinate axes

REFERENCES FOR APPENDIX I

1. Moskowitz, B., Approximate Theory for Calculation of Lift of Bodies, Afterbodies, and Combinations of Bodies, NACA TN-2418

2. Gravalos, F.G., Edelfelt, I H., and Emmons, H., The Supersonic Flow about a Blunt Body of Revolution for Gases at Chemical Equilibrium, 9th Annual Congress, International Astronautical Federation, Amsterdam, August 25-29, 1958

3. Liepmann, H.W., and Lapin, E., Summary of Characteristic Methods for Steady State Supersonic Flows, Douglas Aircraft Co., Report No. SM 13343, May 1959

4. Clippinger, R.F., Giese, J.H., and Carter, W.C., "Tables of Supersonic Flow about Cone-Cylinders," Part II, Complete Flows, BRL Report No. 730, August 1950

5. Chapman, D.R., Kuehn, D.M., and Larson, H.K., Investigation of Separated Flows in Supersonic and Subsonic Streams with Emphasis on the Effects of Transition, NACA TN-3869, March 1957

6. Love, E.S., Base Pressure at Supersonic Speeds on Two-Dimensional Airfoils and on Bodies of Revolution with and without Fins Having Turbulent Boundary Layers, NACA TN-3819, January 1957

7. Howarth, L., Editor, "Modern Development in Fluid Dynamics," High Speed Flow, Vol. II, Oxford at the Clarendon Press, 1953

8. Chapman, D.R., An Analysis of Base Pressure at Supersonic Speeds and Comparison with Experiment, NACA TN-2137, July 1950

9. Morkovin, M.V., Migotsky, E., Bailey, H.E., and Phinney, R.E., Experiments on Interaction of Shock Waves and Cylindrical Bodies at Supersonic Speeds, J.I.A.S., April 1952

AFOSR-106

Directorate of Research Analysis
Air Force Office of Scientific Research
Air Force Research Division, ARDC
Holloman Air Force Base, New Mexico

DYNAMICS OF SEPARATING BODIES - MEASUREMENTS AT MACH 2, 4, AND 5

by H. L. Wackelin and R. O. Fredette

Cook Research Laboratories, a division of Cook Electric Company, Chicago, Illinois

March 1961. 113 pp incl. illus.

Technical Report AFOSR-106

(Contract AF 29(600)-1711) unclassified report

Wind tunnel tests were conducted on a data capsule shape in the interference field of a carrier vehicle model at Mach numbers of 4.0 and 5.0 with limited data at M = 2.0. The data obtained were analysed and a preliminary evaluation made as to the agreement with methods of prediction. It is shown that

(over)

UNCLASSIFIED

UNCLASSIFIED

AFOSR-106

Directorate of Research Analysis
Air Force Office of Scientific Research
Air Force Research Division, ARDC
Holloman Air Force Base, New Mexico

DYNAMICS OF SEPARATING BODIES - MEASUREMENTS AT MACH 2, 4, AND 5

by H. L. Wackelin and R. O. Fredette

Cook Research Laboratories, a division of Cook Electric Company, Chicago, Illinois

March 1961. 113 pp incl. illus.

Technical Report AFOSR-106

(Contract AF 29(600)-1711) unclassified report

Wind tunnel tests were conducted on a data capsule shape in the interference field of a carrier vehicle model at Mach numbers of 4.0 and 5.0 with limited data at M = 2.0. The data obtained were analysed and a preliminary evaluation made as to the agreement with methods of prediction. It is shown that

(over)

UNCLASSIFIED

I. Introduction
II. Wind Tunnel Tests
III. Summary of Data
IV. Data Analysis
V. Applicability of Data
VI. Conclusions
Appendix
1. Wackelin, H. L., and Fredette, R. O.
2. Contract AF 29(600)-1711

UNCLASSIFIED

AFOSR-106

Directorate of Research Analysis
Air Force Office of Scientific Research
Air Force Research Division, ARDC
Holloman Air Force Base, New Mexico

DYNAMICS OF SEPARATING BODIES - MEASUREMENTS AT MACH 2, 4, AND 5

by H. L. Wackelin and R. O. Fredette

Cook Research Laboratories, a division of Cook Electric Company, Chicago, Illinois

March 1961. 113 pp incl. illus.

Technical Report AFOSR-106

(Contract AF 29(600)-1711)

Wind tunnel tests were conducted on a data capsule shape in the interference field of a carrier vehicle model at Mach numbers of 4.0 and 5.0 with limited data at M = 2.0. The data obtained were analysed and a preliminary evaluation made as to the agreement with methods of prediction. It is shown that

(over)

UNCLASSIFIED

I. Introduction
II. Wind Tunnel Tests
III. Summary of Data
IV. Data Analysis
V. Applicability of Data
VI. Conclusions
Appendix
1. Wackelin, H. L., and Fredette, R. O.
2. Contract AF 29(600)-1711

UNCLASSIFIED

AFOSR-106

Directorate of Research Analysis
Air Force Office of Scientific Research
Air Force Research Division, ARDC
Holloman Air Force Base, New Mexico

DYNAMICS OF SEPARATING BODIES - MEASUREMENTS AT MACH 2, 4, AND 5

by H. L. Wackelin and R. O. Fredette

Cook Research Laboratories, a division of Cook Electric Company, Chicago, Illinois

March 1961. 113 pp incl. illus.

Technical Report AFOSR-106

(Contract AF 29(600)-1711)

Wind tunnel tests were conducted on a data capsule shape in the interference field of a carrier vehicle model at Mach numbers of 4.0 and 5.0 with limited data at M = 2.0. The data obtained were analyzed and a preliminary evaluation made as to the agreement with methods of prediction. It is shown that

(over)

UNCLASSIFIED

I. Introduction
II. Wind Tunnel Tests
III. Summary of Data
IV. Data Analysis
V. Applicability of Data
VI. Conclusions
Appendix
1. Wackelin, H. L., and Fredette, R. O.
2. Contract AF 29(600)-1711

UNCLASSIFIED

AFOSR-106

in areas where the flow field is known, estimated values of the derivatives obtained with relatively simple calculation techniques agree reasonably well with the data. A discussion of the direct application of these data to capsule separation analyses is presented.

UNCLASSIFIED

AFOSR-106

in areas where the flow field is known, estimated values of the derivatives obtained with relatively simple calculation techniques agree reasonably well with the data. A discussion of the direct application of these data to capsule separation analyses is presented

UNCLASSIFIED

UNCLASSIFIED

AFOSR-106

in areas where the flow field is known, estimated values of the derivatives obtained with relatively simple calculation techniques agree reasonably well with the data. A discussion of the direct application of these data to capsule separation analyses is presented.

UNCLASSIFIED

UNCLASSIFIED

UNCLASSIFIED

AFOSR-106

Directorate of Research Analysis
Air Force Office of Scientific Research
Air Force Research Division, ARDC
Holloman Air Force Base, New Mexico

DYNAMICS OF SEPARATING BODIES - MEASUREMENTS AT MACH 2, 4, AND 5

by H. L. Wackelin and R. O. Fredette

Cook Research Laboratories, a division of Cook Electric Company, Chicago, Illinois

March 1961. 113 pp incl. illus.

Technical Report AFOSR-106

(Contract AF 29(600)-1711) unclassified report

Wind tunnel tests were conducted on a data capsule shape in the interference field of a carrier vehicle model at Mach numbers of 4.0 and 5.0 with limited data at M = 2.0. The data obtained were analyzed and a preliminary evaluation made as to the agreement with methods of prediction. It is shown that

(over)

UNCLASSIFIED

AFOSR-106

Directorate of Research Analysis
Air Force Office of Scientific Research
Air Force Research Division, ARDC
Holloman Air Force Base, New Mexico

DYNAMICS OF SEPARATING BODIES - MEASUREMENTS AT MACH 2, 4, AND 5

by H. L. Wackelin and R. O. Fredette

Cook Research Laboratories, a division of Cook Electric Company, Chicago, Illinois

March 1961. 113 pp incl. illus.

Technical Report AFOSR-106

(Contract AF 29(600)-1711) unclassified report

Wind tunnel tests were conducted on a data capsule shape in the interference field of a carrier vehicle model at Mach numbers of 4.0 and 5.0 with limited data at M = 2.0. The data obtained were analyzed and a preliminary evaluation made as to the agreement with methods of prediction. It is shown that

(over

UNCLASSIFIED

I. Introduction
II. Wind Tunnel Tests
III. Summary of Data
IV. Data Analysis
V. Applicability of Data
VI. Conclusions
Appendix
1. Wackelin, H. L., and Fredette, R. O.
2. Contract AF 29(600)-1711

AFOSR-106

Directorate of Research Analysis
Air Force Office of Scientific Research
Air Force Research Division, ARDC
Holloman Air Force Base, New Mexico

DYNAMICS OF SEPARATING BODIES - MEASUREMENTS AT MACH 2, 4, AND 5

by H. L. Wackelin and R. O. Fredette

Cook Research Laboratories, a division of Cook Electric Company, Chicago, Illinois

March 1961. 113 pp incl. illus.

Technical Report AFOSR-106

(Contract AF 29(600)-1711)

Wind tunnel tests were conducted on a data capsule shape in the interference field of a carrier vehicle model at Mach numbers of 4.0 and 5.0 with limited data at M = 2.0. The data obtained were analyzed and a preliminary evaluation made as to the agreement with methods of prediction. It is shown that

(over)

UNCLASSIFIED

I. Introduction
II. Wind Tunnel Tests
III. Summary of Data
IV. Data Analysis
V. Applicability of Data
VI. Conclusions
Appendix
1. Wackelin, H. L., and Fredette, R. O.
2. Contract AF 29(600)-1711

AFOSR-106

Directorate of Research Analysis
Air Force Office of Scientific Research
Air Force Research Division ARDC
Holloman Air Force Base, New Mexico

DYNAMICS OF SEPARATING BODIES - MEASUREMENTS AT MACH 2, 4, AND 5

by H. L. Wackelin and R. O. Fredette

Cook Research Laboratories, a division of Cook Electric Company, Chicago, Illinois

March 1961. 113 pp incl. illus.

Technical Report AFOSR-106

(Contract AF 29(600)-1711)

Wind tunnel tests were conducted on a data capsule shape in the interference field of a carrier vehicle model at Mach numbers of 4.0 and 5.0 with limited data at M = 2.0. The data obtained were analyzed and a preliminary evaluation made as to the agreement with methods of prediction. It is shown that

(over)

UNCLASSIFIED

I. Introduction
II. Wind Tunnel Tests
III. Summary of Data
IV. Data Analysis
V. Applicability of Data
VI. Conclusions
Appendix
1. Wackelin, H. L., and Fredette, R. O.
2. Contract AF 29(600)-1711

In areas where the flow field is known, estimated values of the derivativer obtained with relatively simple calculation techniques agree reasonably well with the data. A discussion of the direct application of these data to capsule separation analyses is presented.

UNCLASSIFIED

AFOSR-106

In areas where the flow field is known, estimated values of the derivatives obtained with relatively simple calculation techniques agree reasonably well with the data. A discussion of the direct application of these data to capsule separation analyses is presented.

UNCLASSIFIED

UNCLASSIFIED

AFOSR-106

In areas where the flow field is known, estimated values of the derivatives obtained with relatively simple claculation techniques agree reasonably well with the data. A discussion of the direct application of these data to capsule separation analyses is presented

UNCLASSIFIED

UNCLASSIFIED

AFOSR-106

In areas where the flow field is known, estimated values of the derivatives obtained with relatively simple calculation techniques agree reasonable well with the data. A discussion of the direct application of these data to capsule separation analyses is presented.

UNCLASSIFIED

FOR ERRATA

AD 257 734

THE FOLLOWING PAGES ARE CHANGES

TO BASIC DOCUMENT

ERRATA

AFOSR-106
TECHNICAL REPORT

Contract No. AF 29(600)-1711
Project No. 7856
Task No. 78548

DYNAMICS OF SEPARATING BODIES
VOLUME II
MEASUREMENTS AT MACH 2, 4, AND 5

H. L. Wackelin
R. O. Fredette

March, 1961

Section III, page 36

On graph showing C_m as a function of Y/D for X/D = .625, two lower cu

should read $\alpha = 0^\circ$ and $+15^\circ$ reading down.

Section IV, page 60

On graph showing C_A and A_B and on graph of C_N and A_{CON} as functions

percent exposure, vertical axis ordinates should read 0, .5, 1.0.

Appendix I, Section III

Page 16

Following the equation of motion for the carrier vehicle in center

page, add notation:

θ_o is positive when measured downward from the horizontal

On equation of motion for ejected pilot device at bottom of page, th

last term on the right hand side of the equation should read:

ERRATA

AFOSR-106
TECHNICAL REPORT

Contract No. AF 29(600)-1711
Project No. 7856
Task No. 78548

DYNAMICS OF SEPARATING BODIES
VOLUME II
MEASUREMENTS AT MACH 2, 4, AND 5

H. L. Wackelin
R. O. Fredette

March, 1961

Section III, page 36

On graph showing C_m as a function of Y/D for X/D = .625, two lower curves should read $\alpha = 0^\circ$ and $+15^\circ$ reading down.

Section IV, page 60

On graph showing C_A and A_B and on graph of C_N and A_{CON} as functions of percent exposure, vertical axis ordinates should read 0, .5, 1.0.

Appendix I, Section III

Page 16

Following the equation of motion for the carrier vehicle in center of page, add notation:

θ_o is positive when measured downward from the horisontal

On equation of motion for ejected pilot device at bottom of page, the last term on the right hand side of the equation should read:

$$+ K_p (x - x_p - \lambda_p) \left(1 + \frac{\dot{x} - \dot{x}_p}{k_p}\right)$$

Page 17

Starting on the 4th line of the page. the paragraph should read:

When lines are employed, the mass term $\rho_p (x - x_p)$ is maximum at λ_p, or is equal to $\rho_p \lambda_p$ at the time when full extension of the unstretched length occurs. However, during the period of line stretch, $(x - x_p) > \lambda_p$, the effective mass.....

Page 18

On first line of page, the second algebraic term should read:

$K_c (x_v - x_c - \lambda_c)$

Page 19

Add statement to end of paragraph in middle of page:

....angle of attack at the centroid. This analysis was conducted for bodies whose planes of symmetry are characterized by right angles between all faces, i.e., cylinders and rectangular shapes.

Two equations at bottom of page should read:

$\dot{x}_j = \dot{x}_c - K_j \dot{\theta} \sin (\theta + \tau_j)$

$\dot{y}_j = \dot{y}_c + K_j \dot{\theta} \cos (\theta + \tau_j)$

Page 20

First line on page should read:

where K_j is the distance.....

Page 21

Equation for F_{x_j} should read:

$$F_{x_j} = -\left[\begin{Bmatrix} P_{B_{jE}} \\ P_{F_{jE}} \end{Bmatrix} A_{j_F} + \begin{Bmatrix} P_{B_{j_w}} \\ P_{F_{j_w}} \end{Bmatrix} (A_j - A_{j_E})\right] \cos\left(\theta + j\,\frac{\pi}{2}\right)$$

$$= -\left[B_{j_E} + B_{j_w}\right] \cos\left(\theta + j\,\frac{\pi}{2}\right)$$

Page 22

Fourth equation on page should read:

$$M_{j-} = -B_{jE-}\ a_{jE-} - B_{j_w-} \cdot a_{j_w-}$$

List of Symbols for Appendix I, Page 29

On second line, delete definition given for B and substitute:

B Force on capsule face, lbs

Add definition of K_j:

K_j Distance from centroid of half-face to capsule c.g., ft

On eighth line, delete definition given for P and substitute:

P Pressure on capsule face, lbs/ft^2

END CHANGE PAGES

UNCLASSIFIED